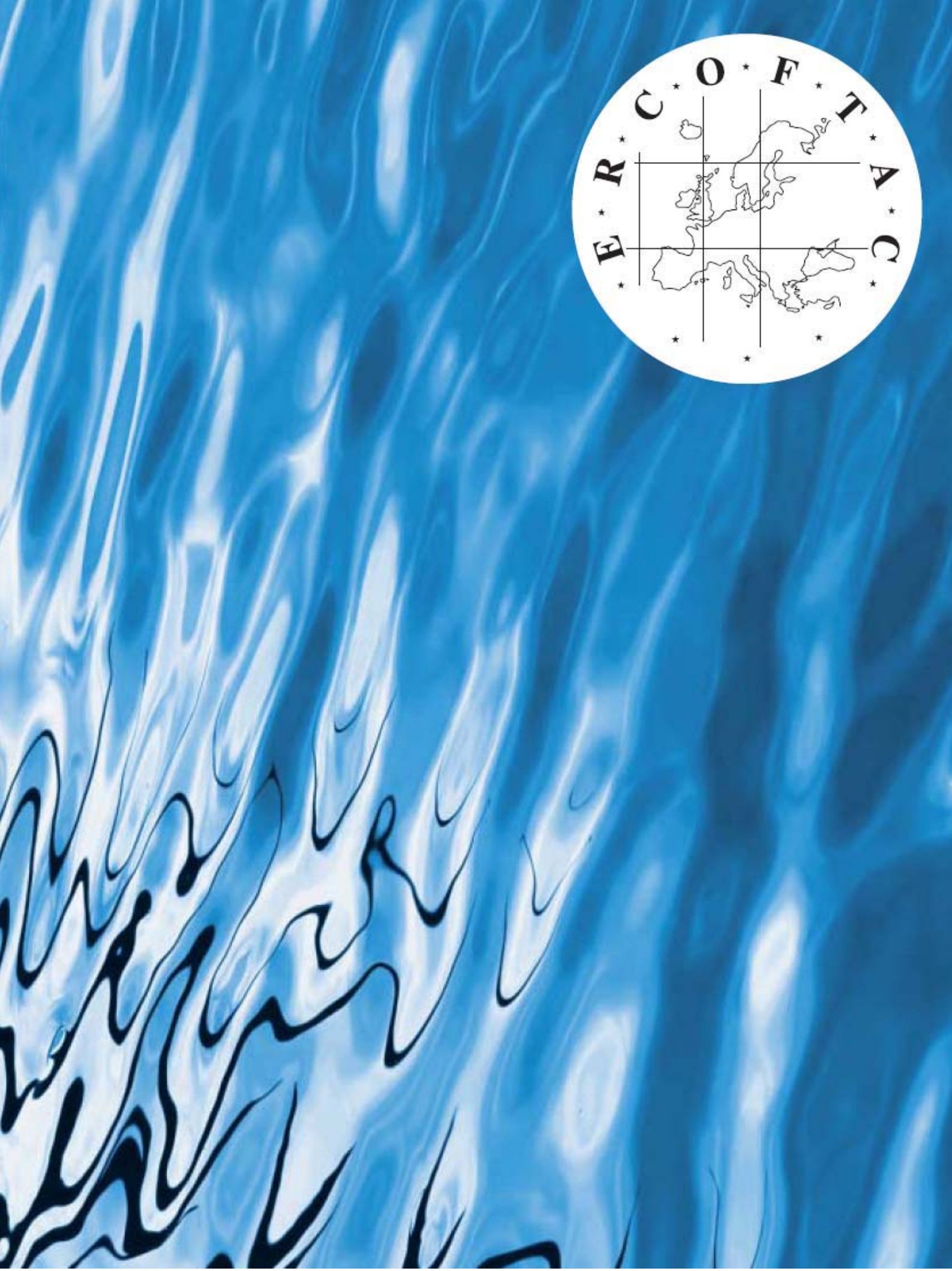
E · R · C · O · F · T · A · C

European Research Community On Flow, Turbulence and Combustion

ERCOFTAC is a leading European association of research, education and industry groups in the technology of flow, turbulence and combustion. The main objectives of *ERCOFTAC* are: To promote joint efforts of European research institutes and industries with the aim of **exchanging technical and scientific information**; to promote **Pilot Centres** for collaboration, stimulation and application of research across Europe; to stimulate, through the creation of **Special Interest Groups**, well-coordinated European-wide research efforts on specific topics; to stimulate the creation of advanced training activities; and to be influential on funding agencies, governments, the European Commission and the European Parliament.

www.ercoftac.org

ERCOFTAC Bulletin 86, March 2011

TABLE OF CONTENTS

SPECIAL THEME

'Fluid Structure Interaction'

SUBMISSIONS

ERCOFTAC Coordination Centre
Laboratory of Heat and Mass Transfer
EPFL-STI-IGM-ERCOFTAC
ME G1 465, Station 9
CH-1015 Lausanne VD
Switzerland

Tel: +41 21 693 3503
Fax: +41 21 693 5960
Email: ercoftac@epfl.ch

HOSTED, PRINTED & DISTRIBUTED BY

ÉCOLE POLYTECHNIQUE
FÉDÉRALE DE LAUSANNE

NEXT *ERCOFTAC* EVENTS

ERCOFTAC Autumn Festival
10th October 2011
TU Darmstadt, Darmstadt, Germany.

ERCOFTAC SPC, IPC & MB-GA Meetings
11th October 2011
TU Darmstadt, Darmstadt, Germany.

The ERCOFTAC Best Practice Guidelines for Industrial Computational Fluid Dynamics

The Best Practice Guidelines (BPG) were commissioned by ERCOFTAC following an extensive consultation with European industry which revealed an urgent demand for such a document. The first edition was completed in January 2000 and constitutes generic advice on how to carry out quality CFD calculations. The BPG therefore address mesh design; construction of numerical boundary conditions where problem data is uncertain; mesh and model sensitivity checks; distinction between numerical and turbulence model inadequacy; preliminary information regarding the limitations of turbulence models etc. The aim is to encourage a common best practice by virtue of which separate analyses of the same problem, using the same model physics, should produce consistent results. Input and advice was sought from a wide cross-section of CFD specialists, eminent academics, end-users and, (particularly important) the leading commercial code vendors established in Europe. Thus, the final document can be considered to represent the consensus view of the European CFD community.

Inevitably, the Guidelines cannot cover every aspect of CFD in detail. They are intended to offer roughly those 20% of the most important general rules of advice that cover roughly 80% of the problems likely to be encountered. As such, they constitute essential information for the novice user and provide a basis for quality management and regulation of safety submissions which rely on CFD. Experience has also shown that they can often provide useful advice for the more experienced user. The technical content is limited to single-phase, compressible and incompressible, steady and unsteady, turbulent and laminar flow with and without heat transfer. Versions which are customised to other aspects of CFD (the remaining 20% of problems) are planned for the future.

The seven principle chapters of the document address numerical, convergence and round-off errors; turbulence modelling; application uncertainties; user errors; code errors; validation and sensitivity tests for CFD models and finally examples of the BPG applied in practice. In the first six of these, each of the different sources of error and uncertainty are examined and discussed, including references to important books, articles and reviews. Following the discussion sections, short simple bullet-point statements of advice are listed which provide clear guidance and are easily understandable without elaborate mathematics. As an illustrative example, an extract dealing with the use of turbulent wall functions is given below:

- Check that the correct form of the wall function is being used to take into account the wall roughness. An equivalent roughness height and a modified multiplier in the law of the wall must be used.
- Check the upper limit on $y+$. In the case of moderate Reynolds number, where the boundary layer only extends to $y+$ of 300 to 500, there is no chance of accurately resolving the boundary layer if the first integration point is placed at a location with the value of $y+$ of 100.
- Check the lower limit of $y+$. In the commonly used applications of wall functions, the meshing should be arranged so that the values of $y+$ at all the wall-adjacent integration points is only slightly above the recommended lower limit given by the code developers, typically between 20 and 30 (the form usually assumed for the wall functions is not valid much below these values). This procedure offers the best chances to resolve the turbulent portion of the boundary layer. It should be noted that this criterion is impossible to satisfy close to separation or reattachment zones unless $y+$ is based upon y^*.
- Exercise care when calculating the flow using different schemes or different codes with wall functions on the same mesh. Cell centred schemes have their integration points at different locations in a mesh cell than cell vertex schemes. Thus the $y+$ value associated with a wall-adjacent cell differs according to which scheme is being used on the mesh.
- Check the resolution of the boundary layer. If boundary layer effects are important, it is recommended that the resolution of the boundary layer is checked after the computation. This can be achieved by a plot of the ratio between the turbulent to the molecular viscosity, which is high inside the boundary layer. Adequate boundary layer resolution requires at least 8-10 points in the layer.

All such statements of advice are gathered together at the end of the document to provide a 'Best Practice Checklist'. The examples chapter provides detailed expositions of eight test cases each one calculated by a code vendor (viz FLUENT, AEA Technology, Computational Dynamics, NUMECA) or code developer (viz Electricité de France, CEA, British Energy) and each of which highlights one or more specific points of advice arising in the BPG. These test cases range from natural convection in a cavity through to flow in a low speed centrifugal compressor and in an internal combustion engine valve.

Copies of the Best Practice Guidelines can be acquired from:

ERCOFTAC ADO
Chaussée de la Hulpe 189 Terhulpsesteenweg
B-1170 Brussels
Belgium

Tel: +32 2 643 3572
Fax: +32 2 647 9398
Email: anne.laurent@ercoftac.be

The price per copy (not including postage) is:

ERCOFTAC members	
First copy	*Free*
Subsequent copies	45 Euros
Students	30 Euros
Non-ERCOFTAC academics	75 Euros
Non-ERCOFTAC industrial	150 Euros

Special Issue on : Fluid Structure Interaction

Elisabeth Longatte[1], Marianna Braza[2]

Coordinators of SIG 41: Fluid Structure Interaction

[1] LaMSID, UMR CNRS-EDF-CEA 2832, Clamart, France

[2] IMFT, UMR 5502 CNRS-INPT-UPS, Toulouse, France

The goal of this Special Issue proposed by the ERCOFTAC Special Interest Group 41 on Fluid Structure Interaction is to gather state-of-the-art research devoted to interfacial modeling and numerical simulation in the field of fluid and solid mechanics coupling. A large panel of topics is addressed including the following numerical and physical aspects: direct and iterative solvers for non-linear fluid solid coupled system computation, interfacial non-matching formulation and discretization, field transfer and interpolation, model reduction, free-surface modeling, hybrid eulerian lagrangian formulations on moving and non-moving grids, interface tracking, stability limit numerical prediction, vortex-induced vibration, turbulence modelling in respect of non-equilibrium effects in interaction with moving solid frontiers.

As far as flow-induced vibrations are concerned, challenge to real scale remains a priority in order to enable industrial investigation of multi-physics multi-scale large size problems. A large variety of configurations is concerned by this issue in several domains like nuclear safety, aeronautics, civil engineering, mechanical structure design, hydrodynamics, naval engineering, biomechanics. The challenge lies in predicting local effects impacting global systems. Therefore the combination of strategies convenient simultaneously for multi-physics, multi-scale and large size system computation is required. Heuristic models based on empirical concepts are often used for design. Based on theoretical and experimental analysis, physics modeling is more and more improved to better capture the fluid-structure interaction in the numerical approaches, enabling local phenomenon reliable prediction with higher accuracy. However fully-coupled non linear fluid solid system computation remains expensive due to the multi-physics patterns and to the large number of degrees of freedom to be involved. In this context, when experimentation is not reachable and numerical simulation is unavoidable but prohibitive, hybrid strategies are involved to take advantage from both numerical local and empiric global solutions.

For these reasons, it is interesting to gather in the present issue several articles dealing with connected issues by using different numerical strategies and showing the numerous possible combination of computational methods. Hybridation of models, optimization of methods as well as High Performance Computing environment are required in order to build the new generation of solvers enabling real size problem computation. This set of publications on advanced numerical methods in the field of fluid structure interaction is a real opportunity for new exchanges in our scientific community and for improvement of understanding, prediction and control of flow-induced vibrations in academic and industrial situations.

Information on the activity of SIG41 and next scheduled workshops can be found in the ERCOFTAC's website.

Immersed Stress Method for solving Fluid-Structure Interaction

E. Hachem[1], S. Feghali[1], T. Coupez[1]

[1] Ecole des Mines de Paris, Centre de Mise en Forme des Matériaux (CEMEF),

UMR CNRS 7635, Sophia-Antipolis, France

Elie.Hachem@mines-paristech.fr

Abstract

A new monolithic approach for solving elastic/rigid body immersed in an incompressible fluid is presented in this paper. The used monolithic formulation gives rise to an extra stress tensor in the Navier-Stokes equations coming from the presence of the structure in the fluid. With each immersed structure comes an appropriate law (rigid, elastic, viscoelastic). The proposed solver must be able then to welcome any behavior law and treat the full monolithic approach by a direct parallel finite element solver. The system is solved using a finite element variational multiscale (VMS) method, which consists in here of a decomposition for both the velocity and the pressure fields into coarse/resolved scales and fine/unresolved scales. The distinctive feature of the proposed approach resides in the efficient enrichment of the extra constraint. This choice of decomposition and spaces enrichment is shown to be favorable for simulating complex immersed structures at high Reynolds number. We assess the behaviour and accuracy of the proposed formulation in the simulation of 2D and 3D examples.

1 Introduction

Fluid Structure Interaction (FSI) is of great relevance in many fields of engineering as well as in the applied sciences and material forming with applications ranging from bioengineering to aerodynamics and from civil engineering to automotive. Often, when interaction effects are essential this comes along with large/small structural deformations and/or with turbulent flows. However, many available approaches may lack robustness especially in such severe situations. The components in all engineering fields are continuously pushed towards higher performance by seeking new developments that must be able to deal with different situations and regimes. In particularly it must be able to treat encountered problems ranging from the mesh adaptation issues to the coupling engines between different codes, and from small/large deformations to low/high Reynolds numbers flows.

Most of the commercial software packages solve FSI problems using an Arbitrary Lagrangian Eulerian (ALE) formulation [1, 2, 3]. The solid domain is treated with a Lagrangian formulation. The nodes belonging to the interface between the solid and the fluid are moved with the solid. The displacement of the nodes in the fluid domain do not depend on the fluid motion, but only ensures the continuity between the fluid and the solid domain, and a good mesh quality. ALE methods are robust and accurate, and do not need any extra degrees of freedom. However, important problems arise if the deformations, displacements and rotations of the solid becomes very important [4, 5, 6].

A higher popularity has been gained recently by partitioned approaches which allow the use specific solver for each domain. The difficulty remains in transfering the information between the codes. The coupling between the two phases can be enforced using different schemes: weakly or strongly coupled version. The former approach manages with just one solution of either field per time step but consequently lack accurate fulfilment of the coupling conditions. The latter requires sub-iterations. The predominant approach consists in solving the problem iteratively, using fixed-point schemes [7] or Newton Krylov methods [8, 9, 10, 11]. Actually, the fixed-point methods with dynamic relaxation seem to be the most interesting variant [12]. This approach allows the use of fluid and solid solvers for each of the two phases. It is accurate and quite efficient but present an inherent instability depending on the ratio of the densities and the geometry of the domain [13]. As a result, the numerical cost increase drastically and coupling algorithms may not converge. For 3D problems, such difficulties become even more severe.

Monolithic approaches have been proposed to overcome these drawbacks. The whole domain (composed by fluid and solid phases) is considered as a single one, meshed by a single grid, and solved with an Eulerian framework. The continuity at the interface is then obtained naturally and there is no need to enforce it, as it was the case in partitioned methods. If the multi-mesh approaches permit the use of classical fluid and solid solvers, monolithic approaches impose the use of an appropriated unique constitutive equation describing both the fluid and the solid domain. Interface tracking, between the two different domains, can be completed by Immersed Boundary (IB) methods [14] where the interface is convected on a Lagrangian way. Other methods such as the fictitious domain [14, 15] treat the coupling between the domains by applying a constraints across the rigid body using a Lagrange multiplier.

Here in this work, a new monolithic method is developped: the Immersed Stress Method. This method can be seen as an extension of the Immersed Volume Method (IVM) [16] to treat real fluid-structure interactions. The motivation of pursuing such general approach comes from the desire of not solving two equations, e.g. one in the solid and another in the fluid, where in some cases; one may still need to provide the boundary conditions between the two domains. Recall also that the

complexity to ensure such conditions is amplified when simulating turbulent fluid structure interactions. When dealing with a large diversity of shapes, dimensions and physical properties of structures, such simulations become rapidly very costly, time consuming and limited. A complete description and details about the immersed volume method but used for a different context (developed previously and applied to thermal couplings) is given in [17, 16].

Therefore, we retain the use of a monolithic formulation for fluid/solid and coupling it to some additional features for accurate resolution, in particular at the interface. The monolithic approach in here is made of a unique mesh in which the different domains are taking place by the level set function. Consequently, different strcutures are immersed in a larger domain of different material properties so that boundary conditions at the interface can be replaced naturally.

The second important ingredient of the approach is the use of anisotropic mesh adaptation [18, 19, 16] at the interface between two different materials. The idea is to apply a fast mesh generation algorithm that allows the creation of meshes with extremely anisotropic elements stretched along the interface, which is an important requirement for FSI problems having internal/boundary layers. It is successfully applied for fixed and some moving objects [17, 16].

The last and most important ingredient focuses more on the finite element solver: on modeling the interaction between the fluid (laminar or turbulent) and the structure in question (rigid, elastic, viscoelastic, etc). For FSI simulations of elastic/rigid body immersed for instance in an incompressible fluid, the global behavior is described by the classical Navier-Stokes equations, with an extra stress tensor. For instantce, we simulate a rigid solid using the Navier-Stokes solver under constrains to impose the nullity of the deformations. This can be done by simply penalizing the strain rate using a very important viscosity in the solid, which can sometimes be sufficient [20, 17]. It is also possible to enforce directly the nullity of the strain by using an Augmented Lagrange Mulptipliers method [21, 22, 23], solved by an iterative Uzawa algorithm. The problem is then solved by adding an extra-stress tensor comming from the presence of the structure in the fluid. Linear or harmonic mixture laws of the mechanical properties characterizing each domain are then applied at the interface.

2 Finite Element Formulation

2.1 Governing equations

The governing equations are considered to be three-dimensional and unsteady. Using a monolithic approach, a unique constitutive equation will be solved on the whole domain, with a variation of the parameters depending on the phase that should be modelled. Recall that the the concept of the Immersed Stress Method (ISM) is based on solving the single set of equations by differentiating the subdomains and refining the mesh at this interface using the level set method. The ISM allows the immersion of any strucutre using the level-set function, mixes the physical properties (ρ and η) and finally applies the anisotropic mesh adaptation at the vicinity of the interface.

The strong form for the whole domain reads then:

$$\begin{cases} \rho(\partial_t \mathbf{v} + \mathbf{v}\cdot\boldsymbol{\nabla}\mathbf{v}) - \boldsymbol{\nabla}\cdot(2\eta_f\boldsymbol{\varepsilon}(\mathbf{v}) + \boldsymbol{\tau_s} - p\ \mathbf{I_d}) = 0 \\ \boldsymbol{\nabla}\cdot\mathbf{v} = 0 \\ \boldsymbol{\varepsilon}(\mathbf{u}) - \dfrac{3}{2E}\boldsymbol{\tau_s} = 0 \\ \partial_t\mathbf{u} + \mathbf{v}\cdot\boldsymbol{\nabla}\mathbf{u} = \mathbf{v} \\ + \text{Boundary conditions} \end{cases} \tag{1}$$

where $\boldsymbol{\tau_s}$ is the extra stress tensor reflecting the presence of the immersed structure (elastic/rigid...) in the incompressible fluid and E is the Young modulus. Note that depending on the value of E, the treated structure will inherit the appropriate law (rigid, elastic, ...).

2.2 Stabilized finite element method

Based on a mesh $\mathcal{K}_h$ of Ω into set of N_{el} elements K, the functional spaces for the velocity, the pressure and the stress are approached by the finite dimensional spaces spanned by V_h, P_h and $\mathcal{T}_h$. The variational multiscale method is used to stabilize the Galerkin formulation and allows the use of equal order continuous interpolations for the velocity and the pressure unkowns (see [24] for details). A piecewise constant interpolation for stresses can be used. It consists in here of a decomposition for both the velocity and the pressure fields into coarse/resolved scales and fine/unresolved scales. The distinctive feature of the proposed approach resides in the efficient enrichment of the extra constraint. We first solve and then we substitute the fine-scale solution into the large-scale problem providing additional terms, tuned by a local time-dependent stabilizing parameter, that enhance the stability and accuracy of the standard Galerkin formulation for the transient Navier-Stokes equations. Such approach can deal with laminar/turbulent FSI problems and can handle large/small deformations. Additionally, when higher accuracy is needed, by applying a robust and fast mesh adaptation it provides a much more computational efficiency than coupling solvers.

The enrichment of the functional spaces for the velocity, pressure and stress solutions is performed as follows: $V_h \oplus V'$, $P_h \oplus P'$ and $\mathcal{T}_h \oplus \mathcal{T}'$. To this end, $\mathbf{v}, p, \boldsymbol{\tau}$ will be approximated as:

$$\mathbf{v} = \mathbf{v_h} + \mathbf{v'} \in \ \mathbf{V_h} \oplus \mathbf{V'}, \ \ \mathbf{p} = \mathbf{p_h} + \mathbf{p'} \in \ \mathbf{Q_h} \oplus \mathbf{Q'} \tag{2}$$

$$\boldsymbol{\tau} = \boldsymbol{\tau_h} + \boldsymbol{\tau'} \in \ \mathcal{T}_h \oplus \mathcal{T}' \tag{3}$$

3 Numerical simulations

We assess the behaviour and accuracy of the proposed formulation coupled to the levelset method in the simulation of 2D and 3D examples. Results show that the present implementation is able to exhibit good stability and accuracy properties using anisotropic mesh adaptation.

In Figure (1), four solids objects with different densities are falling due to gravity in an air-filled channel. The objective of this test, referred as the Tetris benchmark,

is to show the capability of the dynamic mesh adaptation as well as the method to handle high discontinuities of the solids and fluid physical properties. As shown in Figure (2), the convection dominated flows of the surrounding air, the four rigid solids movement as well as the representation of the objects are all well taken into account using one a single domain with one set of equations.

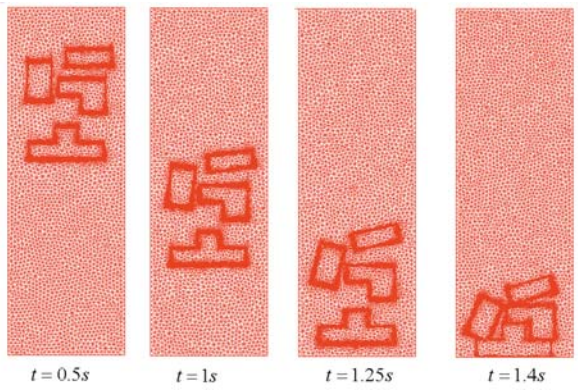

Figure 1: The Immersed Stress Method with dynamic anisotropic mesh adaptation

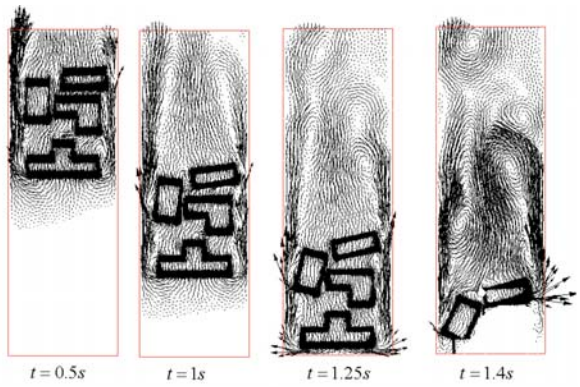

Figure 2: Immersion of four rigid bodies: velocity vectors at different time instants

Figure (3) presents the parallel numerical simulation of unsteady flow around 3D helicopter in forward flight using the proposed monolithic fluid-structure approach with fixed anisotropic mesh adaptation. The mesh generation algorithm allows the creation of meshes with extremely anisotropic elements stretched along the interface, which is an important requirement for FSI problems having internal/boundary layers. The final obtained mesh reflects the capability of the method to render a well respected geometry in terms of curvature, angles and complexity. Contrary to others techniques, this promising method can provide an alternative to body-fitted mesh for very complex geometry.

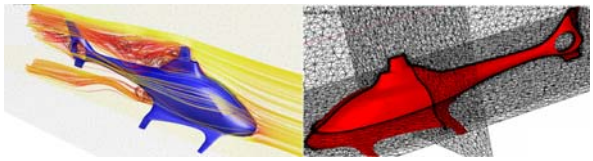

Figure 3: Numerical simulation of unsteady flow around helicopter in forward flight

References

[1] C. W. Hirt, A. A. Amsden, and J. L. Cook. An arbitrary lagrangian-eulerian computing method for all speeds. *Journal of Computational Physics*, 14(3):227–253, 1974.

[2] T. J. R. Hughes, W. K. Liu, and T. Zimmerman. Lagrangian-eulerian finite element formulation for incompressible viscous flow. *Computer Methods in Applied Mechanics and Engineering*, 29(3):329–349, 1981.

[3] J. Donea, S. Giuliani, and J. P. Halleux. An arbitrary lagrangian-eulerian finite element method for transient dynamic fluid-structure interactions. *Computer Methods in Applied Mechanics and Engineering*, 33(1-3):689–723, 1982.

[4] D. Benson. An efficient, accurate, simple ale method for nonlinear finite element programs. *Computer Methods in Applied Mechanics and Engineering*, 72(3):305–350, 1989.

[5] M. Souli, A. Ouahsine, and L. Lewin. Ale formulation for fluid structure interaction problems. *Computer Methods in Applied Mechanics and Engineering*, 190(5-7):659–675, 2000.

[6] R. van Loon, P. D. Anderson, F. N. van de Vosse, and S. J. Sherwin. Comparison of various fluid-structure interaction methods for deformable bodies. *Computers and Structures*, 85(11-14):833–843, 2007.

[7] P. Le Tallec and J. Mouro. Fluid structure interaction with large structural displacements. *Computer Methods in Applied Mechanics and Engineering*, 190(24-25):3039–3067, 2001.

[8] M. A. Fernández and M. Moubachir. A newton method using exact jacobians for solving fluid-structure coupling. *Computers and Structure*, 83(2-3):127–142, 2005.

[9] J-F. Gerbeau and M. Vidrascu. A quasi-newton algorithm based on a reduced model for fluid structure interaction problems in blood flow. *Mathematical Modelling and Numerical Analysis*, 37(4):631–647, 2003.

[10] C. Michler, E.H. E.H. van Brummelen, and R. de Borst. An interface newtonŰkrylov solver for fluidŰstructure interaction. *International Journal for Numerical Methods in Fluids*, 47(10-11):1189Ű–1195, 2005.

[11] J-F. Gerbeau, M. Vidrascu, and P. Frey. Fluid structure interaction in blood flows on geometries coming from medical imaging. *Computers and Structure*, 83(2-3):155–165, 2005.

[12] U. Küttler and A. W. Wall. Fixed-point fluidŰstructure interaction solvers with dynamic relaxation. *Computational Mechanics*, 43(1):61–72, 2008.

[13] P. Caussin, J.-F. Gerbeau, and Nobile F. Added-mass effect in the design of partitioned algorithms for fluid-structure problems. *Computer Methods in Applied Mechanics and Engineering*, 194(42-44):4506–4527, 2005.

[14] C. S. Peskin. The immersed boundary method. *Acta Numerica*, 11:479–517, 2002.

[15] R. Glowinski, T. W. Pan, T.-I. Helsa, and D. D. Joseph. A distributed lagrange multiplier/fictious domain methods for particulate flows. *International Journal of Multiphase flow*, 25(5):755–794, 1999.

[16] E. Hachem, T. Kloczko, H. Digonnet, and T. Coupez. Stabilized finite element solution to handle complex heat and fluid flows in industrial furnace using the immersed volume method. *International Journal for Numerical Methods in Fluids*, pages online, http://dx.doi.org/10.1002/fld.2498, 2010.

[17] Elie Hachem. *Stabilized Finite Element Method for Heat Transfer and Turbulent Flows inside Industrial Furnaces*. PhD thesis, Ecole Nationale Supérieure des Mines de Paris, 2009.

[18] Thierry Coupez. Génération de maillage et adaptation de maillage par optimisation locale. *Revue européenne des éléments finis*, 9:403–423, 2000.

[19] Cyril Gruau and Thierry Coupez. 3D tetrahedral, unstructured and anisotropic mesh generation with adaptation to natural and multidomain metric. *Computer Methods in Applied Mechanics and Engineering*, 194(18-49):4951–4976, 2005.

[20] J. B. Ritz and J. P. Caltagirone. A numerical continuous model for the hydrodynamics of fluid particle systems. *International Journal for Numerical Methods in Fluids*, 30(8):1067–1090, 1999.

[21] R. Glowinski, T.W. Pan, T. I. Helsa, D. D. Joseph, and J. Periaux. A fictitious domain approach to the direct numerical simulation of incompressible viscous flow past moving rigid bodies: application to particulate flow. *Journal of Computational Physics*, 169(2):363–426, 2001.

[22] M. Coquerelle and G.-H. Cottet. A vortex level set method for the two-way coupling of an incompressible fluid with colliding rigid bodies. *Journal of Computational Physics*, 227(21):9121–9137, 2008.

[23] J. Janela, A. Lefebvre, and B. Maury. A penalty method for the simulation of fluid-rigid body interaction. *ESAIM Proceedings*, 14:115–123, 2005.

[24] E. Hachem, Rivaux B., T. Kloczko, H. Digonnet, and T. Coupez. Stabilized finite element method for incompressible flows with high reynolds number. *Journal of Computational Physics*, 229(23):8643–8665, 2010.

A GENERAL PARTITIONED FLUID STRUCTURE INTERACTION MODEL FOR NON-MATCHING UNSTRUCTURED MESH

K. Suresh[1], A. Kumar K. R[1], A. Tripathi[2]

[1] Fluidyn Software and Consultancy (P) Ltd, Bangalore, India

[2] Fluidyn France, Saint-Denis, France

amita.tripathi@fluidyn.com

1 Introduction

Fluid-structure interaction studies are now increasingly being used in many areas. Examples include response of aircraft structures to wind loads, failure analysis of walls of process equipments subjected to transient flow fields, interaction of flow and heat transfer through porous heat exchangers and filters, interaction of electric fields and multi-phase flow fields in electrolysis, coupling of magnetic fields and flow of conducting fluids through cooling channels. Many situations of fluid-structure interaction involve process with a wide range of length and time scales. Hence it is very useful to have a solution method, which is flexible enough to allow the treatment of individual processes according to their characteristic length and time scales and at the same time is accurate and sufficiently coupled. In general two approaches are used in fluidstructure interaction modeling: (a) monolithic and (b) partitioned. A review and comparison of different fluid-structure interaction methods are given by Loon et al. [1]. Also, even though the fluid-structure interaction takes at a surface modeling of some flow and heat transfer processes requires interaction between co-existent volumes. One example is the heat transfer between a fluid and a deforming porous media. In this paper we describe a general three dimensional flexible partitioned fluidstructure interaction solver, Fluidyn-MP, developed to study interaction of flow, stress, temperature, electric and magnetic fields. Section 2 describes different aspects of the model and Section 3 describes two case studies to illustrate the use of this model.

2 Fluid Structure Interaction Model

The computational model includes the equations for multiple fluid flows through porous media, heat and electric conduction and displacements in porous and solid structures, and the additional conditions at the solid-fluid interfaces.

2.1 Fluid Flow Solvers

Fluid flow solvers solve three dimensional unsteady or steady Navier-Stokes equations along with conservation equations for electric, magnetic and any additional user specified scalar fields and specific models for porous media, gaseous and surface reactions and two phase flows. They are based on finite volume methods and are implemented for both the unstructured and multi-block structured mesh. The equations are solved in both steady and transient mode, with the latter using both explicit and implicit methods. All the variables are computed at the element centers and are interpolated on to the nodes to exchange them with the structural solvers. The convective flux calculations are modified to include the mesh movement due to the domain deformation resulting from structural displacement.

2.2 Structural Solvers

The stress and thermal analysis solver for the structural analysis is a finite element code for non-linear transient analysis of structures. The element library includes 2-noded 3D-beam element, 3-noded shell element and 4-noded tetrahedral element and 8-noded hexahedral element. Both geometric and material non-linearity may be handled. Material non-linearity includes elastic-perfectly plastic, elastic-linearly plastic and piecewise linear stress-strain relationship. For thermal analysis the material properties may be constant or temperature dependent (specified as a polynomial function of time).

The stress analysis solver uses convective coordinate approach. The use of convective coordinate approach and incremental strains enables handling problems involving large displacements. The boundary conditions include specified nodal forces, nodal displacements, pressures, body forces and nodal temperatures. The external loading may be constant or time dependent (specified as a piecewise linear function of time).

Temperature distribution in the solid is obtained by solving the steady or unsteady heat conduction equation using finite element method. The thermal boundary conditions include specified boundary temperature, boundary heat flux, element/nodal heat generation, convective and radiation boundary conditions. If there is a specified convective surface present as a fluid boundary to the solid then the convective flux that enters the solid from the fluid according to Newton's law of cooling is calculated using the local heat transfer coefficient and the fluid temperature. Electric and magnetic fields in the structure are also calculated in similar way.

2.3 Fluid-Structure Coupling

In FSI applications, pressure load at fluid boundary faces at F-S interface is transferred to the corresponding struc-

tural boundary faces. The pressure load is converted to nodal forces at structural nodes. The nodal displacements calculated from these external nodal forces are transferred back to the fluid nodes. In CHT applications, the heat flux (in the form of the film coefficient and temperature) at fluid boundary faces is transferred to the corresponding structural faces. The face-centred flux value is transferred to structural nodes for thermal calculation. In the thermal solver, the facecentred flux value is used to compute the nodal heat values for thermal conduction calculation. The resulting nodal temperatures are passed back to the fluid nodes as boundary temperatures.

The above coupling scheme is exact in case of matching mesh (node-node and face-face matching). In this case Fluidyn-MP generates F-S interface data (node-node correspondence and face-face intersection data) using polygon intersection algorithms for tracking fraction of structural face area covered by a fluid face. This process involves specifying required nodal, angular (for non-planar interface) and length tolerances. Complex F-S interface could pose problems by requiring different tolerances to be used in different parts of the mesh for extracting F-S interface data. Also in case of non-matching (dissimilar) mesh at the F-S interface, the load and displacement transfers are not only not straight forward but involve interpolation that may be awkward for some F-S geometries. The problem is compounded in case of non-matching mesh at non-planar F-S interface, due to the presence of gaps and/or overlap in the two meshes.

To facilitate the use of non-matching F-S interfaces, another coupling method is used [2, 3]. The evaluation of loads on the structure induced by the fluid and the displacement of the fluid mesh induced by the structural motion must satisfy the requirement of conservation of work and accuracy. The principle of virtual work is used to ensure conservation of energy. This coupling scheme involves converting facebased values on the fluid boundary face to values on the fluid nodes and using an interpolation matrix to transform fluid nodal values to structural nodal values. Considering a general non-matching interface, this matrix is a non-square matrix. The displacement of CFD grid x_f is expressed in terms of the structural displacements x_s using the transformation matrix [G] as:

$$x_f = [G]x_s$$

The requirement of conservation leads to a corresponding matrix for the transformation of forces:

$$f_s^T dx_s = f_f^T \quad dx_f = f_f^T [G] dx_s$$

$$f_s = [G]^T f_f$$

The coupling for conjugate heat transfer between solid and fluid is done through an exchange of boundary conditions at the F-S interfaces of interest. Like in the case of pressure, the flux and temperature exchange across possibly non-matching F-S interface is done using a suitable transformation matrix. Conservation of heat flux condition ensures accurate exchange of heat flux across the boundary.

2.4 Remeshing

In the case of Fluid-Structure interaction, the structure undergoes deformation due to pressure or heat transfer from the fluid. Consequently, the fluid boundary at the Fluid-Structure interface is displaced. So suitable conditions must be prescribed along the fluid-solid interface expressing that relative sliding of the fluid and the solid is permitted. The conditions that must be prescribed at each point of the interface are: (1) the grid velocity of the fluid coincides with the velocity of the solid, (2) the normal velocity of the fluid coincides with the normal velocity of the solid and (3) the tangential velocity of the fluid is unconstrained. The objective of autoadaptive remeshing is to modify the fluid mesh so as to reduce the distortion and improve the mesh size and aspect ratio of the mesh, which has a direct bearing on the time step. The fluid mesh could become highly distorted if only the fluid boundary is changed. The mesh size at the F-S interface also could become so small as to hinder the progress of solution. Hence the fluid mesh is adapted by moving the nodes of the fluid mesh.

Fluid nodes may be classified as: (1) interior nodes (interior to fluid domain), (2) boundary nodes at the F-S interface, and (3) boundary nodes not at the F-S interface. During remeshing the interior nodes may be moved anywhere within the fluid domain, the boundary nodes at the F-S interface follow the corresponding structural nodes, and the boundary nodes, which are not at the F-S interface, may be modified, subject to the condition that the fluid domain boundary may not change.

3 Case Studies

3.1 Fluid-Structure Interaction: Deformation of Structure

The implemented method has been used to study the fluttering of a wing with symmetrical profile [4]. This is a problem where the flow and structure interacted at a surface. The results obtained by the direct time-domain simulations were in good agreement with the experimental data, in terms of dimensionless flutter velocity and frequency ratio. The section below demonstrates the use of the same model to calculate the deformation of a porous structure due to the flow through and around it.

The physical problem involves a liquid flow around and through a hollow tubular filter causing flow induced vibration (Figure (1)). The filter was modeled both as a solid and a fluid to perform the stress analysis and to study fluid flow through it, simultaneously. Fluid mesh has 134184 elements and 150066 nodes. Structure mesh has 2560 elements and 5186 nodes. All are hexahedral elements. Flow is considered to be incompressible and viscous. Velocity is specified at the inlet and pressure at the outlet. Uniform volume flow rate is specified at the top of the filter to account for the fixed flow rate from that boundary. The filter structure has a volume porosity of 0.84. The nodes of the structure at the top of the filter are completely constrained. All other structural nodes are unconstrained. Initially the pressure and velocity in the whole domain is set to zero, and obtained a steady state solution. Then a small asymmetry is introduced in the flow field to initiate/capture vortices by initializing pressure and velocity in a small region around the filter to zero. The rest of the domain is reinitialized with the steady state results and a transient analysis was performed.

Figure (2) shows the velocity vectors, which indicates the different recirculation zones and the instantaneous flow asymmetry behind the structure due to vortex shedding. Figure (3) shows the instantaneous displacement of and effective stress in the structure due to the pressure dif-

ferential. In this case the transient pressure loading at the external surface of the structure, due to the vortex shedding, and that inside the porous structure due to the flow through the filter are considered. The latter is done using the three dimensional extension of the F-S interface coupling model.

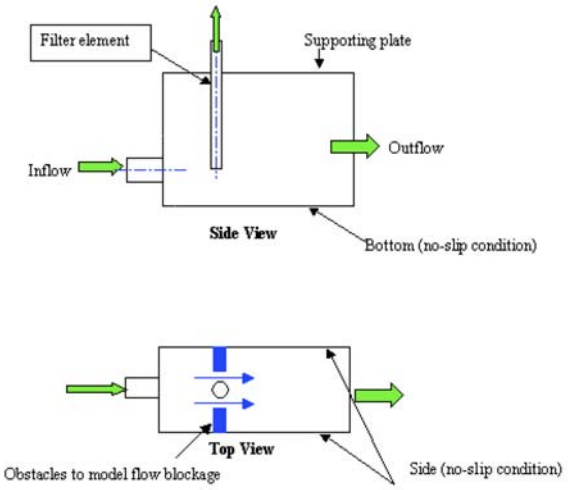

(a) Schematic for the flow through and around a porous structure

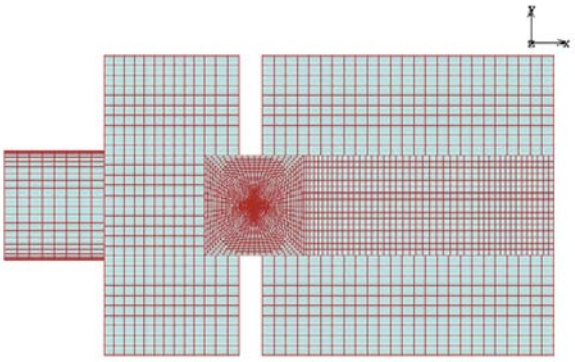

(b) Mesh

Figure 1:

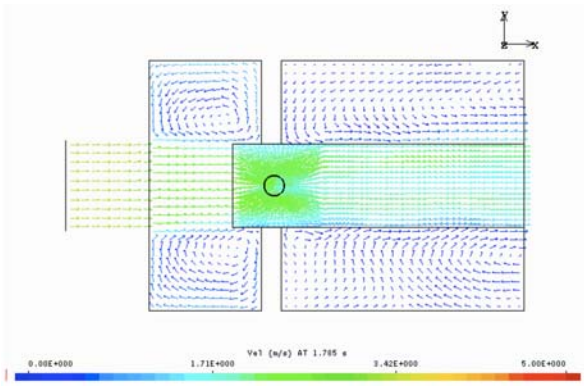

Figure 2: Velocity vectors at an instant

3.2 Fluid-Structure Interaction: Flow and Heat Transfer in Porous Media

The objective of this study is to validate the volume based F-S interaction for conjugate heat transfer with local thermal nonequilibrium model implemented

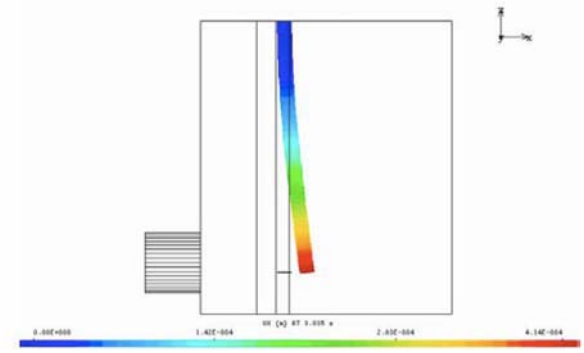

(a) Displacement of structure in the x-direction

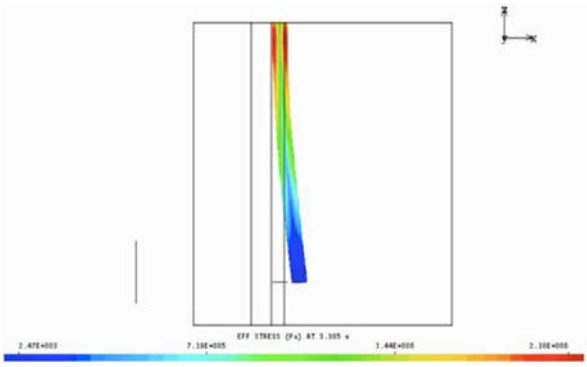

(b) Effective stress in the structure

Figure 3:

in Fluidyn- MP with experimental data of Calmidi and Mahajan [5].

The heat transfer between the porous solid and the fluid flowing through it is modeled using Local Thermal Non-Equilibrium (LTNE) model [5]. In this model, the energy equations are solved separately for the solid and the fluid, and are coupled through the local heat transfer between the solid and the fluid. This model is found to be more appropriate, than the dispersion model (where an effective conductivity is used) when the conductivities of the solid and fluid are highly different or in the presence of large heat generation in the domain.

Figure (4) shows the problem domain. It consists of airflow through aluminium metal foam. In the experiment the foam is heated from one end and the temperature variation at the top surface of the sample along the length is noted with the help of thermocouples. The average Nusselt number is calculated using the average of the measured temperatures along the wall. The Nusselt numbers obtained from the computation, for different flow conditions are compared with the above values.

In this study, the steady volume-averaged momentum equation that governs fluid flow in porous media is considered. The source term accounts for the pressure drop due to viscous friction at the walls of the metal foam and pressure drop due to the form drag. The former is calculated using Darcy's law and the latter is calculated using Forchheimer model. Simulations are done for different inlet velocities. Figure (5) shows the experimental and computed Nusselt numbers for different inlet velocities. Comparison is very good at lower velocities. At higher Reynolds numbers (higher velocities) there is a difference of about 8%. This error can be attributed to due to the average boundary wall temperature specified at the heated wall instead of measured variable temperature. Figure (6) show the longitudinal variation of

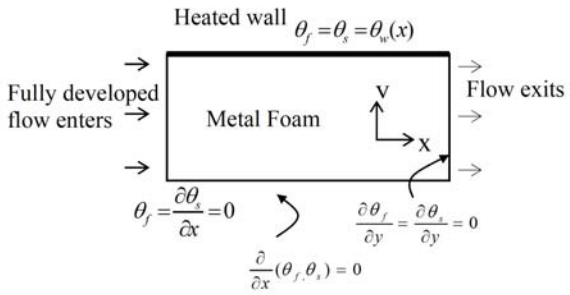

Figure 4: Schematic for flow and heat transfer through porous media

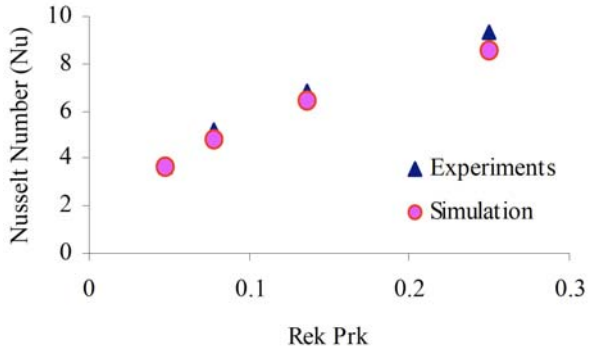

Figure 5: Variation of Nusselt number with product of Reynolds and Prandtl numbers (Re Pr)

temperature in the fluid and the solid, respectively. It is expected that near the inlet the fluid temperature would be much less than the solid temperature, which is correctly captured by the present model.

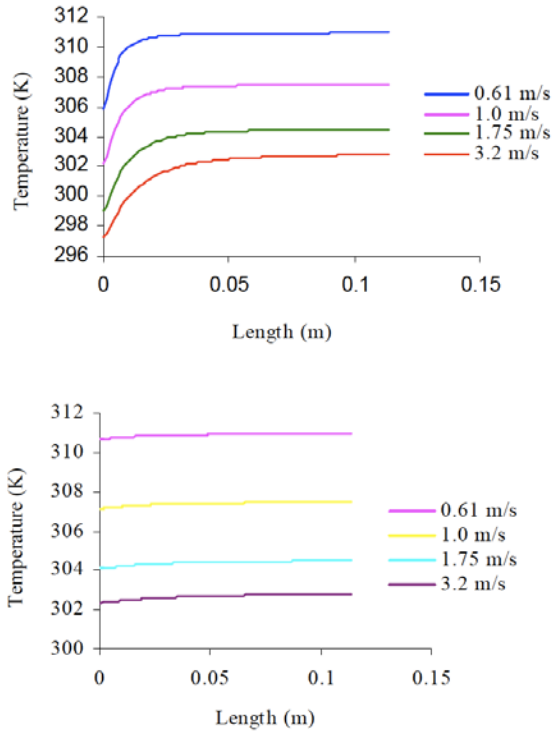

Figure 6: Longitudinal variation of temperature in the fluid (left) and solid (right)

References

[1] R. van Loon, P. D. Anderson, F. N. van de Vosse, and S.J. Sherwin. Comparison of various fluid-structure interaction methods for deformable bodies. *Computers and Structures*, 85:833–843, 2007.

[2] C. Farhat and P. Lesoinne, M. nd Le Tallec. Load and motion transfer algorithms for fluid/structure interaction problems with nonmatching discrete interfaces: momentum and energy conservation, optimal discretization and application to aeroelasticity. *Computer Methods in Applied Mechanics and Engineering*, 157:95–114, 1998.

[3] R.K. Jaiman, X. Jiao, P.H. Geubelle, and E. Loth. Conservative load transfer along curved fluid-solid interface with non-matching meshes. *Journal of Computational Physics*, 218:372–397, 2006.

[4] R. Kumar, P. Jain, S. Ramesh, and J. Humburger. Transonic flutter analysis using a coupled fluid- structure interaction method. In *Seventh Asian Computational Fluid Dynamics Conference*, Bangalore, India, 26-30 November 2007.

[5] V.V. Calmidi and R.L. Mahajan. Forced convection in high porosity metal foams. *Transactions of ASME*, 122:557–565, 2000.

Reduced order model in fluid structure interaction via POD-multiphase formulation

E. Liberge[1], A. Hamdouni[1], M. Pomarede[1,2]

[1] LEPTIAB, University of La Rochelle, Av. M. CREPEAU 17042 La Rochelle Cedex

[2] DCNS, Indret 44620 La Montagne

eliberge@univ-lr.fr

1 Introduction

The computational time is an important issue/task in field of computational mechanics, moreover important when coupled problems are considered. Indeed, for coupled problems, typically fluid structure interaction, a classical method used two solvers, one fluid and one structure, and the smaller time step is used, which increase the computational time. This aspect of the computational mechanic is an important limiting factor for few applications as active control,for which real time is needed or shape optimisation, for which running a computational model for each configuration is too expensive. The objective of the reduced order modelling is to reduced this computational time.

There is different issues to approach the reduced order modelling in fluid structure interaction. Vierendeels *et al.* [1] proposed to reduced the coupling iterations between the fluid and the solid solver. Another approach consists in reducing the computational time either for the fluid or the solid solver, or for both.

For this approach, the most efficient technique in fluid mechanics, the Proper Orthogonal Decomposition [2], has also been used for fluid structure interaction problems.

The difficulty of the POD application for FSI problems is the use of a spatial basis (no time dependent) on time dependant domains. It has been successfully applied for small displacements of the structure by Lieu *et al.* [3]. For bigger displacements Placzek *et al.* [4] proposed a formulation written on the reference datum linked to the solid. It has been successfully applied for the imposed oscillations of an NACA airfoil. Liberge and Hamdouni *et al.* [5] have proposed a multiphase formulation. This formulation is explained in the following sections.

2 The Proper orthogonal Decomposition

The Proper Orthogonal Decomposition (POD) leads to a spatial basis, built from a set af snapshot of the velocity field. This basis is optimal in the kinetic energy sense and has been intensively used as ROM tool in fluid mechanics. The POD has been introduced in this area by [2], in order to extract coherent structures in a turbulent fluid flow. A detailed methodology has already been proposed in the literature [2, 6, 7, 8, 5].

Consider a space $\Omega \subset \mathbb{R}^d$, $d = 1, 2$ or 3, $(O, \mathbf{x_1}, \mathbf{x_2}, \mathbf{x_3})$ a reference datum tied to this space, $\mathbf{T} \subset \mathbb{R}$ an interval, $x \in \Omega$, $t \in \mathbf{T}$. The POD consists in finding a spatial function Φ, in a Hilbert space $\mathcal{V}$, which gives the optimum representation of a field $v \in \mathbf{L^2}(\mathbf{\Gamma}, \mathcal{V})$. Considering M snapshots of the velocity field during a period $\mathbf{T}$, and Φ_i a vector of the POD basis of v, the snapshot POD [9] consists in solving the following eigenvalue problem :

$$\frac{1}{M}\sum_{k=1}^{M}\left(v\left(t_i\right), v\left(t_k\right)\right)A_k = \lambda A_i \quad \text{for} \quad i = 1 \ldots M, \qquad (1)$$

Where $(\bullet, \bullet)$ is the scalar product of $\mathcal{V} = \mathbf{L^2}(\Omega)$. Next, the POD basis (Φ_i) is obtained using the coefficients A_k^i and the snapshots v of the velocity field.

$$\Phi_i(x) = \sum_{k=1}^{M} A_k^i v(x, t_k), \quad \text{for } i = 1, \ldots, M. \qquad (2)$$

This basis is orthonormal and fullfills the free divergence [1] in case of an incompressible fluid, and the relative contribution of each mode i is captured by the eigenvalue λ_i. For a given n, the POD basis (optimal in $\mathbf{L^2}$) is the best decomposition which can be obtained in sense of the kinetic energy.

3 Multiphase ROM-POD formulation

Figure (1) shows a schematic description of the problem domain of interest. Let Ω_f be the fluid domain, Ω_s the solid domain, Γ_I the fluid-solid interface and $\mathbf{n}$ the outward normal of Ω_s. We note Ω the global domain $(\Omega = \Omega_f(t) \cup \Omega_s(t) \cup \Gamma_I(t))$.

A classical use of POD in fluid mechanics consists in building the POD basis from a set of snapshots obtained by a CFD calculation. Next, the Navier-Stokes equations are projected on the truncated POD basis, which leads to a low number of coupled ordinary differential equations. The main idea in fluid structure interaction is to reproduce this scheme. One way consists in reducing the most expensive problem, i.e the computation of the fluid. If an ALE formulation of the Navier-Stokes equations is used, the snaphsots of the velocity field are obtained on a time variant grid, which is not in adequation with the POD formula. Indeed, considering the formula [Eq. (1)], for two differents time steps, the fluid domain is not the same. Consequently, the scalar product of the velocity field at two different time steps doesn't make sense. For

1. In sense of distributions.

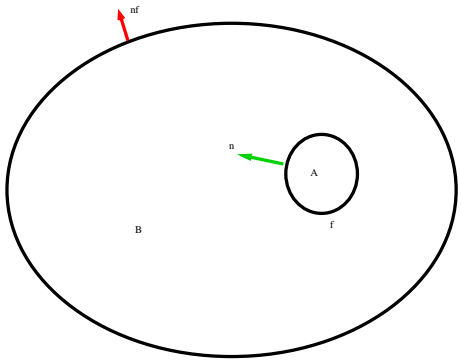

Figure 1: Schematic description of the problem domain

small displacements of the solid domain, the perturbations of the fluid domain are enough small to have any consequence of the computation of the POD basis. Thus, this POD formulation can be used, as shown in [3]. But, for bigger displacement of the solid domain another formulation has to be used.

Liberge and Hamdouni [5] proposed as solution a multiphase ROM approach for fluid structure interaction problems. This approach is similar to the methods which extend the Navier-Stokes equations to the solid domain (immerged boundaries method [10], fictitous method [11]). The snapshots result from a classical fluid structure interaction resolution in ALE, and each snapshot is interpolated from the time variant grid to a fixed one. Next, the POD basis is computed for the global velocity field (fluid and solid) defined on this fixed grid.

The difference with a classical approach is that it is not the fluid equations in ALE which are projected but the multiphase Navier-Stokes equations. The Navier-Stokes equations are extended to the solid domain, by adding a rigid constraint. This approach is explained in the following.

Let v_f be the fluid velocity field and v_s the solid. The global velocity field is :
$\forall x \in \Omega, \forall t \in \mathbf{T}$

$$v\left(x,t\right) = v_f\left(x,t\right)\mathbb{I}_{\Omega_f}\left(x,t\right) + v_s\left(x,t\right)\left(1-\mathbb{I}_{\Omega_f}\left(x,t\right)\right), \quad (3)$$

where $\mathbb{I}_{\Omega_f}$ is the characteristic function of the fluid domain :

$$\mathbb{I}_{\overline{\Omega}_f}\left(x,t\right) = \begin{cases} 1 & \text{if } x \in \overline{\Omega}_f\left(t\right) \\ 0 & \text{else if} \end{cases} \quad (4)$$

The solid constraint in modeled using the following equation :

$$\mathbf{D}\left(v\right) = \frac{1}{2}\left(\bigtriangledown v + \bigtriangledown^T v\right) = 0 \qquad \text{in } \Omega_s. \quad (5)$$

This constraint is penalised in the variational formulation by a viscosity μ_s, that a lagrange multiplier λ is associated with. Considering Γ_f^v the part of the bounadry of Ω where the velicity field is imposed, the following variational formulation associated to this problem is :

$$\begin{aligned}
\mathbf{H}_{v_\Gamma} &= \left\{v | v \in \mathbf{H}^1\left(\Omega\right),\ v = v_\Gamma\left(t\right) \ \text{ on } \Gamma_f^v\right\}, \\
\mathbf{H}^0_{v_\Gamma} &= \left\{v | v \in \mathbf{H}^1\left(\Omega\right), v = 0 \ \text{ on } \Gamma_f^v\right\}, \\
\mathbf{L}^2_0\left(\Omega\right) &= \left\{q \in \mathbf{L}^2\left(\Omega\right) | \int_\Omega q dx = 0\right\},
\end{aligned}$$

$\forall v^\star \in \mathbf{H}^0_{v_\Gamma}$ and $q \in \mathbf{L}^2\left(\Omega\right)$, find $v \in \mathbf{H}_{v_\Gamma}, p \in \mathbf{L}^2_0\left(\Omega\right), \lambda \in \mathbf{H}^1\left(\Omega\right)$ such as :

$$\begin{aligned}
&\int_\Omega \rho\left(\frac{\partial v}{\partial t} + v\cdot\nabla v\right)\cdot v^\star dx - \int_\Omega p\nabla\cdot v^\star dx \\
&+ \int_\Omega \left(1-\mathbb{I}_{\Omega_f}\right)\mathbf{D}\left(\lambda\right) : \mathbf{D}\left(v^\star\right) dx \\
&+ \int_\Omega 2\mu\mathbf{D}\left(v\right) : \mathbf{D}\left(v^\star\right) dx + \int_\Omega q\nabla\cdot v dx = 0,
\end{aligned} \quad (6)$$

ρ and μ are defined on the global domain Ω :

$$\rho = \mathbb{I}_{\Omega_f}\rho_f + \left(1-\mathbb{I}_{\Omega_f}\right)\rho_s \quad (7)$$

$$\mu = \mathbb{I}_{\Omega_f}\mu_f + \left(1-\mathbb{I}_{\Omega_f}\right)\mu_s, \quad (8)$$

Where ρ_f is the fluid density, μ_f the fluid viscosity and the solid viscosity μ_s is the penalisation factor of the rigidity constraint, ρ_s is the solid density and v_Γ is the velocity fluid on Γ_f^v.

Thus a weak formulation is obtained for the global domain Ω with information about fluid and solid domain that are contained in the density ρ and viscosity μ functions.

3.1 Low order dynamical system

3.1.1 First approach

The low order dynamical system has been obtained by choosing POD modes $\Phi_i, i = 1, \cdots, N$ for a virtual velocity field. N is searched as the truncated POD basis captures almost 99% of the total energy. The decomposition of the velocity field on the truncated POD basis is :

$$v = \sum_{i=1}^{N} a_i\left(t\right)\Phi_i\left(x\right),$$

This decomposition is introduced in Eq. (6) and, due to the free divergence of the POD basis, the following dynamical system is obtained :
$\forall t \in [0,T]$ for $n = 1 \ldots N$

$$\begin{cases}
\sum_{i=1}^{N} \frac{da_i}{dt} & A_{in} = \sum_{i=1}^{N}\sum_{j=1}^{N} a_i\left(t\right)a_j\left(t\right)B_{ijn} \\
& \quad + \sum_{i=1}^{N} a_i\left(t\right)C_{in} + E_n + D_n, \\
\frac{\partial \mathbb{I}_{\Omega_f}}{\partial t} & \quad + v\cdot\nabla\mathbb{I}_{\Omega_f} = 0,
\end{cases} \quad (9)$$

with

$$\begin{aligned}
A_{in} &= -\int_\Omega \rho\left(x,t\right)\Phi_i\left(x\right)\cdot\Phi_n\left(x\right)dx, \\
B_{ijn} &= -\int_\Omega \rho\left(x,t\right)\left(\Phi_j\cdot\nabla\Phi_i\right)\cdot\Phi_n\, dx, \\
C_{in} &= -2\int_\Omega \mu\left(x,t\right)\mathbf{tr}\left(\mathbf{D}\left(\Phi_i\right)\cdot\mathbf{D}\left(\Phi_n\right)\right)\, dx \\
E_n &= -\int_\Omega \left(1-\mathbb{I}_{\Omega_f}\right)\mathbf{tr}\left(\mathbf{D}\left(\lambda\right)\mathbf{D}\left(\Phi_n\right)\right)dx,
\end{aligned}$$

The last term D_n takes in account the nonhomogeneous boundary condition and is treated by a penalisation method [12]. There are some differences compared to the low order dynamical system obtained using POD basis in classic fluid mechanics [8, 13]. In fact coefficient $A, B, \cdots$

are time variant and must be computed at each time step. λ is computed using an Uzawa algorithm. The computational cost at each time step should be considered as a limitation of the method, but in fact for a small number of POD modes the computational expense is less as compared to that of a FSI problem solved with the ALE method. This method does not require a remeshing step and secondly, the initial problem is transformed into a low order set of ordinary differential equation.

3.1.2 Second approach

The computational time can also be reduced by the obtention of a system with non-time dependent coefficients. The decomposition of the characteristic function $\mathbb{I}_{\Omega_s}$ on a POD basis Φ^c, and the decomposition of the Lagrange multiplier on the same basis of the velocity field yields the following :

$$\begin{aligned} &a)\ \mathbb{I}_{\Omega_s}(x,t) = \sum_{i=1}^{N_c} b_i(t)\,\Phi_i^c(x), \\ &b)\ \lambda(x,t) = \sum_{i=1}^{N_l} c_i(t)\,\Phi_i(x), \end{aligned} \tag{10}$$

N_c and N_l denote the number of POD modes retained for the characteristic function and the Lagrange multiplier. N_l is chosed equal to N.

It leads to the following dynamical system :
$\forall\ i = 1, \cdots, N\ p = 1, \cdots, N_c$

$$\begin{aligned} &\rho_f \frac{da_n}{dt} + (\rho_s - \rho_f) \sum_{k=1}^{N}\sum_{p=1}^{N_c} \frac{da_k}{dt} b_p \mathcal{A}_{pkl} \\ &+\rho_f \sum_{k=1}^{N}\sum_{l=1}^{N} a_k a_l \mathcal{B}^1_{kln} + 2\mu_f \sum_{k=1}^{N} a_k \mathcal{C}^1_{kn} \\ &+ (\rho_s - \rho_f) \sum_{k=1}^{N}\sum_{l=1}^{N}\sum_{p=1}^{N_c} a_k a_l b_p \mathcal{B}^2_{pkln} \\ &+2(\mu_s - \mu_f) \sum_{k=1}^{N}\sum_{p=1}^{N_c} a_k b_p \mathcal{C}^2_{kpn} \\ &= \sum_{h=1}^{N_l}\sum_{p=1}^{N_c} b_p c_h \mathcal{D}_{phn} + \mathcal{G}_n, \end{aligned} \tag{11}$$

$$\begin{aligned} &a)\ \frac{db_p}{dt} + \sum_{k=1}^{N}\sum_{l=1}^{N_c} a_k b_l \mathcal{E}_{klp} = 0, \\ &b)\ \sum_{p=1}^{N_c}\sum_{k=1}^{N} b_p a_k \mathcal{F}_{pkn} = 0, \end{aligned} \tag{12}$$

$$\begin{aligned} \mathcal{A}_{pkl} &= \int_\Omega \Phi_p^c \Phi_k \Phi_l dx \\ \mathcal{C}^2_{kpn} &= \int_\Omega \Phi_p^c \mathbf{Tr}\left(\mathbf{D}(\Phi_k)\,\mathbf{D}(\Phi_n)\right) dx, \\ \mathcal{B}^1_{kln} &= \int_\Omega (\Phi_k \nabla \Phi_l)\cdot \Phi_n dx \\ \mathcal{C}^1_{kn} &= \int_\Omega \mathbf{Tr}\left(\mathbf{D}(\Phi_k)\,\mathbf{D}(\Phi_n)\right) dx, \\ \mathcal{B}^2_{klpn} &= \int_\Omega \Phi_p^c\,(\Phi_k \nabla \Phi_l)\cdot \Phi_n dx \\ \mathcal{D}_{phn} &= \int_\Omega \Phi_p^c \mathbf{Tr}\left(\mathbf{D}(\Phi_h)\,\mathbf{D}(\Phi_n)\right) dx, \\ \mathcal{E}_{klp} &= \int_\Omega (\Phi_k \cdot \nabla \Phi_l^c)\,\Phi_p^c dx \\ \mathcal{F}_{pkn} &= \int_\Omega \Phi_p^c \mathbf{Tr}\left(\mathbf{D}(\Phi_k)\,\mathbf{D}(\Phi_n)\right) dx. \end{aligned} \tag{13}$$

The Eq. (12).a) is the reduction of the convection equation of the characteristic function and the Eq. (12).b) is the reduction of the rigid constraint Eq. (5) defined on the solid domain. Thus, an algebric differential equation system, whose coefficients can be computed once, is obtained.

In the present paper, two low order dynamical systems, which transformed the initial problem into a more simple system of ordinary differential equation in $a_i(t)$ with low degrees of freedom have been presented. In practice, a basis using only a few POD modes takes more than 90% of the kinetic energy. The methods will be compared in the next section.

4 Application

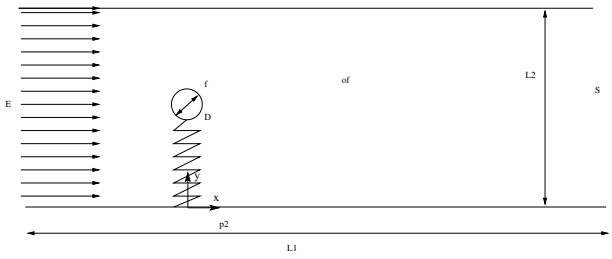

Figure 2: Schematic description

The method has been tested on the configuration described on Figure (2), a cylindrical rigid body, attached to a spring, has been immersed in a fluid flow at Reynolds number Re = 1690.

For the fluid parameters, we consider the fluid density $\rho_f = 1000$ kg.m^{-3}, the viscosity $\mu_f = 0.001$ kg/m.s, the inlet velocity $v_\Gamma = 3.38 \cdot 10^{-2}$m.s^{-1}. The solid parameters are the radius $R = 0.025$ m, the mass equal to m$_s = 11.78\ 10^{-1}$ kg, which implies a solid density equal to $\rho_s = 60$ kg.m^{-3}. The stiffness of the spring was chosen $k = 0.559$ N $\cdot$ m^{-1} and the damping to 2.7825 kg $\cdot$ s^{-1}.

The low order dynamical systems is built with 6 POD modes. Table (1) compares the computational time using the STARCD software and the multiphase ROM, the first approach (F.A) and the second (S.A).

The gain in term of CPU times obtained by the multiphase-ROM is significant.

Figure (3) compares temporal coefficients obtained by the low-order dynamical system (Eq. (11)) and POD direct. The temporal coefficient a'_2 is plotted versus a'_1.

Table 1: Comparison of CPU times

	STARCD ALE	F. A.	S. A.
CPU time	726	143	21

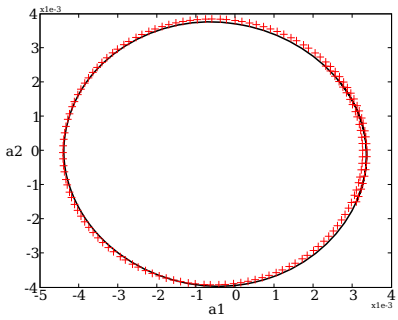

Figure 3: Limit cycle a_2' versus a_1' : −, POD direct solution; +, obtained by ROM with 6 POD modes

If the low-order dynamical system is run for time period longer than the snapshot period, an outline circle is observed. This circle can be used to study the stability of the solution. The plot of a_2 versus a_1 has to approach the outline of this circle as much as possible.

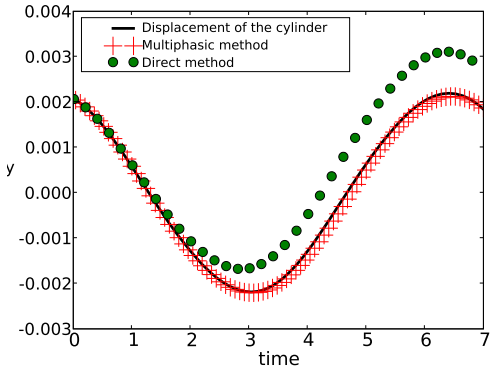

Figure 4: Position of gravity centre : −, initial solution; +, obtained by our ROM method with 6 modes; •, obtained by the direct method with 6 modes

Figure (4) plots the position of the gravity center according to axis $\mathbf{x_2}$ (the displacement has been blocked along $\mathbf{x_1}$). The result has also been compared with a classical POD approach, which consists in projecting the Navier-Stokes equations without taking account that the fluid domain is moving. The same number of POD modes has been considered for both, the direct method and the method proposed in this article. The result obtained by low order dynamical system agrees with the results of the reference case. Moreover, the ROM give good description of the solid displacement for a period longer than the snapshot period (the blue curves on the Figure (5)).

The velocity field is also well rebuild as shown on the figure Figure (6)

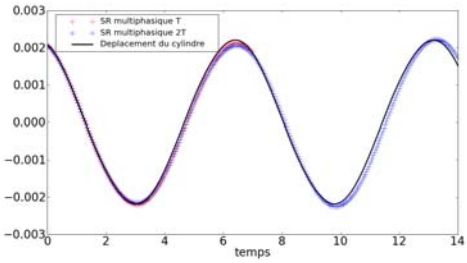

Figure 5: Position of gravity centre : −, initial solution; +, obtained by our ROM method with 6 modes; •, obtained by the ROM for a longer period

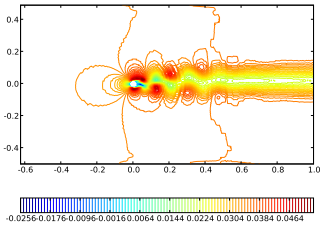

(a) $v\,(150,1)$

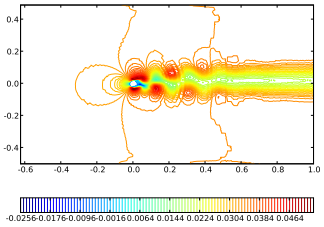

(b) $\tilde{v}\,(150,1)$

Figure 6: First component of the velocity field. UP : snapshot velocity field; DOWN : obtained by low-order dynamical system

5 Conclusion

The Reduced Order Modelling in fluid structure interaction is a research field in important development. The most efficient approach today are using the POD, with few variants according the problem studied. For important displacements of the solid domain, the multiphase-ROM approach proposed in this paper give an important gain of computational time, and a good prediction of the displacement of the solid. This method uses a multiphase formulation of the Navier-Stokes equations, extending the Navier-Stokes equations to the solid domain and adding a rigid constraint on the solid domain.

References

[1] J. Vierendeels, L. Lanoye, J. Degroote, and P. Verdonck. Implicit coupling of partitioned fluid-structure interaction problems with reduced order models. *Computers & Structures*, 85:970–976, 2007.

[2] J.L. Lumley. The structure of inhomogeneous turbulent flows. *Atmospheric Turbulence and Radio Wave Propagation*, vol. In A.M. Yaglom and Tararsky:166–178, 1967.

[3] T. Lieu, C. Farhat, and M. Lesoinne. Reduced-order fluid/structure modeling of a complete aircraft configuration. *Computer Methods in Applied Mechanics and Engineering*, 195(41-43):5730–5742, 2006.

[4] R. Ohayon A. Placzek, D.-M. Tran. "nonlinear pod-based reduced-order models for aeroelastic compressible flows". In *International Forum on Aeroelasticity and Structural Dynamics*, Seattle, 21-25 juin 2009.

[5] E. Liberge and A. Hamdouni. Reduced order modelling method via proper orthogonal decomposition (pod) for flow around an oscillating cylinder. *Journal of Fluids and Structures*, 26(2):292–311, 2010.

[6] P. J. Holmes, G. Berkooz, and J. L. Lumley. *Turbulence, Coherent Structures, Dynamical Systems and Symmetry*. Cambridge Monographs on Mechanics, 1998.

[7] G. Berkooz, P. Holmes, and J. Lumley. The proper orthogonal decomposition in the analysis of turbulent flows. *Annual review of fluid Mechanics*, 25:539–575, 1993.

[8] C. Allery, C. Beghein, and A. Hamdouni. Applying proper orthogonal decomposition to the computation of particle dispersion in a two-dimensional ventilated cavity. *Communications in nonlinear science and numerical simulation*, 10(8):907–920, December 2005.

[9] L. Sirovitch. Turbulence and the dynamics of coherent structures, part i : Coherent strucures, part ii : Symmetries and transformations, part iii : Dynamics and scaling. *Quarterly of Applied Mathematics*, 45(3):561–590, 1987.

[10] C. S. Peskin. *Flow patterns around heart valves: A digital computer method for solving the equation of motion*. PhD thesis, Albert Einstein College of Medicine, 1972.

[11] N.A. Patankar, P. Singh, D.D. Joseph, R. Glowinski, and T.-W. Pan. A new formulation of the distributed lagrange multiplier/fictitious domain method for particulate flows. *International Journal of Multiphase Flows*, 26:1509–1524, 2000.

[12] C. Allery. *Contribution à l'identification des bifurcations et à l' étude des écoulements fluides par des systémes d'ordre faible (POD)*. PhD thesis, Université de Poitiers, 2002.

[13] E. Liberge, M. Benaouicha, and A. Hamdouni. Low order dynamical system for fluid rigid body interaction problem using pod method. *Int. Jnl. of Multiphysics*, 2(1):59–81, 2008.

Fluid-Structure Interaction: A Brief Review of Existing Strategies

Mina Ya-alimadad[1], Keith Davey[1], Robert Prosser[1]

[1] School of Mechanical, Aerospace and Civil Engineering, the University of Manchester

mina.ya-alimadad@postgrad.manchester.ac.uk

Abstract

This article is provides a brief review of the major existing strategies in the simulation of fluid-structure interaction (FSI) and comments on their advancement towards the development of general approaches that are robust and accurate, even when large deformations exists.

1 FSI Challenges and Existing Strategies

The need for more accurate results in many engineering simulations has necessitated consideration of multiple, coupled physical processes. FSI is one of the most important categories of such analyses which in general are challenging in terms of both modelling and computational issues. Extensive research has been carried out in this field and satisfactory results are now being obtained in a number of areas of engineering interest. Many software packages now include modules that allow limited analysis of certain types of FSI problem. Nonetheless, much remains to be done to develop robust, accurate and less case-specific approaches for industrial applications [1].

When tackling FSI problems, one should consider five aspects: the fluid and the structure spatial models; the treatment of their interface, time stepping and supplementary algorithms [2]. The combination of the strategies implemented in tackling the problem must satisfy conditions such as energy conservation, time accuracy, stability, etc (see [2] for a more comprehensive list).

There are two computational coupling strategies; the monolithic and the partitioned approaches. The former is based on the fully-coupled discretization of the governing equations of the fluid and the solid which renders complete control over the implementation of the solvers. The approach lacks software modularity. It can also be very burdensome to set up, which leads to high computational costs. Most engineering applications exhibit complex behaviour in both the solid and fluid domains and thus the partitioned approach is used instead [3, 4]]. With this approach, separate solvers are used for the fluid and the structure fields which exchange information and exert their respective influence via their boundary conditions. Hence there is an opportunity to select optimal solvers for each field [5, 6]. The partitioned strategy has proved to be the most convenient and flexible approach [4]. The challenge then lies in the exchange of information between the two solvers at the interface; this is accompanied by concerns about stability, accuracy and the convergence of staggered time stepping schemes [6].

Undoubtedly FV and FE are the most commonly used methods for tackling CFD and CSM calculations [7]. In the FSI field, many strategies have been deployed in transferring data between solid elements and fluid cells. Having reviewed these methods, it is obvious that they all have their strong and weak points depending on the applications. However it is apparent that significant work is being done in tackling the challenges that arise from the exchange of data between two different methods. An FSI algorithm is needed to ensure appropriate coupling between the interfaces [8, 9].

One key issue is that of the deformation of the fluid mesh as it follows the structural mesh displacements. This movement contradicts the Eulerian description of the fluid. There are two classes of principle approach in dealing with this aspect [10]: those that let the fluid mesh move (mesh moving strategies) and those that are based on the Eulerian description of the fluid mesh (fixed grid strategies). A mixture of the two can also be used.

The most commonly used approach of the first category is the Arbitrary-Lagrangian-Eulerian (ALE) approach [1, 11] in which the fluid control volume can track the structural deformations at the interface. This method permits differing fluid and structure mesh densities but coupling and matching at the common boundary of the fluid-structure (FS) interface is the main challenge [12]. However, even the best ALE methods are followed by an expensive and time consuming re-meshing/mesh update technique [1], when large deformations occur [10]. This is because the method requires some prior knowledge of the solution, which for large deformations, is not readily available [12].

In the fixed-grid approach, the solid mesh can move through the fluid mesh. Moreover, the FS interface divides the fluid domain into a physical and a fictitious field to be discretized and solved. The problem with such methods is that it is impossible to decouple fully the two fluid fields with respect to the kinematic and stress fields and thus additional time-consuming calculations are required for the fictitious field [10].

Two important examples of such methods are the Immersed Boundary (IB) method and the Distributed Lagrangian Multiplier/Fictitious Domain (DLM/FD) method (which are used for incompressible flows), the Lagrangian structure mesh moves on top of the fluid mesh and forces the fluid material inside the structure to deform with the structure [12]. In IB methods the fluid and structure interact through distributed nodal forces and by interpolating nodal velocities between the two domains, through a smoothed approximation of the Dirac delta function. The benefit of this method is that the FS interface is tracked automatically [13]. A drawback of DLM/FD methods is that the structural degrees

of freedom are not removed [1]. When used with volume occupying structures, both methods require the coupling to be carried out between the fictitious flow field and the structure field. This results in incompressible deformation of the structure and the production of artificial viscosity terms. This can create additional errors in complex physical problems [12].

Another fixed-grid approach is the XFEM method, which originated as a method to track discontinuities such as cracks, and is now being used in the FSI field [12, 13] with the aim of reducing some of the problems with the strategies mentioned above. This method enriches the approximation space to make it possible to capture weak and strong discontinuities [14]. One obvious characteristic of this method is that there is no influence of the fictitious fluid domains and thus computations can be performed much faster. Whilst this method is not dependent on the mesh resolution, one must choose the most appropriate Lagrangian multiplier method, which is an outstanding issue of research [12].

In general, a fixed grid approach that can be applied to general FSI problems involving incompressible flows requires: 1) the physical and fictitious flow region are physically decoupled to avoid energy transfer across the interface; 2) the coupling takes place along the interface; 3) the fluid and structure mesh sizes are independent and; 4) the fictitious domain can be switched off for increased efficiency [3, 12].

Overall the existing fixed grid methods do not satisfy one or more of the above criterions and several proposals exist in solving the shortcomings [1]. In comparison to fixed grid methods, correctly implemented ALE schemes may be used as a comparator in terms of accuracy, stability and generality [12] except for large deformations cases.

A second major issue in FSI problems is that of non-matching meshes at the FS interface. Non-matching meshes imply that the interface is based on nodally conforming meshes along the interface [8] and there maybe gaps and overlaps between the meshes [6]. This is because FV methods are less accurate and hence they require much finer meshes to represent the flow [5, 6]. Consequently an interpolation or projection method is required to transfer information between the fluid and the solid. Several strategies have been introduced to couple the non-matching meshes [5]. It is important that the method used ensures global conservations of energy and loads over the interface, as well as maintaining accuracy, and conservation of the order of the coupled solvers as well as their computational efficiency[5].

In general the interface methods can be segregated into three categories: 1) primal i.e. there are no additional interface variables (AIV); 2) dual: dual type AIVs are introduced and; 3) primal-dual: dual and primal type AIVs are introduced [2]. These three classes of methods can be used in both partitioned and monolithic approaches if suitable. The simplest method is a primal method known as nearest neighbour interpolation in which information obtained from the nearest neighbouring point in the other mesh. This method is accurate when the degree of misalignment of the meshes is low. A more accurate method is the projection method in which a point or an element is orthogonally projected to another to obtain data of that mesh [5]. Another primal method derives from spline based methods. A common dual type method is the Mortar scheme which is founded on the usage of Lagrangian multipliers [2, 8]. The application of Mortar methods in the FSI field is very recent [5]. A primitive method of the primal-dual category is the Localized Lagrangian Multiplier (LLM) scheme. In this method a kinematic frame is placed between the fluid and structure at their common interface. Multipliers are located at the interface between each domain and the kinematic frame.

As mentioned previously the selection of the correct algorithm can be a difficult task. A review of some of these methods is presented in [5], but it is clear that the current state of art is far from definitive.

In considering the existing strategies, it is apparent that while there is significant scope for developing less case-specific approaches than the traditional methods currently used in CFD and CSM, there is as yet no consensus that a single strategy could be developed to cover all the attributes mentioned in [2]. Thus it seems that the methods themselves could be the root of the problem.

One could look at the transport equations of a continuum and argue that the fluid and structure equations are essentially identical, and that their differences have risen from the way they have been developed to suit the physics of the system they represent. In fact FVM can be thought of as a special case of FEM with a Galerkin weighting [15]. Indeed many attempts have been made in using FVM and FEM in tackling structural and fluid problems, respectively [15]. Some of these have resulted in useful techniques such as the flow-condition-based interpolation (FCBI) finite element scheme [7] which enables the usage of coarse fluid meshes [15]. An important development is the usage of cell-vertex FVM in which the displacement and stress variables are stored at the vertices of the cells, thereby enabling the use of the method with distorted meshes [7]. Despite these developments, it is evident that research in this area is somewhat compartmentalised into extensions of either fluids or structures. This emphasises just how different the various methodologies are and why transferring data between them is somewhat problematic.

Meshless Methods (MMs), as exemplified by, say Smoothed Particle Hydrodynamics (SPH) were introduced with an aim to eliminate the problems of mesh-based methods originating from making approximations based on a mesh. Such problems include errors due to low quality or distorted meshes, the need for re-meshing and the inability to model discontinuities. An important benefit of MMs is that they are capable of treating problems both with moving discontinuities and large deformations easily and robustly [6]. The drawback of the MMs is that the shape functions require high-order integration to be correctly computed. Moreover, the treatment of essential boundary conditions can be complicated. As a consequence, in general, MMs are more expensive computationally than FEM [6].

2 Concluding Remarks

This paper is concerned with the coupling of fluid solid interaction. Despite the significant number of developments in this area, it is evident that current research is somewhat compartmentalised into extensions of either fluids-based or structures-based approaches. This emphasises just how different the various methodologies are and why transferring data between them is somewhat problematic. The following conclusions can be drawn from this brief discourse:

- Partitioned strategies are preferred over monolithic approaches because they are more flexible;

- The ALE method provides a good reference test against which other schemes can be contrasted;
- No single method presently provides the complete solution;
- A possible new direction is to re-examine the fundamentals to homogenise solid and fluid formulations for improved coupled analysis.

References

[1] Wolfgang Wall, Axel Gerstenberger, Peter Gamnitzer, Christiane Förster, and Ekkehard Ramm. Large deformation fluid-structure interaction advances in ale methods and new fixed grid approaches. In *Fluid-Structure Interaction*, Lecture Notes in Computational Science and Engineering, pages 195–232. Springer Berlin Heidelberg, 2006.

[2] CA Felippa, KC Park, and MR. Ross. A classification of interface treatments for fsi. In *Fluid Structure Interaction II*. Springer, 2010.

[3] F. Cirak and R. Radovitzky. A lagrangian-eulerian shell-fluid coupling algorithm based on level set. In *Computers and Structures*. Elsevier, 2005.

[4] T. Gallinger, A. Kupzok, U. Israel, K.-U. Bletzinger, and R. Wüchner. A computational environment for membrane-wind interaction. In *Kassel University Press*. Gmbh, 2009.

[5] A. de Boer, AH van Zuijlen, and H Bijl. Review of coupling methods for non-matching meshes. In *Computer Methods in Applied Mechanics and Engineering*. Elsevier, 2007.

[6] RK Jaiman, X Jiao, P. H. Geubelle, and E. Loth. Assessment of conservative load transfer for fluid-solid interface with non-matching meshes. In *International Journal for Numerical Methods in Engineering*. Wiley Online Library, 2005.

[7] Klaus-Jürgen Bathe and Hou Zhang. A flow-condition-based interpolation finite element procedure for incompressible fluid flows. *Computers and Structures*, 80:1267–1277, 2002.

[8] Hyun-Gyu Kim. A new coupling strategy for fluid-solid interaction problems by using the interface element method. *International Journal for Numerical Methods in Engineering*, 81:403–428, 2010.

[9] Folco Casadei and Serguei Potapov. Permanent fluid-structure interaction with non-conforming interfaces in fast transient dynamics. *Computer Methods in Applied Mechanics and Engineering*, 193:4157–4194, 2004.

[10] Klaus-Jürgen Bathe and Hou Zhang. A mesh adaptivity procedure for cfd and fluid-structure interactions. In *Computers and Structures*. Pergamon Press, Inc., 2009.

[11] W. A. Wall, A. Gerstenberger, U. Küttler, and U. M. Mayer. An xfem based fixed-grid approach for 3d fluid-structure interaction. In *Fluid Structure Interaction II*, volume 73 of *Lecture Notes in Computational Science and Engineering*, pages 327–349. Springer Berlin Heidelberg, 2010.

[12] Axel Gerstenberger and Wolfgang A. Wall. An eXtended Finite Element Method/Lagrange multiplier based approach for fluid-structure interaction. *Computer Methods in Applied Mechanics and Engineering*, 197:1699–1714, 2008.

[13] L.T. Zhang and M. Gay. Immersed finite element method for fluid-structure interactions. *Journal of Fluids and Structures*, 23:839–857, 2007.

[14] Vinh Phu Nguyen, Timon Rabczuk, Stéphane Bordas, and Marc Duflot. Meshless methods: A review and computer implementation aspects. *Mathematics and Computers in Simulation*, 79:763–813, 2008.

[15] Guohua Xia and Ching-Long Lin. An unstructured finite volume approach for structural dynamics in response to fluid motions. *Computers and Structures*, 86:684–701, 2008.

U-RANS SIMULATION OF FLUID FORCES EXERTED UPON AN OSCILLATING TUBE ARRAY IN AXIAL FLOW AT LARGE KEULEGAN-CARPENTER NUMBERS

L. Divaret[1], P. Moussou[2], O. Cadot[3], J. Berland[4], O. Doaré[3]

[1] EDF R&D, Analysis in Mechanics and Acoustics Dpt, Clamart, France

[2] LaMSID UMR CNRS EDF 2832, Clamart, France

[3] UME, ENSTA ParisTech, Palaiseau, France

[4] EDF R&D, Fluid Dynamics, Power Generation and Environment Dpt, Chatou, France

lise.divaret@edf.fr

Abstract

This paper presents a CFD simulation of the fluid flow and of the fluid forces generated by large lateral displacements of cylinder arrays in the presence of an axial turbulent flow. A Morison-like expansion of the force consisting in an inertial term and a drag term is proposed, and the dependency of the dimensionless coefficients as functions of the Keulegan Carpenter number, of the Stokes number and of the axial Reynolds number are investigated.

1 Introduction

In the nuclear industry, the seismic design of reactor cores requires the structural analysis of fuel rod assemblies undergoing transient excitations. The fuel assemblies are classically described by vibrating beams, and the fluid is usually taken into account with the help of an added mass and an added damping coefficient incorporated into the structure model [1]. Such a representation is of current usage, but recent advances in CFD have made feasible thorough evaluation of the fluid forces nowadays.

In Power Water Reactor plants, fuel assemblies are constituted of stacks of 17 by 17 rods with a diameter D equal to about 9 mm, and a pitch to diameter ratio equal to about 1.33. The steady state axial fluid velocity reaches values equal to 5 m/s, which corresponds to an axial Reynolds number of the order of 10^5. In standard calculations, the amplitude of the lateral displacement of a fuel assembly during a seism can reach a few diameters, and the corresponding frequencies range from 5 to 20 Hz. The velocity of a rod can hence reach values up to 2 m/s, which implies that the displacement-induced fluid flow is also turbulent. The dimensionless oscillation amplitude can be described by the so-called Keulegan-Carpenter (KG) number [2], equal to 2π X/D, where X is the lateral rod displacement: in the framework of seismic analysis, the KG number varies from 0.1 to 20.

The scientific literature provides data about large amplitude oscillations of cylinders arrays in quiescent fluid, whereas studies of axial flows are focused on small lateral displacements [3]. There does not seem to exist a large amount of reference data dealing with axial flow and a large amplitude of the lateral displacement. Some experiments [4] have shown that the equivalent structural damping could reach values exceeding 30 %, and CFD simulations [5] have corroborated this order of magnitude.

The purpose of the present paper consists in evaluating the unsteady fluid forces exerted upon a rigid tube array moving laterally with KG numbers varying from 0.1 to 20. The system under study is kept as simple as possible, in order to facilitate the identification of the key parameters, and in order to better understand the physics of the fluid flow

The choice of a controlled sine displacement is made to facilitate the analysis of the fluid dynamics. Such a representation cannot be used as it stands for seismic analysis, for non-linear terms in the fluid forces forbid to expand a transient displacement in Fourier terms. However, this approach constitutes a first step in the understanding of fluid dynamics.

2 Approach

For the sake of efficiency, the simplest possible configuration is considered, namely, a 3 by 3 cylinder array inside a rectangular box in two dimensions. Such a simplified representation is to be used the following way: the central cylinder stands for the inner fuel rods, the four corner cylinders stand for the corner cylinders of a fuel assembly, and the four lateral cylinders stand for the outer rods of a fuel assembly. It is here assumed that the presence of a series of rods is screened by one single row of cylinders.

The cylinders have the same diameter as the actual fuel rods, i.e., 9 mm, and they are separated by gaps equal to 3 mm. A rectangular box is arranged around the cylinder array, with a gap equal to 2 mm in the y-direction, and a variable gap in the x-direction. The displacement of the cylinder array is a controlled sine oscillation with a frequency varying from 2 to 15 Hz and an amplitude varying from 0.05 to 4 diameters. An axial flow is imposed, with an average value inside the array varying from 2.5 to 7 m/s. The dimensionless values associated with these figures are given in Table (1): the case number 2 is chosen as reference.

As shown in Figure (2), the fluid mesh around the cylin-

ders is constituted of hexahedra only as required by the best practice in fluid dynamics, with a small width in the axial direction associated with one cell. The mesh generator *GMSH* [6] was used to generate it; it exhibits 19560 cells. The skew ratio of the cells is always lower than 0.5, and the maximum edge ratio is equal to 1.9.

Unsteady Reynolds Averaged Navier Stokes (URANS) simulation is performed with the help of the finite volume fluid dynamics solver *Code_Saturne* [7] using the Arbitrary Lagrangian Eulerian method (see for instance [8] for a detailed description of the ALE). The choice was made to use a $k-\epsilon$ model with a standard two-scale law.

A 2D simulation is performed by applying periodic conditions in the axial direction, i.e., by forcing the upper and lower velocity vectors to coincide. The net flow in the axial direction is generated by the addition of a momentum source term to the Navier-Stokes equations, which compensates the friction force along the cylinder walls and the box walls. Such a procedure ensures a two-dimensional solution of the fluid dynamics equations, without forcing the velocity nor the pressure at the mesh boundaries.

The ALE method is applied in its simplest form: the displacement of the boundaries of the fluid domain are prescribed, and the mesh is automatically compressed and expanded with the help of a Laplacian algorithm which keeps the mesh almost unchanged close to the cylinders.

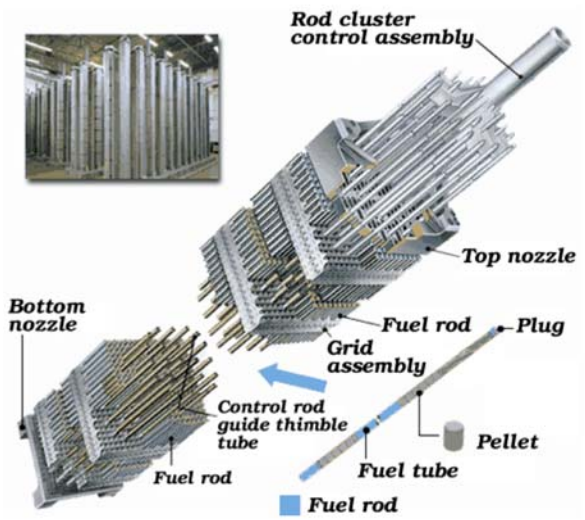

Figure 1: Sketch of a fuel assembly, from the WNA website `www.world-nuclear.org`

The calculations are performed with an 8 processor Linux station: in the reference case, 20000 initial time steps of 0.2 ms are first dedicated to the stabilization of the axial flow pattern, followed by a smooth transition to a final series of controlled oscillations of the cylinder array during 15000 time steps. The Courant-Friedrichs Lewy (CFL) number obtained is lower than 4.

3 Flow pattern and unsteady forces

Visualization of the fluid flow are achieved with the help of the free software Paraview [9]. The unsteady forces obtained during the calculations are illustrated in the reference case by the following figures, where the fluid velocity in the x-direction and the axial component of the vorticity are plotted. The x-direction goes from left to right in the Figure (3) and Figure (4), the y-direction form bottom to top and the z-direction is the axial direction, perpendicular to the Figure (3) and Figure (4).

A simple flow pattern is observed, with flow separation downstream of each cylinder and the formation of a wake behind the last row of cylinders. The unsteady vortices in the wake appear to vanish quite quickly, most probably because of the turbulent axial flow. It can be also be observed that the leading cylinders at the beginning of the backwards displacement interact with the residual vortices as shown in the fourth subfigure, which corresponds to an intermediate time shortly after the maxi-

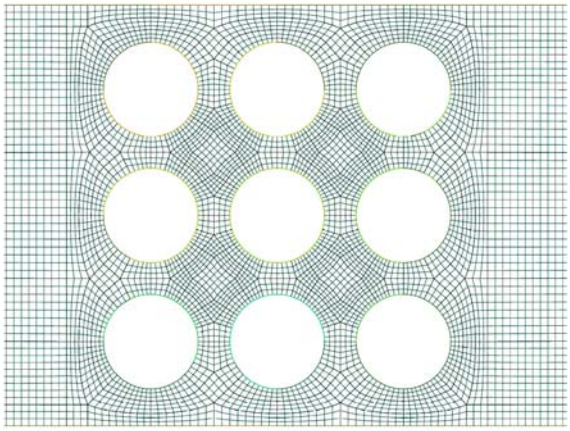

Figure 2: Partial view of the cylinder array mesh, the lateral parts are not shown

Table 1: Flow and oscillation conditions

Case #	Keulegan Carpenter	Stokes	Axial Reynolds	Confinement
1	12.56	**162**	37622	11.5
2	12.56	405	37622	11.5
3	**6.28**	405	37622	11.5
4	**0.31**	405	37622	11.5
5	**25.12**	405	37622	11.5
6	12.56	**810**	37622	11.5
7	12.56	405	**17442**	11.5
8	12.56	405	**54566**	11.5
9	12.56	**1215**	37622	11.5
10	12.56	405	37412	5
11	12.56	405	37320	3
12	12.56	**243**	37622	11.5
13	12.56	**324**	37622	11.5
14	12.56	**648**	37622	11.5
15	**0.69**	405	37622	11.5
16	**0.2**	405	37622	11.5
17	12.56	**972**	37622	11.5
18	**2.51**	405	37622	11.5

mum displacement. The fluid forces exerted upon the

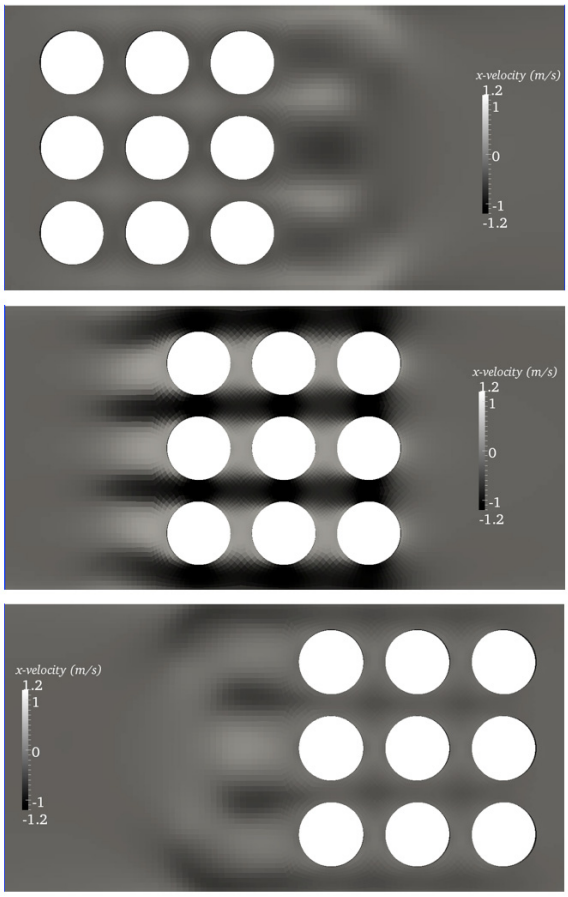

Figure 3: Sketch of the x-velocity along one cycle of oscillation, in ms^{-1}

cylinders exhibit a sine-like shape, with a phase difference with the array displacement equal to about -0.95 in the reference case illustrated in Figure (5) and Figure (6). This phase shift indicates that the drag force dominates in the range of displacement amplitude and of fluid velocities considered, and that inertial effect are also present. Such a description overlooks unsteady effects like the interaction of cylinders with the wake vortices, but it is meaningful as a first approximation. It is worth mentioning the fact that the axial velocity does not adapt instantaneously to the position of the tube array, as illustrated in Figure (7): the axial velocity in the wake of the cylinders remains close to zero during a part of the oscillation cycle. This results probably from axial inertia combined to the vanishing velocity condition along the cylinder walls.

4 Inertia and drift coefficients

A simple attempt to fit the computed forces can be based on the Morison expansion originally derived for single cylinders in quiescent flow, namely:

$$F_x^{Morison} = -\alpha_m \frac{\pi \rho D^2}{4} \ddot{X} - \alpha_d \frac{\rho D}{2} |\dot{X}| \dot{X}$$

where α_m is the dimensionless coefficient of the added mass term, assumed to be proportional to the acceleration of the cylinder. In the above expression, the drag term follows a quasi-steady law, and unsteady effects are overlooked. Nevertheless, such an expression has the

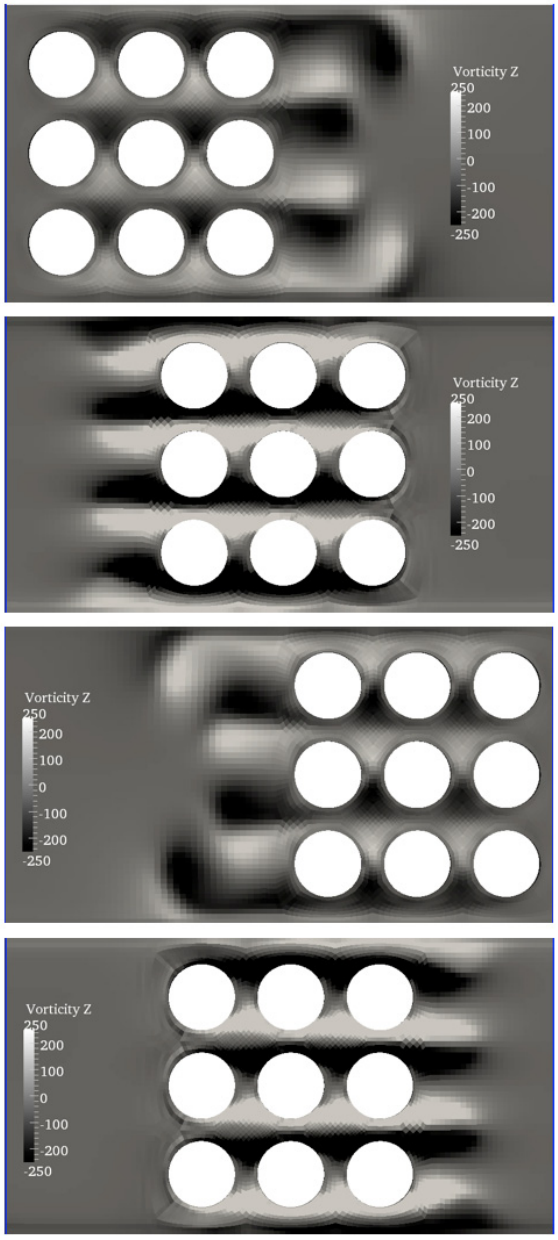

Figure 4: Sketch of the axial vorticity along one cycle of oscillation, in s^{-1}

merit of simplicity, and as the term $|\dot{X}|\dot{X}$ is reasonably close to a sine, the identification of a couple of dimensionless coefficients α_m and α_d is straightforward.

Following this line of reasoning, it is proposed to expand the x-forces in Morison-like coefficients according to

$$F_x = \omega^2 \left(\alpha_m \frac{\pi \rho D^2}{4} sin\omega t A - \alpha_d \frac{\rho D}{2} |cos\omega t| cos\omega t A^2 \right)$$

where ω and A are the circular frequency and the amplitude of the oscillation, respectively. The coefficients obtained that way are still related to the drag and to the fluid inertia, but they may depend on the oscillation parameters, especially the frequency and the amplitude. Such an expansion cannot cover all the details of the fluid flow, and presumably not the interaction of the cylinder array with the axial flow. It is used in the present study because it the simpler expansion that can be proposed.

The coefficients obtained throughout least square estimations for four out of nine cylinders are plotted in the

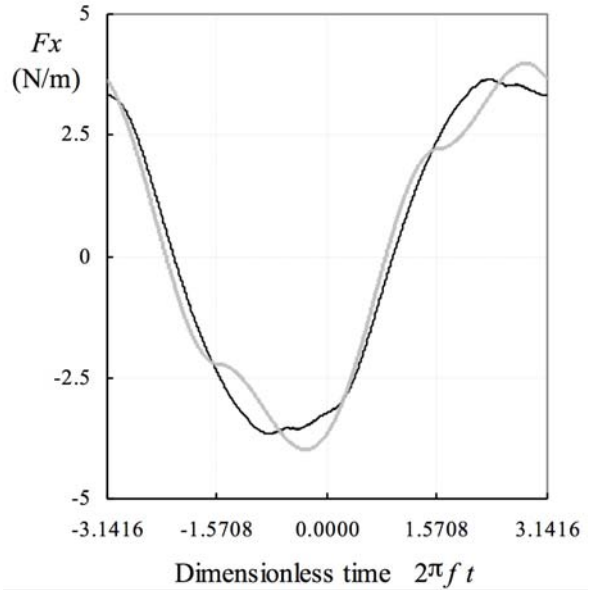

Figure 5: Evolution of the x-component of the force exerted upon the upper center cylinder during one cycle of oscillation, for a displacement of the array proportional to sin2πft. Black line: result of the computation of the reference case, gray line: Morison-like fit of the result of the computation (see next Section)

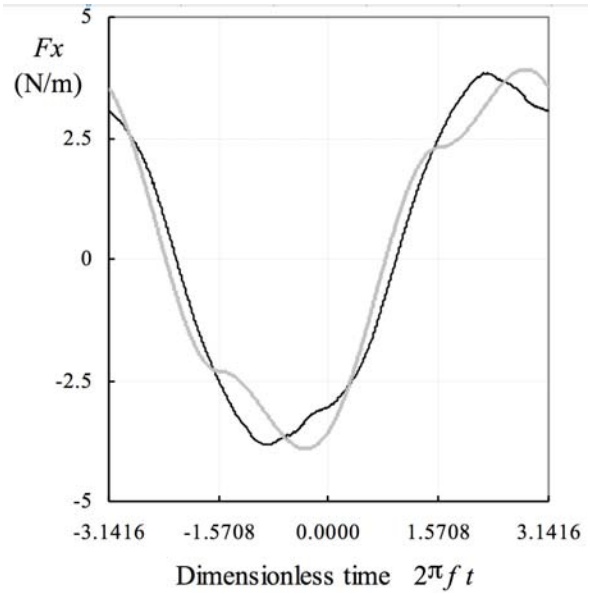

Figure 6: Evolution of the x-component of the force during one cycle of oscillation for the central cylinder for a displacement of the array proportional to sin24πft.. Black line: result of the computation of the reference case, gray line: Morison-like fit of the result of the computation (see next Section)

next figures as functions of parameters listed in Table (1), i.e., the dimensionless amplitude (KG), the dimensionless frequency fD^2/ν, a.k.a. Stokes number, and the axial Reynolds number. The width of the box was not found to have a significant influence on the coefficients in the range of widths tested (see Table (1)).

It appears that the mass and the drag coefficients obtained that way are, as an order of magnitude, close to unity. These values are consistent with the classical values of the added mass of a single cylinder estimated by a potential flow model ($\alpha_m = 1$, see for instance [10]) and

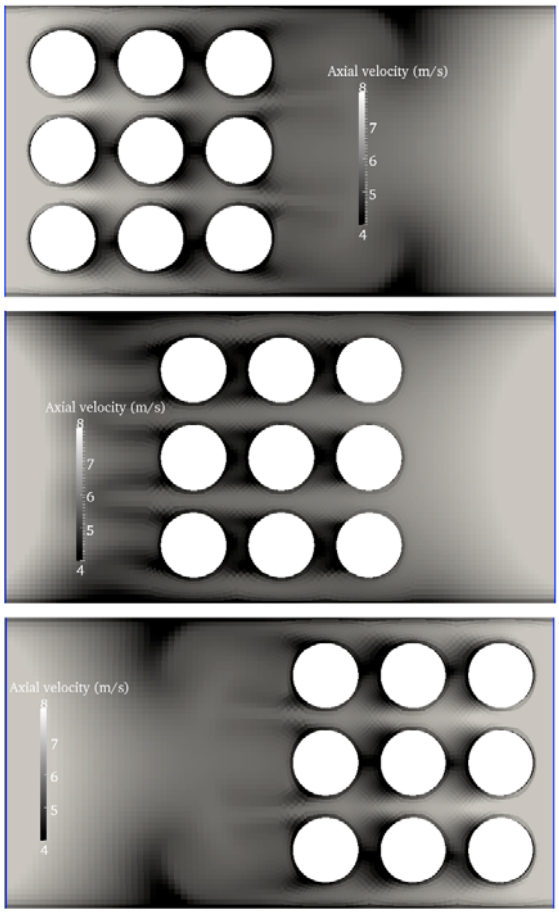

Figure 7: Sketch of the axial velocity along one cycle of oscillation for the reference case, in s^{-1}

with the drag coefficient of a cylinder which is close to unity in a wide range of Reynolds numbers ($\alpha_d \sim 1$, see for instance [11]).

As can be seen in Figure (8), a strong dependency of the drag coefficient with the Keulegan Carpenter number is observed. The strong increase of α_d for small values of KC seems to indicate that the scale laws of the above equations may require some further elaboration.

5 Perspectives

A CFD calculation of the fluid forces exerted upon a 3 by 3 array of cylinders with large Keulegan Carpenter could be achieved with URANS and ALE. Further work is needed to experimentally validate the principle of this calculation, and special attention should be given to the two dimensional nature of the fluid flow. Another aspect of the approach deals with the nature of the confinement; one effects the alpha coefficients to significantly be altered if the surrounding box was opened on both ends. Further calculation are required to investigate it.

Nevertheless, the approach of the present paper constitutes a first attempt to grab the essential features of large lateral displacements of cylinder arrays in the presence of axial flow.

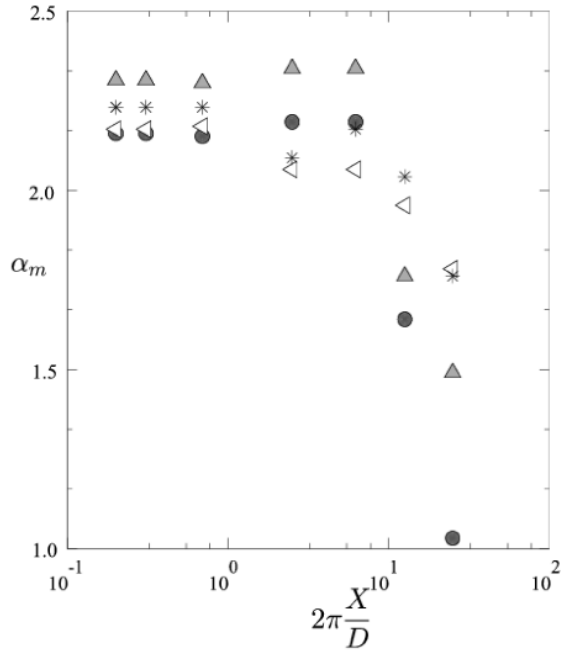

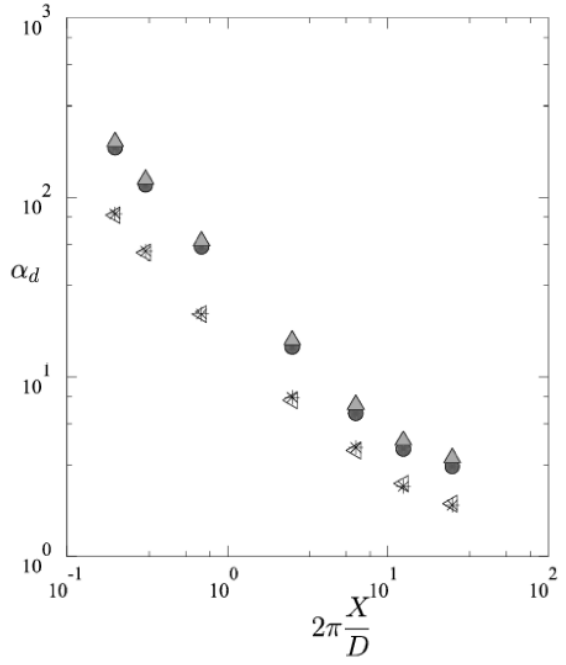

Figure 8: Mass and drag coefficients vs. Keulegan Carpenter number. •:center cylinder, ◁:left central cylinder, △:central upper cylinder, ⋆: upper left cylinder

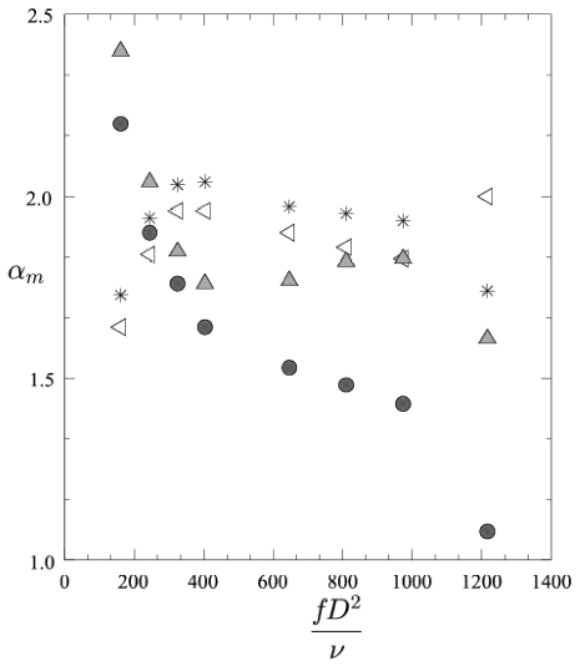

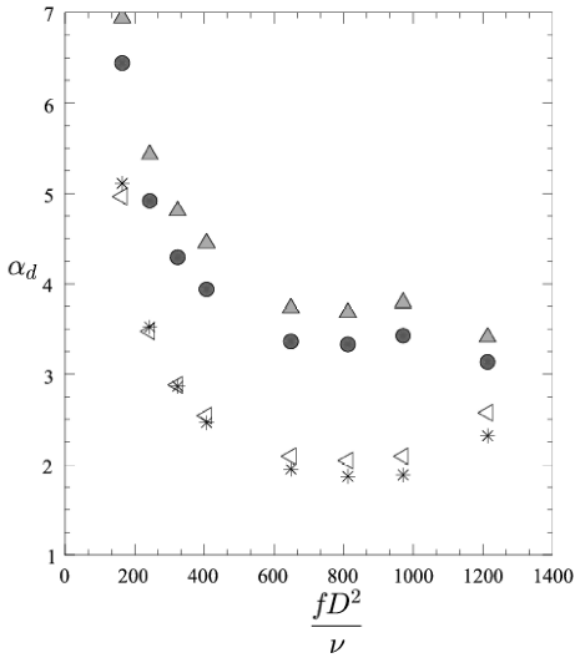

Figure 9: Mass and drag coefficients vs. Stokes number. •:center cylinder, ◁:left central cylinder, △:central upper cylinder, ⋆: upper left cylinder

Acknowledgements

The authors express their gratitude to Miss Marie Clement for paving the way to the different CFD tools used in the present study.

References

[1] J.F. Sigrist and D. Broc. Homogenisation method for the modal analysis of a nuclear reactor with internal structures modelling and fluid-structure-interaction coupling. *Nuclear Engineering and Design*, 237:431–440, 2007.

[2] R.D. Blevins. *Flow-induced Vibrations*. Krieger, Florida, 2001.

[3] M. P. Paidoussis. Slender structures and axial flow. In *Fluid-Structure Interactions*. Elsevier, 2004.

[4] B. Collard, S. Pisapia, S. Bellizzi, and F. Witters. Pwr fuel assembly modal testing and analysis. *Pressure Vessels and Piping*, 465, 2003.

[5] B. Ladouceur, J. Woilliez, and M. Fontaine. Fuel assembly damping for accident studies: an analytical approach. Structural behaviour of fuel assemblies for water cooled reactors, Note IAEA TECDOC 1454, 2004.

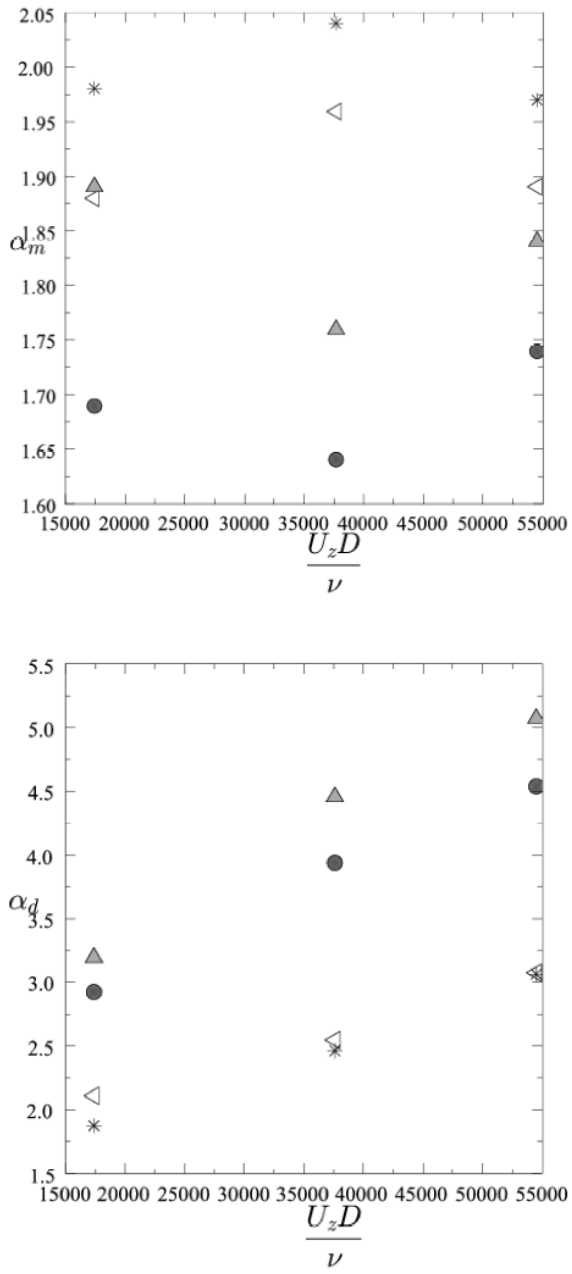

Figure 10: Mass and drag coefficients vs. axial Reynolds number Stokes number. •:center cylinder, ◁:left central cylinder, △:central upper cylinder, ⋆: upper left cylinder

[6] C. Geuzaine and J.-F. Remacle. Gmsh: a three-dimensional finite element mesh generator with built-in pre- and post-processing facilities. *International Journal for Numerical Methods in Engineering*, 79:1309–1331, 2009.

[7] F. Archambeau, N. Méchitoua, and M. Sakiz. A finite volume code for the computation of turbulent incompressible flows–industrial applications. *International Journal of Finite Volumes*, 1:1–59, 2004.

[8] T. Belytschko, W.K. Liu, and B. Moran. *Nonlinear Finite Elements for Continua and Structures*. Wiley, 2000.

[9] J. Ahrens, B. Geveci, and Ch. Law. Paraview: An end-user tool for large data visualization. In C.D. Hansen and C.R. Johnson, editors, *Visualization Handbook*. Elsevier, 2005.

[10] L. M. Milne-Thomson. *Theoretical Hydrodynamics*. Dover Publication, 1968.

[11] R.D. Blevins. *Applied Fluid Dynamics Handbook*. Krieger, Florida, 1992.

Coupling a 3D Navier-Stokes with free-surface model with geometrically non-linear structures

C. Kassiotis[1]

[1] Saint-Venant Laboratory for Hydraulics, Université Paris-Est

(Joint Research Unit EDF R&D, CETMEF, École des Ponts ParisTech)

6 quai Watier, BP 49, 78401 Chatou, France

christophe.kassiotis@enpc.fr

Abstract

In this work we discuss a way to compute the interaction between free-surface flows and nonlinear structures. The approach chosen rely on a partitioned strategy that allows to solve strongly coupled fluid-structure interaction problem. The software coupling is ensured in an efficient way using the Communication Template Library (CTL). Numerical examples presented herein concern 2D validations case but also 3D problems with a large number of equations to be solved.

1 Introduction

The recent and dramatic events in Japan underline the need of accurate predictions for civil engineering structures in interaction with free surface flows. In most of the current applications, the fluid loading is applied statically on the construction, taking into account its dynamics and the interaction effects with only security coefficients. Obviously, the problem is coupled (the more a coastal protection resists, the higher the fluid level, and therefore the loading is), and there is a need to compute both the resistance of structures and the flow main characteristics, especially when the failure occurs.

In this work we focus on fluid-structure interaction problems, with free-surface flows. The free-surface flow problem is described by the Navier-Stokes equations with two phases (water and air), set in an ALE framework [1, 2, 3] and discretized with a VOF strategy [4, 5, 6, 7] For the structure part, it is natural to follow material point motion in a Lagrangian formulation and a discretization with FEM [8].

For the coupled problem, the monolithic approach is abandoned in favor of the partitioned approach [9, 10, 11, 12, 13, 14, 15, 16, 17]. The latter is preferred for its modularity and the possibility of re-using existing software. The partitioned approach used here is based on a simple fixed-point strategy based on the Block Gauss-Seidel algorithm (DFMT-BGS) with an adaptive relaxation parameter [18] that shows sufficient performances for the example proposed. The properties as well as stability of the implicit coupling DFMT-BGS algorithms used herein are presented in detail in [19].

In this work, a general fluid-structure interaction framework based on existing software was used. This framework was built using the middleware Communication Template Library (CTL) [20] which offers good performances, and can therefore be used for scientific computing of large systems. An important feature is the possibility to couple types of software product that were initially not programmed to be coupled (here `FEAP` for the structure and `OpenFOAM` for the fluid), even if they are based on different discretization techniques (respectively FV for the fluid and FE for the structure) and were programmed in different languages, `C++` and `Fortran`. For more details on the implementation, see [21]

The outline of this paper is as follow: in the subsequent section we present the chosen formulations for the structure and fluid sub-problem. In Section 3, we describe the coupling between the fluid and the structure sub-problems. In Section 4, we give and comment the results of illustrative numerical examples dealing with free-surface flow impacting a structure in two and three-dimensions as well as comparison with existing works. The concluding remarks are given in the last section.

2 Description of the free surface flows and the structures

We will not here gives the detailled PDE for the structure and the fluid, but give directly the semi-discrete form of the problem. For the structure, it can be set in a matrix notation by using the real valued vectors $\mathbf{u}_s \in \mathbb{R}^{n_{d-o-f}}$ that give a discrete approximation of the 3D displacement vector field $\boldsymbol{u}_s$:

$$\mathcal{R}_s(\mathbf{u}_s;\boldsymbol{\lambda}) := \mathbf{M}_s\ddot{\mathbf{u}}_s + \mathbf{f}_s^{\text{int}}(\mathbf{u}_s) - \mathbf{f}_s^{\text{ext}}(\boldsymbol{\lambda}) = \mathbf{0} \quad (1)$$

where $\mathbf{M}$ is the mass matrix, $\mathbf{f}_s^{\text{int}}$ with a geometrically nonlinear problem, and $\mathbf{f}_s^{\text{ext}}$ the consistent nodal forces. Here the $\boldsymbol{\lambda}$ represents the boundary forces computed from the fluid flow problem and imposed on the fluid-structure interface. In order to complete the discretization process, the time integration of the structure problem can be carried out by using standard time-stepping schemes [8]. In particular, the Generalized HHT-α method is used herein.

The semi-discrete form of the discretized fluid problem can be written in a matrix form as follows. The discrete fluid mesh motion considers that $\mathbf{u}_m$ is imposed by the motion of the interface $\mathbf{u}$:

$$\mathcal{R}_m(\mathbf{u}_m;\mathbf{u}) := \mathbf{K}_m\mathbf{u}_m - \mathbf{D}_m\mathbf{u} = \mathbf{0} \quad (2)$$

where $\mathbf{D}_m$ is a projection/restriction operator and $\mathbf{K}_m$ governs the extension of the boundary displacement.

The (discrete) volume fraction $\boldsymbol{\iota}$, the 3 components of velocity $\mathbf{v}$ and pressure p are coupled through a set of non-linear equations. Written in a matrix forms, it gives the following semi-discrete problem:

$$\begin{aligned}&\mathcal{R}_f(\boldsymbol{\iota}, \mathbf{v}_f, \mathsf{p}_f; \mathbf{u}_m)\\ &:= \begin{bmatrix} \mathbf{M}_\iota \dot{\boldsymbol{\iota}} + \mathbf{N}_\iota(\mathbf{v}_f - \dot{\mathbf{u}}_m)\boldsymbol{\iota} \\ \mathbf{M}_f(\boldsymbol{\iota})\dot{\mathbf{v}}_f + \mathbf{N}_f(\boldsymbol{\iota}, \mathbf{v}_f - \dot{\mathbf{u}}_m)\mathbf{v} + \dots \\ \qquad \dots \mathbf{K}_f(\boldsymbol{\iota})\mathbf{v}_f + \mathbf{B}_f \mathsf{p}_f - \mathbf{f}_f(\boldsymbol{\iota}) \\ \mathbf{B}_f^T \mathbf{v}_f \end{bmatrix} \\ &= \mathbf{0}\end{aligned} \tag{3}$$

where $\mathbf{M}_\iota$ and $\mathbf{N}_\iota$ are the matrices associated to the advection problem of the fluid volume fraction, $\mathbf{M}_f$ is a positive definite mass matrix, $\mathbf{N}_f$ is an unsymmetric advection matrix, $\mathbf{K}_f$ is the conduction matrix describing the diffusion terms, and $\mathbf{B}_f$ is for the gradient matrix, whereas $\mathbf{f}_f$ is the discretized nodal loads on the flow. This matrix form also takes into account the boundary conditions; special care has to be taken concerning the discretization of boundary conditions – and especially normal flux – when using the Finite Volume Method [22].

One way to solve the flow problem is to consider a monolithic solver handling all equations simultaneously. Another way is to consider a split between the mesh motion, the volume fraction advection, the momentum and the continuity equations, and to use an operator split-like procedure often referred to the *segregated approach* [23]. This approach is favored for its computational efficiency compared to the monolithic scheme. Indeed, even with a simple fixed point iteration strategy its cost is less important than that of the monolithic approach for large size problems [24]. In the work presented herein, the segregated approach will be used because of its efficiency.

3 Coupling strategy and implementation

By enforcing the continuity of primal variables at the interface we can eliminate the energy errors that characterize the explicit interface matching. When coupling incompressible flow with structure, the implicit interface matching is required for stability reason, as proved in [19]. This ought to be done by iterating on the following residual to reduce its value below the chosen tolerance:

$$\boldsymbol{r}_{N+1} := \boldsymbol{u}_{s,N+1} - \boldsymbol{u}_{f,N+1} \simeq 0 \quad \leq \mathtt{TOL} \tag{4}$$

In this way we obtain an implicit algorithm requiring more than one iteration to enforce the interface matching condition. The chosen order of iterations, corresponds to the Block-Gauß-Seidel algorithm for fluid-structure interaction problem [14]. Let us note that not only the value at synchronization points T_n or T_{n+1}, but also the interpolated evolution of variables have to be exchanged in the entire time-interval $t \in [T_n, T_{n+1}]$ when the time steps are not matching between fluid and structure subproblems.

Contrary to explicit algorithms which generate spurious energy at the interface, the present implicit interface matching algorithm enforce the same evolution of the primal variables at the fluid-structure interface. In other words, an iterative solution for primal (displacements) continuity as well as the dual (forces) equilibrium equations at the interface is performed by using the Picard iteration:

$$\boldsymbol{u}_{N+1}^{(k+1)} = \mathcal{G}\left(\boldsymbol{u}_{N+1}^{(k)}\right); \qquad \mathcal{G} = {\mathcal{S}_s}^{-1} \circ -\mathcal{S}_f \tag{5}$$

where $\mathcal{S}_f$ and $\mathcal{S}_s$ are Steklov-Poincaré operators for fluid and structure defined as define in [15]. These operators can be formulated using transfer operators and equations (Eq. (1)), (Eq. (3)) and (Eq. (2)):

$$\mathcal{S}_s = \mathcal{T}_s^{\boldsymbol{\lambda}} \circ \mathcal{R}_s \circ \mathcal{T}_s^{\boldsymbol{u}}; \qquad \mathcal{S}_f = \mathcal{T}_f^{\boldsymbol{\lambda}} \circ \mathcal{R}_f \circ \mathcal{R}_m \circ \mathcal{T}_s^{\boldsymbol{u}} \tag{6}$$

where the transfer of structure displacement to fluid-structure interface displacement is $\mathcal{T}_s^{\boldsymbol{u}}$, the transfer of fluid displacement to interface displacement $\mathcal{T}_s^{\boldsymbol{\lambda}}$, the transfer of structure stresses to the interface $\mathcal{T}_f^{\boldsymbol{u}}$ and the transfer of fluid stresses to the interface $\mathcal{T}_f^{\boldsymbol{\lambda}}$.

The Picard iterations will continue until convergence of interface residual is achieved:

$$\boldsymbol{r}_{N+1}^{(k)} = \boldsymbol{u}_{s,N+1}^{(k)} - \boldsymbol{u}_{f,N+1}^{(k)} = \mathcal{G}\left(\boldsymbol{u}_{N+1}^{(k)}\right) - \boldsymbol{u}_{N+1}^{(k)} \tag{7}$$

It is clear that this fixed-point algorithm based on Picard iterations has the main drawback that the search directions for $\boldsymbol{u}$ and $\boldsymbol{\lambda}$ variables at the interface do not exploit any information from the fixed-point function $\mathcal{G}$ nor the Steklov-Poincaré operators $\mathcal{S}_f$ and $\mathcal{S}_s$. Therefore, quite a few iterations may be needed to reach the convergence.

The stability of such a coupling algorithm is studied in [19]. We give a formal proof of potential numerical instability due to the *added-mass effect* also observed in [16, 10]. In order to improve the convergence of the DFMT-BGS method, we can use a relaxed update:

$$\boldsymbol{u}_{N+1}^{(k+1)} = \boldsymbol{u}_{N+1}^{(k)} + \omega^{(k)}\ \boldsymbol{r}_{N+1}^{(k)} \tag{8}$$

Our favorite choice for constructing $\omega^{(k)}$ is using a secant methods which can keep the cost of each iteration as low as possible. The Aitken's relaxation strategy has been extensively used in fluid-structure interaction [15, 18], and shown sufficient performances to be used in the following.

The use of different different solvers, for the fluid and the structure part, do not provide in general a matching mesh at the interface. Furthermore, even for matching meshes, as the geometries of the domains are not the same on both sides of the interface, an optimal numbering of the nodes can lead to different orders for the interface nodes. In the examples proposed herein, only this latter point is of interest. Last but not least, different discretization techniques (Finite Element versus Finite Volume) or different order p of the polynomials can be used for constructing solution to fluid-structure interaction problem. In the domain of FE applied to mechanical engineering, extensive literature can be found on how to build a consistent interpolation for both subproblems at the interface [25]. For the fluid-structure interaction problems, an interesting review can be found in [26]. In our framework, it was decided not to favor any mesh-based representation of the interface, since, in the most general case, the fluid problem can also be solved by a meshfree-based method [27]. Namely, an interpolation strategy relying on radial basis function is here chosen. This method has already been employed for FSI in [28, 29].

The algorithm presented here is simple to implement. We use for this work the Communication Template Library (CTL, see [30, 20]) that allows to re-use existing codes in a generic way, either called as libraries on the same computer, or as remote executables through network. With the CTL, we are able to couple existing stand-alone software, in a quite straightforward way, even if they are programmed in different langages (`Fortran` for the structure part, `C++` for the fluid part), and to conserve the inner parallelism of each component. For more details on the implementation, the reader is invited to see [21].

4 Numerical simulation

The problem solved is a 3D generalization of dam-breaking event that brings about a sloshing wave impact on a rigid [31, 5] or flexible structure as presented in 2D in [32, 33]. At initial time $t = 0s$, a the three-dimensional water column starts falling down under the gravity loading and eventually hits the obstacle placed in the way. The flexible obstacle is a slender plate-like body made of elastic material that can undergo large deformation. The chosen dimension of the problem, as well as the boundary conditions are given in Figure (1). Let us note that we propose to use open boundary conditions far from the obstacle in order to avoid the water bounces-back and hits again the structure after breaking off the walls. For that reason, only the left and bottom planes of the fluid domain are defined as non-slipping walls, while the others are defined with boundary condition of atmospheric pressure.

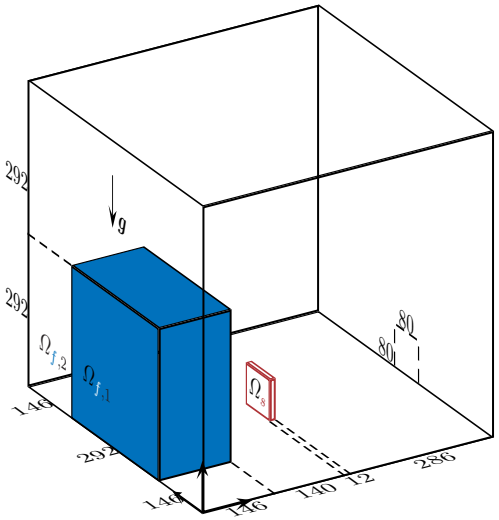

Figure 1: Three-dimensional water column impacting an obstacle: geometry (given in mm) and boundary conditions

The material properties are chosen as follows: the density and the kinematic viscosity are $\rho_{f,1} = 1\times10^3 kg.m^{-3}$ and $\nu_{f,1} = 1 \times 10^5 m.s^{-1}$ for the high density fluid (water in the reservoir), versus $\rho_{f,2} = 1 \times 10^3 kg.m^{-3}$ and $\nu_{f,2} = 1 \times 10^6 m.s^{-1}$ for the low density fluid (air in the remaining part of the domain). The mesh motion problem is solved by using a Laplacian smoothing material where the diffusion coefficient is a quadratic inverse function of the distance to the interface between solid and fluid.

The results are computed for two meshes with the chosen discretization and the number of cells given in Tab. Table (1). For the finest grid, around 64, 60 and 40 cells are used in $\boldsymbol{e}_x$, $\boldsymbol{e}_y$ and $\boldsymbol{e}_z$ direction. The mesh is refined gradually refined around the structure, and initially the cell dimensions are between 8.9×10^{-8} and 3.2×10^{-5}. For this finest grid, the maximum skewness of the mesh observed is 2.947, that does not generate too large errors. The fluid is handled by second order space discretization and a Van Leer limiter is used for the advection terms. The time integration scheme employed in this computation is implicit Euler. For such a scale of modeling it is not required to consider surface tension between the two fluids. For this problem the fluid computation is parallelized, but reduction of the CPU time is obtained by using a Generalized Algebraic-MultiGrid (GAMG) linear solver. Note that small time steps are required for the explicit solution of the phase function indicator equation, as well as the half-implicit nature of the coupling between the momentum predictor and the pressure corrector.

For the structure part, we propose here to use three-dimensional elements with quadratic shape functions, where each element has 27 nodes. The material properties used for the solid are: a neo-Hookean elastic material with Young's modulus $E_s = 1 \times 10^6 Pa$ and Poisson's ratio $\nu_s = 0$ and a density $\rho_s = 2500kg \cdot m^{-3}$, which can represent finite deformation. The time integration is carried out by a Generalized-α scheme with the same parameters as the one used for the 2D case.

	fluid d-o-f	solid d-o-f	number of time steps
Coarse	63×10^3	1.1×10^3	1×10^5
Fine	520×10^3	6.6×10^3	1×10^5

Table 1: Number of d-o-f for coarse and fine discretization of the three-dimensional dam-breaking problem

The computation of the coupled problem (with total number of d-o-f given in Tab. Table (1)), is carried out by an implicit iterative scheme. The results of fluid and solid computations are matched for a time step of 1×10^{-4} for the coarse and 2×10^{-5} for the fine discretization. The coupling scheme used is DFMT-BGS with Aitken's relaxation. The initial parameter is $\omega = 0.25$ and the predictor is of order 1. The absolute tolerance considered is:

$$\|\boldsymbol{r}_N^{(k)}\| \leq 1 \times 10^{-6} \tag{9}$$

The number of iterations required to reach the convergence criteria is given in 2(a). Note that there is no iteration required before the water hits the structure since the effect of air flow can almost be deemed negligible with respect to the structure. The number of iterations required for the coarse and fine mesh is small. This propertie is observed for most of the simulation carried out with free-surface flow when the convergence of the pressure solver is easily reached. For the finest grid, the total time required to perform the whole coupled simulation on a single $3.0GHz$ Intel processor is $279 \times 10^3 s$.

In Figure (3), the high density fluid domain is represented, as well as some part of the fluid mesh and the structure displacement. The first $0.1s$ of the simulations, the water column falls under the gravity loading. There is no effect whatsoever on the structure until the high density flow reaches its bottom. The maximum amplitude of the motion is obtained at $t = 0.25s$, before the

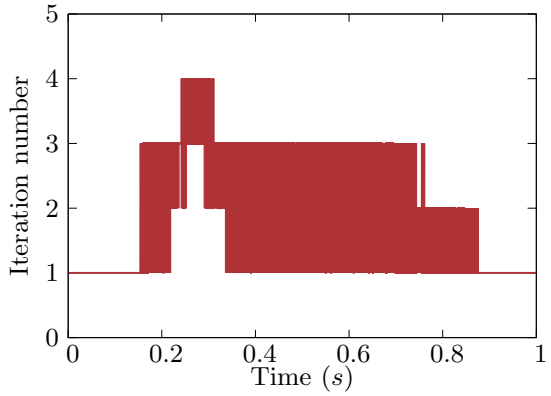

(a) Number of iterations in order to make the DFMT-BGS algorithm converge for the three-dimensional dam-breaking problem

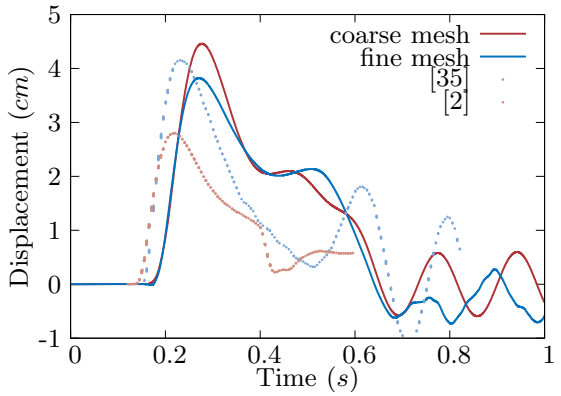

(b) Three-dimensional dam break example: obstacle displacement in e_x direction of center point of the top face $(40; 6; 80)$ and comparison with 2D models [33, 32]

Figure 2: Results of three-dimensional simulations

solid comes back to its initial position and oscillates after the shock.

In 2(b) the motion of the extremity of the solid obstacle is plotted. Contrary of the two-dimensional example, small drops of high density fluid are not interacting with the obstacle after the main shock. Therefore, the motion of the flexible structure remains fairly smoothed and it is rather well described with the coarsest grid. We present for comparison the results obtain with 2D models using either a monolithic stabilized-FEM strategy [32] or tight coupling strategy between a FV and FEM solver [33]. The use of 2D models ad well as the difference in strategy explain the differences observed (our results are closer for a 2D simulation, as presented in [34]).

5 Conclusions

The proposed solution method allows to perform coupled simulations and obtain reliable solution to complex fluid-structure interaction by using the existing codes, that were initially developed to support either fluid or structure motion computation. This is achieved thanks to the use of the component technology [21, 20] providing the coupling between existing software products. Therefore, the proposed solution method for fluid-structure interaction can utilize very different discretization strategies to obtain the optimal accuracy; The case in point concerns FE for the structure and FV for the fluid. The use of these popular methods for the fluid and solid parts allows to benefit from the advanced features of the two families of methods, each developed by the experts from the corresponding domain. Accordingly, on the fluid side, it is possible to use a very efficient semi-implicit solver for incompressible flow (PISO), inverse techniques (Algebraic Multigrid) or advanced models for free-surface flows. A very good performance of the proposed technology for fluid-structure interaction is illustrated with 2D and 3D models for dam breaking examples, which also involve flexible obstacles.

Even if the convergence is quite easy to achieve, the use of semi-implicit coupling strategy [35] could by a good way to decrease the computational cost without loosing accuracy. An other point of interest is the extension of this work to more complex behavior, for both the fluid (turbulence, non Newtonian flows, debris flows...) and the structure (non-linear behavior, cracks and failure).

References

[1] Charbel Farhat, Philippe Geuzaine, and Céline Grandmont. The discrete geometric conservation law and the nonlinear stability of ale schemes for the solution of flow problems on moving grids. *Journal of Computational Physics*, 174(2):669–694, 2001.

[2] I. Demirdžić and Milovan Perić. Space conservation law in finite volume calculations of fluid flow. *International Journal for Numerical Methods in Fluid*, 8(9), 1988.

[3] C. W. Hirt, A. A. Amsden, and J. L. Cook. An arbitrary Lagrangian-Eulerian computing method for all flow speeds. *Journal of Computational Physics*, 135(2):203–216, 1997.

[4] Denis Dutykh and Dimitrios Mitsotakis. On the relevance of the dam break problem in the context of nonlinear shallow water equations. *Discrete and Continous Dynamical System – Series A*, Accepted, 2009.

[5] O. Ubbink and RI Issa. A method for capturing sharp fluid interfaces on arbitrary meshes. *Journal of Computational Physics*, 153(1):26–50, 1999.

[6] R. J. Sobey. Linear and Nonlinear Wave Theory. Lecture note, Leichtweiß-Institut für Wasserbau, Braunschweig, 1998.

[7] J. J. Stoker. *Water Waves: The Mathematical Theory and Applications*. Wiley-Interscience, New-York, 1992.

[8] Adnan Ibrahimbegović. *Nonlinear solid mechanics: Theoretical formulations and finite element solution methods*. Springer, 2009.

[9] Charbel Farhat and M. Lesoinne. Two efficient staggered algorithms for the serial and parallel solution of three-dimensional nonlinear transient aeroelastic problems. *Computer Methods in Applied Mechanics and Engineering*, 182:499–515, 2000.

[10] P. Le Tallec and J. Mouro. Fluid structure interaction with large structural displacements. *Computer Methods in Applied Mechanics and Engineering*, 190(24-25):3039–3067, 2001.

[11] Hermann G. Matthies and Jan Steindorf. Partitioned strong coupling algorithms for fluid-structure interaction. *Computers and Structures*, 81:805–812, 2003.

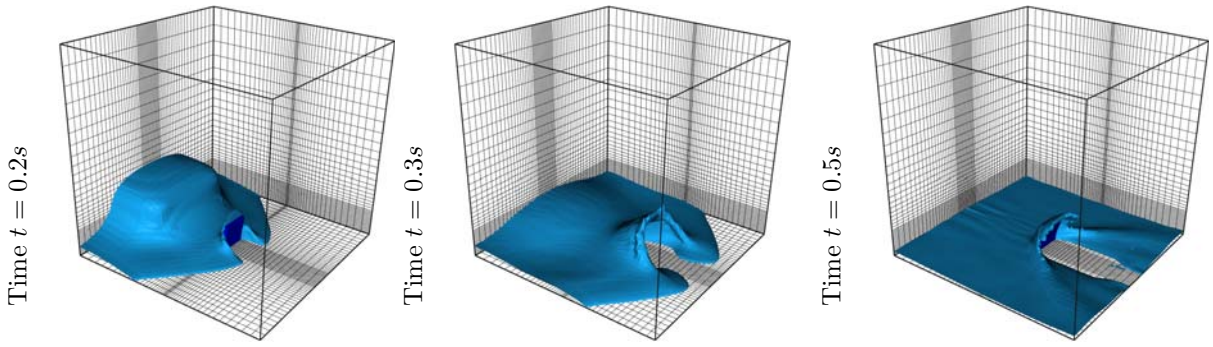

Figure 3: Tri-dimensional dam break problem. Evolution of the free surface and motion of the structure.

[12] P. Causin, J.-F. Gerbeau, and Fabio Nobile. Added-mass effect in the design of partitioned algorithms for fluid-structure problems. *Computer Methods in Applied Mechanics and Engineering*, 194(42-44):4506–4527, 2005.

[13] M. Á. Fernández and M. Moubachir. A Newton method using exact Jacobians for solving fluid–structure coupling. *Computers and Structures*, 83(2-3):127–142, 2005.

[14] Hermann G. Matthies, Rainer Niekamp, and Jan Steindorf. Algorithms for strong coupling procedures. *Computer Methods in Applied Mechanics and Engineering*, 195:2028–2049, 2006.

[15] Simone Deparis, Marco Discacciati, Gilles Fourestey, and Alfio Quarteroni. Fluid-structure algorithms based on Steklov-Poincaré operators. *Computer Methods in Applied Mechanics and Engineering*, 195(41-43):5797–5812, 2006.

[16] Christiane Förster, Wolfgang A. Ramm, and Ekkehard Ramm. Artificial added mass instabilities in sequential staggered coupling of nonlinear structures and incompressible viscous flows. *Computer Methods in Applied Mechanics and Engineering*, 196:1278–1291, 2007.

[17] M. Á. Fernández, J.-F. Gerbeau, A. Gloria, and M. Vidrascu. Domain decomposition based Newton methods for fluid-structure interaction problems. In *ESAIM: Proceedings*, volume 22, pages 67–82. edp-sciences.org, 2008.

[18] Ulrich Küttler and Wolfgang A. Wall. Fixed-point fluid-structure interaction solvers with dynamic relaxation. *Computational Mechanics*, 43(1):61–72, 2008.

[19] Christophe Kassiotis, Rainer Niekamp, Adnan Ibrahimbegović, and Hermann G. Matthies. Partitioned procedure for strongly coupled fluid-structure problems. Part I: implicit algorithm, stability analysis and validation examples. *Computational Mechanics*, Published online, 2010.

[20] Rainer Niekamp, Damijan Markovič, Adnan Ibrahimbegović, Hermann G. Matthies, and Robert L. Taylor. Multi-scale modelling of heterogeneous structures with inelastic constitutive behavior: Part II–software coupling implementation aspects. *Engineering Computations*, 26:6–28, 2009.

[21] Christophe Kassiotis, Rainer Niekamp, Adnan Ibrahimbegović, and Hermann G. Matthies. Partitioned procedure for strongly coupled fluid-structure problems. Part II: implementation aspects, re-using existing software as components and nested parallel computations by using CTL. *Computational Mechanics*, Published online, 2010.

[22] Jean-Michel Ghidaglia and F. Pascal. The normal flux method at the boundary for multidimensional finite volume approximations in cfd. *European Journal of Mechanics/B Fluids*, 24(1):1–17, 2005.

[23] S. V. Patankar. *Numerical heat transfer and fluid flow*. Hemisphere Publishing Corporation, Washington, DC, 1980.

[24] Joel H. Ferziger and Milovan Perić. *Computational Methods for Fluid Dynamics*. Springler-Verlag, Berlin, Germany, 3^{rd} edition, 2002.

[25] C.A. Felippa and K.C. Park. Synthesis tools for structural dynamics and partitioned analysis of coupled systems. *NATO Advanced Research Workshop (eds. A. Ibrahimbegović and B. Brank)*, pages 50–111, 2004.

[26] A. de Boer, A. H. van Zuijlen, and H. Bijl. Review of coupling methods for non-matching meshes. *Computer Methods in Applied Mechanics and Engineering*, 196(8):1515–1525, 2007.

[27] RA Dalrymple and BD Rogers. Numerical modeling of water waves with the SPH method. *Coastal engineering*, 53(2-3):141–147, 2006.

[28] JJ Monaghan. Smoothed particle hydrodynamics. *Annual review of astronomy and astrophysics*, 30(1):543–574, 1992.

[29] A. Beckert and H. Wendland. Multivariate interpolation for fluid-structure-interaction problems using radial basis functions. *Aerospace Science and Technology*, 5(2):125–134, 2001.

[30] Damijan Markovič, R. Niekamp, Adnan Ibrahimbegović, H. G. Matthies, and R. L. Taylor. Multi-scale modeling of heterogeneous structures with inelastic constitutive behavior : Mathematical and physical aspects. *International Journal of Engineering Computations*, 22:664–683, 2005.

[31] GN Bullock, C. Obhrai, DH Peregrine, and H. Bredmose. Violent breaking wave impacts. Part I: Results from large-scale regular wave tests on vertical and sloping walls. *Coastal Engineering*, 54(8):602–617, 2007.

[32] Elmar Walhorn, Andreas Kölke, Björn Hübner, and Dienter Dinkler. Fluid-structure coupling within a monolithic model involving free surface flows. *Computers and Structures*, 83(25-26):2100–2111, 2005.

[33] R. Baudille and M. E. Biancolini. Modelling FSI problems in FLUENT: a dedicated approach by means of UDF programming. In *Proceedings of the European Automotive CFD Conference, Frankfurt, Germany*, 2005.

[34] Christophe Kassiotis, Adnan Ibrahimbegović, and Hermann G. Matthies. Partitioned solution to fluid-structure interaction problems in application to free-surface flows. *European Journal of Mechanics – B/Fluids*, 29:510–521, 2010.

[35] M. Astorino, F. Chouly, and M. Á. Fernández. An added-mass free semi-implicit coupling scheme for fluid-structure interaction. *Comptes Rendus Mathematique*, 347(1-2):99–104, 2009.

Simulation of fluid flow in a tube bundle system using a POD-ROM approach

M. Pomarède[1,2], E. Liberge[1], A.Hamdouni[1], E. Longatte[3], and J.-F. Sigrist[2]

[1] LEPTIAB, University of La Rochelle, Av. M. CREPEAU 17042 La Rochelle Cedex, France

[2] DCNS,Indret 44620 La Montagne, France

[3] LaMSID - UMR CNRS/EDF 2832, 1 Av. du Général de Gaulle 92141 CLAMART Cedex, France

marie.pomarede@dcnsgroup.com

1 Introduction

The running rate of a nuclear power plant or on-board stokehold steam boiler intrinsically induces several vibratory levels, especially concerning the boiler tube bundle [1, 2, 3, 4]. It is shown that fluid-elastic instabilities can occur in such a configuration [5, 6, 7], leading to a certain destruction of one or more tubes: this is why the study and a precise comprehension of this vibrations phenomenon are crucial. But, this good comprehension stays difficult because of the high number of parameters that play a role in vibrations generation [8, 9].The high resource level that is necessary to set up this fluid/structure interaction problem is a still a problem: accurate and robust numerical codes have to be developed [10, 11] and, to be as close as possible to real conditions, a fully 3D turbulent flow has to be computed [12], added to the cost of the structure coupling. In an industrial configuration, such a computation is not possible, first because of the resource cost, second because of the CPU time involved.

We propose an alternative that could offer perspectives in the study of tube bundle vibrations, using reduced models. Theses models are well-known and widely used in the domain of fluid mechanics [13, 14] as well as structure mechanics [15], but they still represent a challenge within the frame of fluid/structure interaction [16, 17]. They however could give a better comprehension of the physics of this fluid/structure interaction problem, making possible the access to some parameters or information. The reduced model that we propose to set up in this paper is the Proper Orthogonal Decomposition (POD) [18, 19], which is used in many fields [20, 18, 21].
This paper is organized as follows: vibrations problems of tube bundle of heat exchangers are quickly recalled. Then, Proper Orthogonal Decomposition is described as well as its potential contribution specifically for this crucial question of tube bundle vibrations. Finally, in the third part, first numerical results in the use of POD are proposed and perspectives for a future work are exposed.

2 The heat exchanger tube bundle and its vibrations problems

On-board stokehold steam boilers of water pressurized reactors (WPR) and civil nuclear steam boilers contain a tube bundle that is constituted of long, fine and numerous tubes that are close from each other. Thus, because of the surrounding flowing fluid, theses tubes are leaded up to vibrate. A very large number of specific parameters have to be considered while studying this configuration. Main variables used in this paper are depicted in Table (1): Classically, the motion equation of one tube is

Variable	Definition
ρ	Fluid density ($kg.m^{-3}$)
μ	Fluid dynamic viscosity ($kg.m^{-1}.s^{-1}$)
D	Diameter of one tube (m)
P	Step between two tube diameters (m)
$[M]$	Total mass matrix
$[C]$	Damping matrix
$[K]$	Stiffness matrix

Table 1: Main variables of the system

the following:

$$[M]\{\ddot{Q}(t)\} + [C]\{\dot{Q}(t)\} + [K]\{Q(t)\} = \{F_{\text{ext}}\} \qquad (1)$$

where $\{Q(t)\}$ represents the motion generalized coordinates vector, $\{F_{\text{ext}}\}$ is the fluid forces vector to which the tube is subjected.
Before presenting different tubes excitation phenomena, it is necessary to redefine dimensionless numbers that govern the fluid flow, the Reynolds number and the Strouhal number. These dimensionless numbers are respectively defined as:

$$\mathcal{R}_e = \frac{\rho U_p D}{\mu} \; ; \; S_t = \frac{f_s D}{U_p} \qquad (2)$$

The step fluid velocity U_p takes into account the tube confinement. It is defined as $U_p = U_\infty \dfrac{P}{P-D}$ where U_∞ is the equivalent mean flow velocity which would have been imposed in an infinite domain. f_s is the vortex-shedding frequency, when vortices appear behind the tube.

Four vibratory excitation mechanisms are susceptible to exist under transversal flow: turbulent excitation, vortex-induced vibration, acoustic resonance and fluid-elastic instability. Fluid-elastic instability is the most spectacular vibratory excitation phenomenon [22][23]: it leads to a very quick ruin of the tubes that have been

excited. For theses grounds, researchers particularly focused on this mechanism in order to avoid it at all costs. A very large number of models, empirical or semi-empirical, have been proposed in the hope of avoiding such a situation. But, flow passing a tube bundle is a system containing a very high number of degrees of freedom, so a precise analytical description of exciting efforts is not possible; moreover, several modes can be excited, considering relatives cylinders motions. For each vibration mechanism, experimental data have been collected and exploited by various authors in order to define criteria to respect [6][24][25]. Sometimes, semi-analytical models have been developed, particularly in the case of the fluid-elastic instability phenomenon; see [23] for example. Moreover, CFD models have been set up in order to avoid experimental costs and to observe a large number of parameters. Fluid-elastic instability stays very hard to model because of the number of parameters that are involved. The numerical modelling of interactions between fluid and structure motions is still a challenge in such a configuration, because a complete numerical resolution of the fluid-structure interaction in a tube bundle in functioning regime cannot be carried out. In this context, the use of Reduced Order Models (ROM) can be a solution to achieve the realization of such a study. A ROM allows solving a problem which formulation contains the bulk of the system information with a reduced number of degrees of freedom. In the framework of fluid dynamics studies, the criterion that ensures the fact that "the bulk of the system information" is kept can be an energetic criterion. Using this criterion, the optimal approach is the well known Proper Orthogonal Decomposition (POD). This method is the subject of next section; its potential application for the study of fluid-structure interactions in tube bundles is also developed.

3 Proper Orthogonal Decomposition (POD)

In classic computational fluid dynamics studies, approximated Navier-Stokes equations are computed on a bi-dimensional of three-dimensional domain Ω for a time interval $[0, T]$. In the case of a large three-dimensional domain, and if the flow is turbulent, calculation times can be very long. Moreover, if a parametric study has to be set up, it is necessary to lead as many calculations as there are values of the parameter in question to test. The Proper Orthogonal Decomposition allows saving calculation time on computations, and provides a projection basis that can be reused in parametric studies: in an industrial context, theses advantages have to be taken into account. Proper Orthogonal Decomposition has notably been introduced by Lumley [26] within the framework of coherent structure extraction of turbulent flows. A rigorous description of POD can be found in [18] for example; a large amount of domains are interested in using POD techniques, see [21], [16], [27] for example. Here we briefly present the POD formulation. Let us consider a domain Ω of the set of all real numbers and a time interval $[0, T]$ where T is a real maximal date. Spatial and time variables are respectively $x \in \Omega$ and $t \in [0, T]$. Let $v(x, t)$ be the unknown field, for example the velocity field (unknown of Navier-Stokes equations), with $v(x, t) \in H(\Omega, T)$, H is a Hilbert space. Proper Orthogonal Decomposition consist in determining a determinist basis $\{\Phi_n\}_{n=1,..,N}$ of functions which give the optimum representation of the field $v(x, t)$. N is the size of the POD basis. A practical approach of POD has been proposed by Sirovich [28], it is called Snapshot POD: this method is based on making the most of samples of experimental or numerical data. Let consider M snapshots of the velocity field $v(x, t)$ (these snapshots can be equally taken from an experimental or numerical set), these snapshot have been sampled during a period T. Snapshot POD consist in solving the following eigenvalue problem:

$$\sum_{k=1}^{M} \frac{1}{M} \big(v(t_i), v(t_k)\big)_{L^2(\Omega} A_k = \lambda A_i \qquad (3)$$

For each $i = 1, ..., M$, where λ contains eigenvalues. Each element of the POD basis is a linear combination of snapshots, coefficients are A_n^k, $n = 1, ..., N$:

$$\Phi_n(x) = \sum_{n=1}^{M} A_n^k v(x, t_n) \qquad n = 1, ..., N \qquad (4)$$

The POD basis $\{\Phi_n\}_{n=1,..,N}$ has interesting characteristics: it is orthonormal and if we study an incompressible flow, each element of the basis (each POD mode) satisfies the incompressibility condition as well as the boundary conditions of the problem. For a given $n \in [1, 2, ..., N]$, the energetic contribution of the POD mode Φ_n is captured by the corresponding eigenvalue λ_n and the eigenvalues are ranked in descending order $(\lambda_1 > \lambda_2 > ... > \lambda_N)$. Thus, the Proper Orthogonal Decomposition is optimal in an energetic sense. When POD modes $\{\Phi_n\}_{n=1,..,N}$ are determined, a low order dynamical system is solved. For that, the partial differential equations are projected on the POD basis constructed for the field $v(x, n)$. Then, a system of ordinary differential equations, which size N^* is less or equal to the POD basis size, is obtained. To determine this size N^*, an energetic criterion is used, based on eigenvalues of the problem; then the POD basis is truncated to N^* modes.

4 Tube bundle configuration

A tube bundle configuration is then proposed in order to be closer to the problem we are interested in. However, the chosen configuration remains simple: a 2D domain and only one tube and its neighbors are considered, with periodic boundary conditions. Thus, the domain is representing an infinite regular tube bundle. Reynolds number of this case is $\mathcal{R}_e \simeq 2600$. First, the central tube remains fixed. Figure (1) gives the global fluid velocity flow for two different dates in the time interval $[0, T]$, and Figure (2) shows vorticity and stream lines that enhance recirculation zones. The case where the

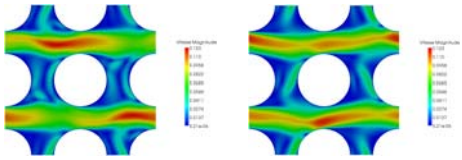

a) $t = 40.05s$ b) $t = 41.05s$

Figure 1: Snapshots of global velocity field in the tube bundle configuration

central tube is allowed to move in transverse direction has also been treated. Figure (3) represents the central tube displacement along y-direction, *i.e.* the cross-flow

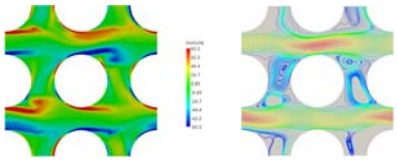

a) Vorticity b) Stream lines

Figure 2: Recirculation zones in fluid domain

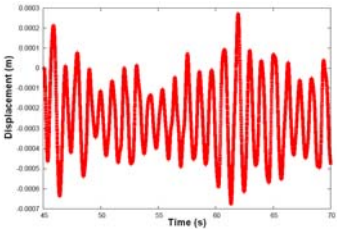

Figure 3: Temporal evolution of the central tube displacement along y-direction.

direction. Only the fixed case has been treated with the POD approach. The fluid-structure interaction with model reduction will be implemented in a future work. For the moment, for either fixed or moving configuration, no turbulence model has been considered. One of the improvements for the present study will thus consist in the use of a model that could better represent the physics of the phenomenon. Thus, POD method has been implemented on the fixed configuration; first POD modes magnitude can be observed on Figure (4). When

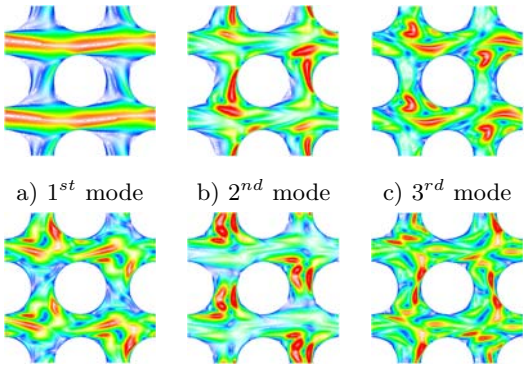

a) 1^{st} mode b) 2^{nd} mode c) 3^{rd} mode

d) 4^{th} mode e) 5^{th} mode f) 6^{th} mode

Figure 4: First POD modes for instantaneous flow field in fixed tube bundle configuration

POD modes are obtained, the following step is to project Navier-Stokes equations on these POD modes for the present tube bundle configuration and compare the fluid flow field obtained after projection to the original set of snapshots. From now on, the fluid flow configuration obtained thanks to the complete calculation is considered as a reference, even if it is not representing a real configuration. The important part of the present work is to check the POD reduced order model efficiency to reproduce a velocity field. A future work will consist in working on cases that can be compared to literature, in order to check if the complete calculation of the flow is correct. To the authors' knowledge, present configuration has not been numerically studied (inline 2D square array of fixed tubes at Reynolds number $\mathcal{R}_e \simeq 2600$). However, the CFD code used in this study, *Code_Saturne* [29], has been validated for fluid-structure interactions in various tube bundle configurations; see [30][10][31]. Time coefficients obtained thanks to a direct POD computation are constructed knowing POD modes and velocity field from the complete calculation:

$$a_n(t) = \big(v(x,t), \Phi_n(x)\big)_{L^2(\Omega)} \quad \forall n = 1, ..., N^* \tag{5}$$

Using incompressible Navier-Stokes equations:

$$\begin{cases} \dfrac{\partial v}{\partial t} + (v \cdot \nabla)v &= -\dfrac{1}{\rho}\nabla p + \nu \Delta v \\ \nabla \cdot u = 0 \end{cases} \tag{6}$$

where p is the pressure field and ρ, ν respectively flow density and cinematic viscosity. Low-order dynamical system obtained from the projection on the POD basis is:

$$\begin{aligned} \frac{da_i}{dt} = &- \sum_{n=1}^{N^*} \sum_{m=1}^{N^*} a_n(t) a_m(t) B_{nmi}(x) \\ &- \nu \sum_{n=1}^{N^*} C_{ni}(x) a_n(t) - D_i(x) \end{aligned} \tag{7}$$

for each $i = 1, ..., N^*$, with spatial coefficients B, C, D defined in Table (2); $\mathbf{n}$ is the unit vector normal to the fluid-structure interface. Coefficient D cannot be calculated through the reduced-order model, since information is only given for the velocity field. Thus, it is necessary to model this coefficient. Various solutions exist to obtain the new pressure field. In this paper, coefficient D has not been modelled yet; it is a short-term perspective for our future work. Figure (5) represents the comparison between the fluid velocity field from the complete calculation and the fluid velocity field obtained after the projection of Navier-Stokes equations on the POD basis on the same time period. 1000 snapshots have been taken to constitute the data sample on one pseudo-period of the velocity signal. The POD basis is constituted of $N^* = 20$ modes. A stabilization technique has been used for the dynamical system with an additional viscosity, which value is adapted to the projection on each POD mode, as proposed in [13], in order to improve the system response. Observation of Figure (5) shows that the reduced-order model gives satisfying results in the reconstruction of the velocity flow field for the fixed tube bundle configuration. The challenge now consists in treating the case of a bundle which tubes are allowed to move. As the Proper Orthogonal Basis is fully spatial and based on time snapshots, its use within a fluid-structure interaction resolution is not immediate. Indeed, if the numerical sample from which the snapshots are extracted has been obtained thanks to a moving mesh technique, the construction of the POD basis has no sense, since the POD modes are not time-dependants. Thus, in the case

Coefficient	Definition
B_{nmi}	$\big((\Phi_n \cdot \nabla)\Phi_m, \Phi_i\big)_{L^2(\Omega)}$
C_{ni}	$\big(\nabla\Phi_n, \nabla\Phi_i\big)_{L^2(\Omega)}$
D_i	$\frac{1}{\rho}\big(p, \Phi_i \cdot \mathbf{n}\big)_{L^2(\partial\Omega)}$

Table 2: Spatial coefficients of the POD reduced model for incompressible Navier-Stokes equations

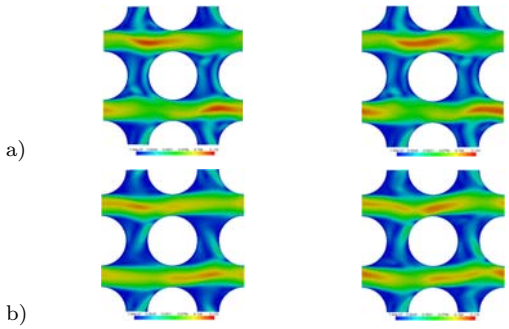

Figure 5: Comparison between global velocity field obtained with a complete calculation vs. the reduced-order model solution at a) t= 40.042 s and b) t = 40.802 s.

of fluid-structure interaction problems, an extension of the Snapshot POD is necessary. This has been proposed by Liberge and Hamdouni [16] who propose to work on a static spatial domain using a projection of snapshots. This method will be applied to the tube bundle configuration in a future work.

5 Conclusion

In this paper, the crucial problematic of vibratory excitation of a heat exchanger tube bundle is presented. Fluid-elastic instability is one of the most violent vibration mechanisms and a lot of studies have been led in order to define the critical fluid velocity and avoid such a phenomenon. This problematic is well known but not well understood. A way to improve our comprehension of tube bundle vibrations is to work with reduced order models (ROM). The most widespread ROM method, called Proper Orthogonal Decomposition (POD) and its properties are briefly presented. First applications to the tube bundle are proposed; future work will consist of taking into account the fluid-structure interaction thanks to Liberge et al. works [16] and modelling the pressure term.

References

[1] Bendjeddou Z. *Simulation numérique de vibrations induites par écoulement dans un faisceau de tubes.* Thèse de doctorat, Université de Lille, 2005.

[2] Chen S.S. *Flow Induced Vibrations of Circular Cylindrical Structures.* Hemisphere, 1987.

[3] Gorman D.J. Pettigrew M.J. Vibration of heat exchanger tube bundles in liquid and two-phase cross flow. *Flow-Induced Vibration Design Guidelines*, 52:89 – 110, 1981.

[4] Pettigrew M.J. Rogers R.J., Taylor C. Fluid effects on multispan heat exchanger tube vibration. In *Pressure Vessels & Piping, San Antonio.*, 1984.

[5] Bressler M.M. Blevins R.D. Acoustic resonances in heat exchangers, part ii: Prediction and suppression of resonance. *Journal of Pressure Vessel Technology*, 109:282–288, 1987.

[6] Chen S.S. Instability mechanisms and stability criteria of a group of circular cylinders subjet to cross-flow. Part I: Theory ; Part II: Numerical Results and Discussion. *Journal of Vibration, Acoustics, Stress and Reliability in Design*, 105:51–58, 1983.

[7] Jendrzejczyk J.A. Chen S.S. Experiments on fluid elastic instability in tube banks subjected to liquid cross flow. *Journal of Sound and Vibration*, 78:355–381, 1981.

[8] Taylor C.E. Pettigrew M.J. Fluidelastic instability of heat exchanger tube bundles: Review and design recommendations. *Journal of Pressure Vessel Technology*, 113:242–256, 1991.

[9] Taylor C.E. Pettigrew M.J. Vibration analysis of shell-and-tube heat exchangers: an overview - part 1: flow, damping, fluidelastic instability. *Journal of Fluids and Structures*, 18:469–483, 2003.

[10] Huvelin F. *Couplage de codes en interaction fluide-structure et applications aux instabilités fluide-élastiques.* Thèse de doctorat, Ecole doctorale des Sciences Pour l'Ingénieur de Lille, 2008.

[11] Abouri D. Sigrist J.F. Numerical simulation of a non-linear coupled fluid-structure problem with implicit and explicit coupling procedures. In *Pressure Vessel and Piping Conference, Vancouver, 25 - 28 July*, 2006.

[12] Lesoinne M. Farhat C. Improved staggered algorithms for the serial and parallel solution of three-dimensional non-linear transient aeroelastic problems. *AIAA Journal*, 182:1774–1757, 1996.

[13] Cazemier W. *Proper Orthogonal Decomposition and low dimensional models for turbulent flows.* Thèse de doctorat, Groningen University, Holland, 1997.

[14] Sagaut P. Couplet M., Basdevant C. Calibrated reduced-order pod-galerkin system for fluid flow modelling. *Journal of Computational Physics*, 207:192–220, 2005.

[15] Païdoussis M.P. Amabili M., Sarkar A. Reduced-order models for nonlinear vibrations of cylindrical shells via the proper orthogonal decomposition method. *Journal of Fluids and Structure*, 18:227–250, 2003.

[16] Hamdouni A. Liberge E. Reduced order modelling method via proper orthogonal decomposition (pod) for flow around an oscillating cylinder. *Journal of Fluids and Structures*, 26:292–311, 2010.

[17] Shyy W. Utturkar Y., Zhang B. Reduced-order description of fluid flow with moving boundaries by proper orthogonal decomposition. *International Journal of Heat and Fluid Flow*, 26:276–288, 2005.

[18] Berkooz G. Holmes P., Lumley J.L. *Turbulence, Coherent Structures, Dynamical Systems ans Symmetry.* Cambridge Monographs on Mechanics, Cambridge University Press, 1996.

[19] Volkwein S. Kunisch K. Galerkin proper orthogonal decomposition methods for parabolic systems. *Numerische Mathematik*, 40:117–148, 2001.

[20] Païdoussis M.P. Amabili M., Sarkar A. Experimental and numerical pod study of the coanda effect used to reduce self-sustained tones. *Mechanics Research Communications*, 31:105–120, 2004.

[21] Lesoinne M. Lieu T., Farhat C. Reduced-order fluid/structure modeling of a complete aircraft configuration. *Computer Methods in Applied Mechanics and Engineering*, 195:5730–5742, 2006.

[22] Blevins R.D. Fluidelastic whirling of a tube row. *ASME Journal of Pressure Vessel Technology*, 96:263 – 267, 1974.

[23] Price S.J. A review of theoretical models for fluidelastic instability of cylinder arrays in cross-flow. *Journal of Fluids and Structures*, 9:3147–3170, 2001.

[24] Weaver D.S. Lever J.H. On the Stability of Heat Exchanger Tube Bundles, Part I: Modified Theoretical Model. *Journal of Sound and Vibration*, 107:375–392, 1986.

[25] Taylor C.E. Pettigrew M.J. Vibration analysis of shell-and-tube heat exchangers: an overview - part 2: vibration response, fretting-wear, guidelines. *Journal of Fluids and Structures*, 18:485–500, 2003.

[26] Lumley J.L. The structure of inhomogeneous turbulence. In A.M. Yaglom and V. I. Tatarski, editors, *Atmospheric Turbulence and Wave Propagation*, pages 166–178. 1967.

[27] Verdon N. *Un système dynamique d'ordre réduit basé sur une approche APR-POD pour l'étude de l'interaction écoulement turbulent-particules.* Thèse de doctorat, Université de La Rochelle, 2007.

[28] Sirovich L. Turbulence and the dynamics of coherent structures, parts I-III. *Quarterly of Applied Mathematics*, 45:561–590, 1987.

[29] Sakiz M. Archambeau F., Mechitoua N. *Code_Saturne* : a finite volume code for the computation of turbulent incompressible flows - industrial applications. *International Journal of Finite Volumes*, 1, 2004.

[30] Laurence D. Benhamadouche S. Les, coarse les, and transient rans comparisons on the flow across a tube bundle. *International Journal of Heat and Fluid Flow*, 24:470–479, 2003.

[31] Souli M. Longatte E., Bendjeddou Z. Methods for numerical study of tube bundle vibrations in cross-flows. *Journal of Fluids and Structures*, 18:513–528, 2003.

CHIMERA METHOD APPLIED TO THE SIMULATION OF STATIC AND MOVING CONFINED OBJECTS

Thibaut Deloze[1], Yannick Hoarau[1] and Jan Dušek[1]

[1] Institut des Mécaniques des Fluides et des Solide (IMFS)

Université de Strasbourg 2 rue de Boussingault, F-67000 Strasbourg

Abstract

We have developed at IMFS a three-dimensional parallel automatic overlapped grid method to solving steady and unsteady viscous flow. The finite-volume Navier-Stokes solver used, is based on the dual time-stepping artificial compressibility scheme. Overlapped grids are used to discretize complex wall confined geometries. A criterion based on the local nearest wall distance allows to account for multiple overlapping. The communication at the interface of overlapped grids is provided by interpolation in buffer layers. The chimera method has been applied to study the flow around confined bodies: a 2D static cylinder in a channel, a sphere uniformly translating near a wall or in a tube and a 2D cylinder falling in a channel.

1 Solution Method

We have implemented the chimera method in our Navier-Stokes Multi-Block (*NSMB*) code [1, 2, 3]. The NSMB code solves the compressible Navier-Stokes equations using a finite volume formulation on Multi-Block structured grids. Various spatial discretization schemes are available like Jameson's central difference [4], Roe [5] or AUSM+ [6]. The time integration is based on the full matrix implicit LU-SGS (Lower-Upper Symmetric Gauss-Seidel) method and on the dual-time stepping. In the present work, the artificial compressibility method [7] is employed. NSMB is parallelized using the Message Passing Interface.

The chimera method is based on the management of independent overlapped grids. It significantly simplifies the generation of meshes. This method provides a good alternative to unstructured grids. The principle is to decompose any complex geometry into simple sub-domains independently meshed with curvilinear grids. Beyond simplifying the mesh generation, this technique offers a powerful and simple solution to manage moving bodies.

The pioneers of the chimera method were Benek et al. [8]. The huge possibilities offered by this approach explain its successful use in many and diverse applications like high-speed reaction flow [9, 10, 11], blood flow [12], combustion [13], aerodynamics [14, 15, 16, 17, 18, 19, 20], flow around ships [21], separation of the spacecraft orbiter from boosters [22] or aerodynamic noise [23]. It is associated with other numerical tool to increase efficiency (such as Automatic Mesh Refinement (AMR) coupled with chimera method [24] for example).

In NSMB, the chimera method follows four main steps described here :

- 1^{st} *step :* the overlapped cells are detected based on their coordinates.
- 2^{nd} *step :* the nature of the overlapped cell is determined. Following [25], three kinds of overlapped cells exist :
  a) Calculated cells : the values come from the resolution of the Navier-Stokes equations.
  b) Interpolated cells : the flow values are obtained by interpolation on grids where the governing equations are solved.
  c) Hole cells (or blanked/masked cells) : these values are never used in the discretization scheme nor in the overlapped boundary conditions so they are not interpolated nor calculated.
- 3^{rd} *step :* the interpolations parameters are computed.
- 4^{th} *step :* the values are interpolated.

These steps can be grouped into two categories: the first one includes the steps 1 to 3 and represents the chimera set-up. During these steps, the grids are analysed and the overset parameters are defined. These steps depend only on the grid definition. The second category includes the 4^{th} step and represents the communication itself. For static grids, the meshes do not change and the chimera set-up needs to be performed only once. In case of relative grid motion, the modification of the coordinates requires a repetition of chimera set-up. The static and mobile cases can be studied in the same way but a particular attention on the computation time of the chimera set-up is required for moving grid. These steps are now more detailed :

Detection of overlapped cells

The search of overlapped cells is based on a test of inclusion on the coordinates. In order to accelerate the search, the mapping of coordinates in a virtual uniform Cartesian grid is performed. This method is well known as the *bucket method* [26, 27, 28]. An inverse mapping algorithm creates an index array that link virtual grid to the real coordinates. The search begins on the virtual grid and it continues on the physical associated grid points. The creation of link array is time consuming but the gain in the research is significant (at least a factor 20).

Another issue concerns the points that are inside a solid body. In this case, the cells are not detected as overlapped cells. To remove these cells, two methods are implemented: for simple cases (cylinder, sphere) we use an analytical function and for general cases, for more

complex geometry we compute the dot product of the vector from the nearest wall cell center to cell center and the vector of the associated wall normal vector. If the dot product is negative, the cell is in the solid region, otherwise the cell is out of the solid region. The general method is 30 times more expensive than the first one for the configuration of a sphere in a tube, with 6 millions of cells and 65 000 wall cells.

Determination of the nature of overlapped cells

The second step of the chimera method is the definition of the nature of the overlapped cells (calculated, interpolated or hole). In this step, among several overlapped cell, the best candidate to predict the flow state (calculated cell) and to give the flow solution to the other cells (interpolated cells) is chosen. The criterion that justifies the choice is based on the best resolution of the physical problem. We distinguish four techniques based on the criteria associated to the following quantities: user-defined grid ranking, user-defined cell quality, cell size, nearest local wall distance.

For simple overset, the definition on an overlapped hierarchy of each block is enough for the cell type selection. All the cells of the highest ranking of the grid are defined as calculated cells. This solution is simple and fast but not suitable for complex overlapped layers where the definition of chimera grid ranking given by the user is then needed. Based on the fact that the cell size is a criterion indicating the best discretization, Siikonen et al. [28] or Liao et al. [29] justify this choice by assigning the *calculated cells* type to the smallest ones. This criterion is locally adapted, automatic and requires no user input. A third criterion is added to the previous one and based on a user-defined cell quality. This way the user can force a specific kind of cell (calculated or interpolated) by associating to this cell a high quality value. This technique can force cell type by protecting or immunising specific cells but the user input is binding and does not follow the grid movement. The cell size in the wall-normal direction was introduced by Landmann [25]. The selection use the intersection segment between normal nearest wall and cell boundary. This technique is fully automatic and it is based on an important physical quality: the boundary layer. This test requires to search for the nearest wall and to calculate the intersection for each cell. In order to find a lighter, accurate and automatic criterion, we developed a similar criterion based on the distance from a cell to the nearest local wall. The nearest local wall is the wall in the same block where the cell is defined (Figure (1)). With this criterion, the overlapped cell with the smallest local near wall distance is calculated and the others are interpolated. This approach guarantees the resolution of Navier-Stokes equations in the nearest wall region and consequently each boundary layer is accurately computed. Moreover, this technique is based on the local wall distance and this quantity does not change with moving grid (an update is needed only for deformed meshes) whereas the criterion based on the wall normal intersection need an update after each grid movement.

In the case of the sphere in a circular tube, the criterion based on the cell size complicates the generation of the mesh. The same problem may be encountered in the configuration of a sphere near a plane wall. The cell aspect ratio of the near wall mesh is not the same as that of the spherical wall mesh and the cell volume is very difficult to control. In our case of a sphere in a tube with a cylindrical grid overlapped by a spherical grid, the criterion based on the volume does not give a proper solution. The new criterion based on the local near wall distance give the best answer. The Figure (2) represents the visualisation of the calculated cells in the 3 planes crossing the sphere centre for various criteria.

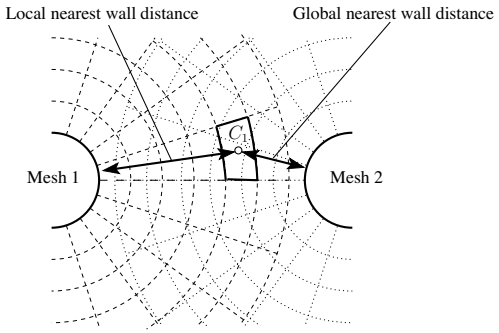

Figure 1: Definition of local nearest wall distance and global nearest wall distance for the cell C_1 of the mesh 1 in the configuration of two overlapped polar meshes.

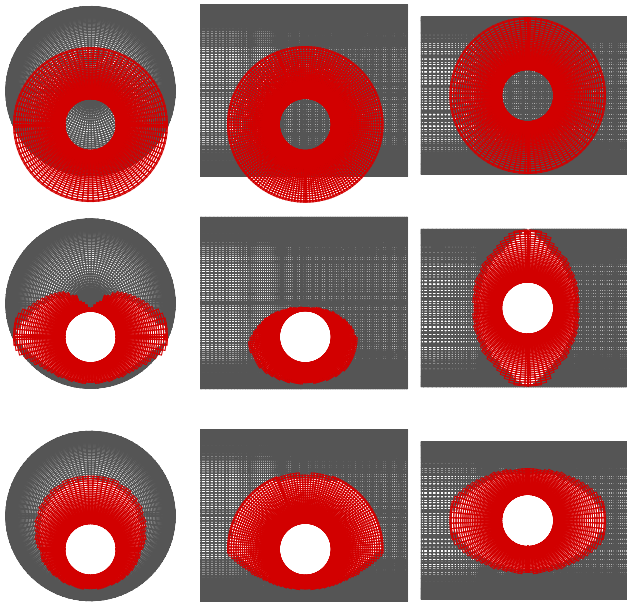

Figure 2: Visualisation of the calculated cells for the chimera cell selection before cell selection (1^{st} row), using cell volume criterion (2^{nd} row) and using the nearest local wall distance criterion (3^{rd} row) for the cross section of the tube (1^{st} line), the streamwise plane in the symmetric plane (2^{nd} line) and streamwise plane perpendicular to the symmetric plane (3^{rd} line)

Interpolation

The interpolation is a key element of the chimera method. It allows the transfer of flow information between overlapped grids. In NSMB, the whole state vector ($W = (p, \rho u, \rho v, \rho w)^T$ for the artificial preconditioned system) is interpolated and three interpolations are implemented: the trilinear, the tetravolumic and the weighted inverse distance interpolations.

The weighted inverse distance interpolation is based on the distance between the points. Its implementation is simple and the stencil of points is very flexible. The

formula used is given by the following relation :

$$f_M = \frac{\sum_{i=1}^{N} \frac{f_i}{d_i^\alpha}}{\sum_{i=1}^{N} \frac{1}{d_i^\alpha}} \quad (1)$$

where N is the number of the stencil points, f_i the value at the point i, α is the weighting exponent (in our case equal to 2) and d_i is the distance from the stencil point i to the interpolation point M.

The second interpolation is the tetravolumic interpolation based on the tetrahedral volumes composed by the four nearest cell centres. The interpolation weights are given by the opposite of the tetrahedral volume. For the two-dimensional example of the Figure (3), the formula is given by :

$$f_M = \sum_{i=A,B,C} W_i f_i$$
$$\text{with } W_A = \frac{V_{BCM}}{V_{ABC}}, W_B = \frac{V_{ACM}}{V_{ABC}} \text{ and } W_C = \frac{V_{ABM}}{V_{ABC}}$$

with W the weight of the interpolation and V_{ACM} the volume of the triangle (ABC). In three dimensions, the triangle volume is replaced by the tetrahedral volume.

The last interpolation is the trilinear one. We use a trilinear interpolation based on a linear interpolation in each direction. In the two-dimensional example of the Figure (3), the first linear interpolation yields the values f_Q and f_P then a second linear interpolation provides f_M. In three-dimensions, three steps of linear interpolation are required.

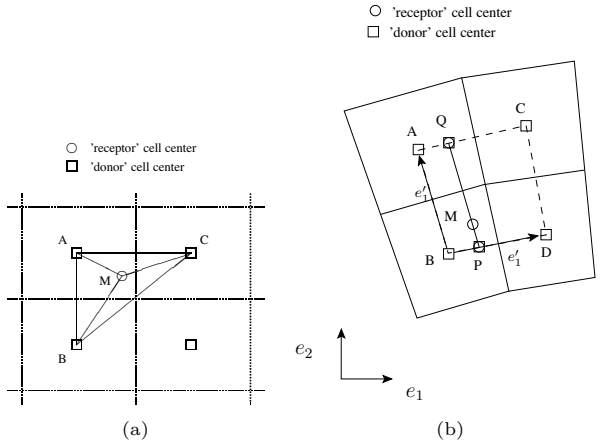

Figure 3: Schemes of the principle of the tetravolumic interpolation (a) and the trilinear interpolation (b).

2 Results on static objects

2.1 Cylinder in uniform translation parallel to the walls

The first study is about an uniform forced motion of a cylinder in a quiescent fluid between two plates. For the simulation, the plate walls are give the same velocity of the inlet velocity. Two distinct overlapped grid are used in this case: the first one is a polar mesh refined around the cylinder and the second is a Cartesian grid with refinement near the lateral walls. The upstream length L_u is equal to $10d$ where d is the diameter of the cylinder and the downstream length L_d is equal to $25d$. The number of cells is equal to 354 964 cells. The two plates are separated by $3.3d$.

Two parameters are studied, the distance L/d which represents the dimensionless distance between the bottom plate and the centre of the cylinder ($[0.6 - 1.65]$) and the Reynolds number ($[10 - 40]$ and 100).

For the steady flow, the same behaviour than the unconfined cylinder is found for the drag coefficient: it diminishes with increasing Reynolds number and for a fixed Reynolds number, it increases with L/d. The drag of the confined cylinder is much higher than the unconfined one. Concerning the lift and the torque coefficients, they are negligible for the free stream cylinder or when the cylinder is in the middle of the two plates but their values increases when L/d diminishes. This is due to the fact that the lower vortex behind the cylinder vanishes when the cylinder get close to the lower wall. At a fixed location, the lift and the torque decrease with increasing Reynold number. The torque coefficient is due entire to the viscous effect and naturally decreases with the increase of Reynolds number.

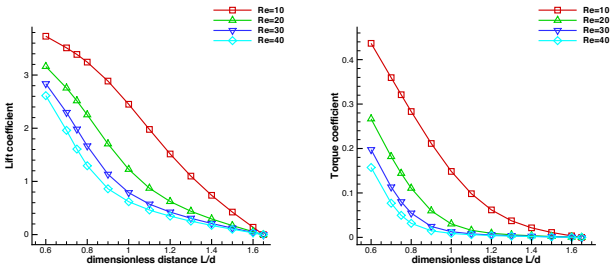

Figure 4: Influence of the dimensionless distance L/d number over the lift coefficient (left) and the torque coefficient (right).

Lei et al. [30] studied the vortex shedding suppression for flow over a circular cylinder near a plat boundary and find a critical distance where the unsteady state became steady. For the Reynolds number equal to 100, the critical distance between the centre of the cylinder and the wall is equal to $1.5d$. The main difference with our study is that in Lei et al. case there is only one bottom wall.

The vortex shedding suppression occurs for $L/d =]0.7 : 0.75[$. Versus dimensionless distance L/d, the amplitude of the variation of the drag coefficient increases until $L/d = 0.9$ and then decrease. The amplitude of the lift coefficient is bigger than the one of drag coefficient and the behaviour is increasing when L/d increases. The frequency of the vortex shedding is smaller near the wall than on the middle of the channel. Concerning the evolution of the Strouhal number (2.1), the wall proximity tends to slow down the vortex sheeding and the Strouhal shows a saturation for a distance to the wall L/d higher than 1.1.

2.2 Flow over a sphere translating along a plane wall

We now consider the configuration of an interaction between a sphere and a moving wall. We simulate the flow past a sphere in a uniform translation parallel to a plane wall which has been previously reported by Zeng et al. [31] and Takemura & Magnaudet [32]. The parameters for this configuration are the distance between the sphere centre and the wall (L/d) and the Reynolds number $Re = U.d/\nu$, with U the velocity of the sphere

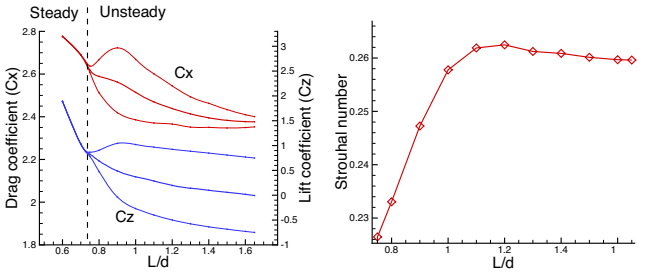

Figure 5: Mean, maximum and minum of the drag, lift coefficients and Strouhal number versus dimensionless distance L/d and for $Re = 100$.

translation and ν the viscosity of the fluid. The geometry is meshed with a first Cartesian grid, which is refined along the plane wall, and a second spherical one, which is refined near the sphere wall. The criterion for chimera cell selection is based on the definition of a boundary layer for the background grid where the cells are always calculated. Elsewhere the cells of spherical mesh are calculated. The motion of the sphere is implemented with the wall condition of the plate and with an inlet boundary condition. The mesh for parallel simulations is decomposed into 32 sub-blocks. The range of the Reynolds number is $10 \leq Re \leq 250$ and the studied distance is $L/d = 1$ and $L/d = 0.75$.

The presence of the plane wall breaks the axisymmetric geometry, and at all Reynolds numbers a lift force exists. Two mechanisms are the source of this force (Takemura & Magnaudet [32]): the first one is related to the strong interaction between the wall and the wake of the sphere. The Figure (6) shows the isovalues of the streamwise velocity in the wall normal plane for the case $Re = 200$ and $L/d = 1.00$. The distribution of the flow looses the up/top asymmetric and it results into a lift force directed away from the wall. The second mechanism is related to the high velocity in the gap associated to a low pressure. This behaviour gives a force with opposite direction (attractive force) to the first mechanism. The resultant force tends to push the sphere away from the wall. The streamlines plotted along the streamwise wall normal plane (Figure (7)) represents the vortex structure for $Re = 200$ and $L/d = 0.75$. The same case performed by Zeng et al. [31] is plotted sideline our results for comparison (Figure (7)). The overset border is not visible and proves one more time that the chimera communication is sufficient. Zeng et al. [31] found the same representation of the flow reproduced in Figure (7).

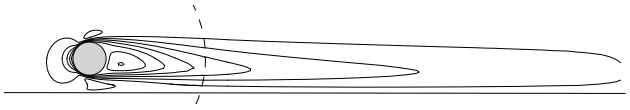

Figure 6: Isovalues of the streamwise velocity in the plane normal to the wall (-0.3 to 1.1 with a increment of 0.2)

The results on the aerodynamic coefficients are in good agreement with those of Zeng et al. [31] for both the drag and lift coefficients (Figure (8)). The differences between the results of Zeng et al. [31] and ours remain below 1%.

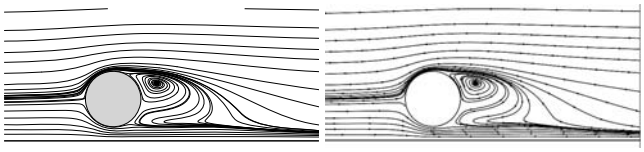

Figure 7: Streamlines in the plane normal to the wall for the case $Re = 200$, $L/d = 0.75$ for the present study (left) and extract to Zeng et al. [31] (right)

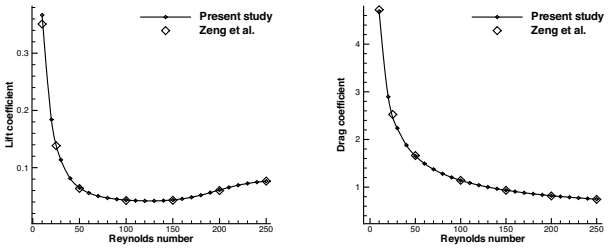

Figure 8: The drag and lift coefficient for L/d = 1.00 and versus Reynolds numbers

2.3 Flow over a sphere translating along a circular pipe

The last simulation on fixed objects consists in the study of the flow around a sphere in uniform translation along a tube. The translation is constant and it is parallel to the pipe wall. This study is similar to the sedimentation of a sphere in a tube. The parameters are the sphere diameter d, the tube diameter D, the velocity of the sphere U, the viscosity of the fluid ν, the smallest distance L between the centre of the sphere and the tube wall. This problem can be characterised by three dimensionless parameters: the diameters ratio (D/d), the Reynolds number $Re = Ud/\nu$ and the distance L/d. The range of the studied Reynolds number is $50 \leq Re \leq 350$ to stay in steady flow. Two distances L/d are considered, one correspond to the sphere on the tube axis ($L = D/2$) and the second is out the tube axis, $L/d = 1$. Two confinements are chosen ($D/d = 3.3$ and 5) and two distances L/d are considered.

Firstly, the configuration with the sphere out axis is treated. Like the sphere near a plane wall, the spatial configuration is non-axisymmetric that gives rise for all Reynolds number to a non axisymmetric flow. The visualisation of the velocity field shows a good continuity of the flow at the chimera border (Figure (9)). The downstream velocity is maximum in the narrow gap associated with a low pressure. This characteristic has already been observed in the last case of the sphere translating along a plane wall. This flow acceleration results to an attraction force of the sphere to the wall because of the low pressure area. But the asymmetric distribution of the vortex up/down confers to the sphere a more important force in the opposite direction. The resultant force is a repulsive one.

The value of the force in the tube is greater than the one near a plane wall (Figure (10)). This behaviour is not obvious but it can be explained by the tube confinement: the vortex behind the sphere is stronger and induce a

higher repulsive force. The pipe wall increase the drag coefficient. The lower is the diameter of the pipe, the more the drag coefficient is affected and increases. This behaviour is not surprising and the experimental observation shows the same effect on the sedimentation of a particle in a vertical pipe. For the effect on the lift force, the behaviour is more complex. The confinement and the proximity of the wall increases the lift force which corresponds to a repulsive force. The lift coefficient is composed by a viscous and a pressure part. For small Reynolds number ($Re \leq 100$), the viscous effect dominates and decreases with increasing Reynolds number. When the viscous part of the lift force does not dominate and the pressure effect increases, the lift force increases ($Re \geq 120$). The Hopf bifurcation appears for closer critical Reynolds number than the one described for non-confined sphere.

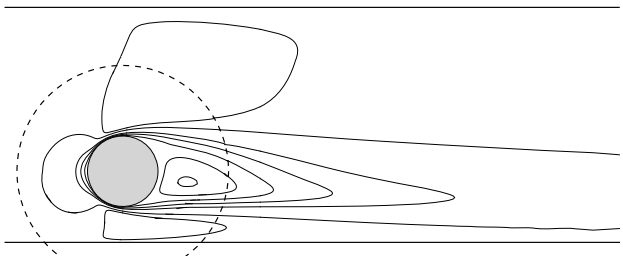

Figure 9: The isovalues of the velocity on the slide Oxy

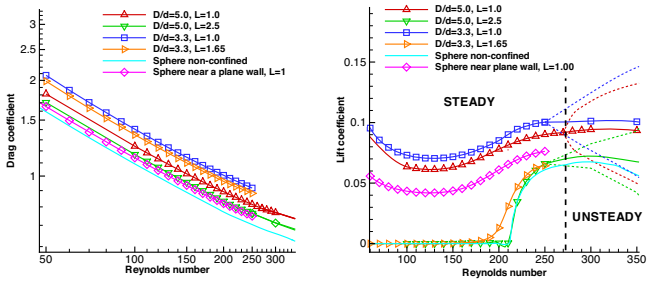

Figure 10: Drag and lift coefficient induced by the flow around a sphere

3 Free cylinder falling in a channel

In this section, the movement of a 2D cylinder falling in a channel is simulated with the chimera approach. The influence of the initial position and the Galileo number, defined as $Ga = \sqrt{\dfrac{gd^3\rho_f\left(\rho_b - \rho_f\right)}{\mu^2}}$ or $Ga = \sqrt{\dfrac{gd^3\rho_f\left(\beta - 1\right)}{\nu^2}}$ is studied. g is the gravity acceleration, ρ_f and ρ_b respectively the densities of the fluid and the body and μ the viscosity of the fluid.

The two fixed parameters are the diameter ratio (D/d) equal to 3.3 where D is the channel height and d the cylinder diameter, the density ratio ($\beta = \rho_f/\rho_b$) equal to 2. The varying parameters are the Galileo number Ga and the initial transverse position y_0. The range of the Galileo number studied is $151 \leq Ga \leq 300$. The results are compared to the simulation of a unconfined falling cylinder in order to determine the influence of the wall.

Trajectories

The following movement equation is solved and coupled with the Navier-Stokes equations :

$$\ddot{x}_i == g_i\left(1-\beta\right) + \frac{2\beta}{\pi}\,C_i \tag{2}$$

$$\ddot{\alpha}_i = \frac{16}{\pi}\,\beta\,C_{m,i} \tag{3}$$

The trajectory for $Ga = 200$ (Figure (11)) is different depending whether the cylinder is confined or not, and for the confined configuration, if the initial position is in the middle plane or not. For the unconfined falling cylinder, a deviation of the transverse position appears in the first part. In the second part of the trajectory, the transverse position oscillates around a value that is not equal to the initial transverse position. For the confined falling cylinder with $y_0 = 0$, the deviation doesn't exist and for the periodic pattern, the transverse oscillation is located around the initial value (i.e. the middle axis). For the confined falling cylinder with $y_0/d = -0.65$, the first part is different when the cylinder is placed symmetry axis. The second part of the periodic oscillation is similar to the one with $y_0 = 0$, with an oscillation around the middle axis and the same frequency and amplitude. Yu et al. [33] found the similar behaviour in the case of the sedimentation of a cylindrical particle in a channel. The first motion of the particle is the migration to the channel axis. This approach of the centerline is not monotone and Yu et al. [33] described this movement as a "wagging motion". They explain the variation by the vortex shedding under the critical Reynolds number.

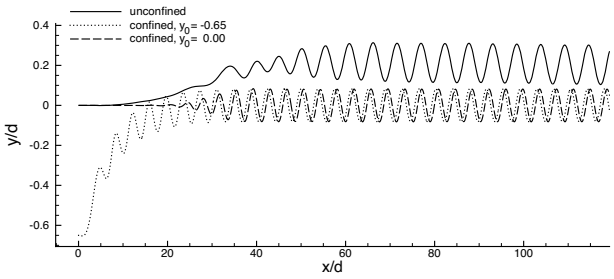

Figure 11: Trajectories for $Ga = 200$

The temporal variation of the velocity components is represented in Figure (12). The dimensional time (t^*) is non-dimensionalised with the terminal velocity U_t by the relation $t = t^* d/U_t$. The behaviour of the x-component is linear and dominated by the strong gravity effect. The y-component is dominated by the wake induced force. In this case, the Von Kármán vortex shedding produces a periodic oscillations. For $Ga = 200$, the amplitude of the transverse oscillation is equal to 0.09801 for unconfined configuration and 0.08155 for the both confined configurations. Those amplitudes are less than 3% of the distance between the channel walls. The confinement decreases the amplitude of the transverse oscillations but increases its frequency. We will discuss after the correlation between the Strouhal and the Reynolds number.

Moreover, the confinement fixes the axis of the oscillation to the centre axis between the two walls.

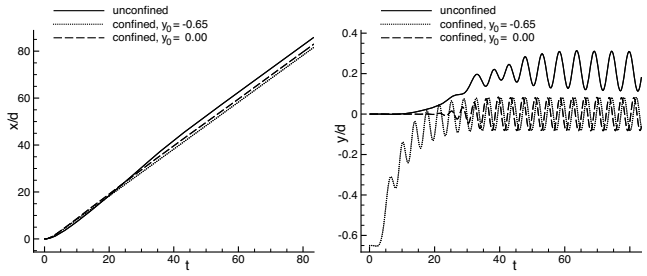

Figure 12: Components of the position x/d and y/d versus the dimensionless time for $Ga = 200$

Velocities of the cylinder

The velocity is represented by the Reynolds number $Re = U.d/\nu$, with ν the kinematic viscosity. The x-component of the velocity (gravity direction) is represented by Re_x and the y-component (transverse direction) by Re_y. The variation of Re_x is composed of three parts (Figure (13)). When dropped the cylinder has no velocity and the first part is an acceleration phase with a strong increase of the falling velocity. The second step, called over-shoot, is a phase during which the increase of velocity stops and even decreases due to the the onset of the vortex shedding. This over-shoot is more visible for the unconfined falling cylinder than for the confined configuration. The last phase of the motion is a periodic oscillation of the velocity about a constant mean value ($\overline{Re_x}$).

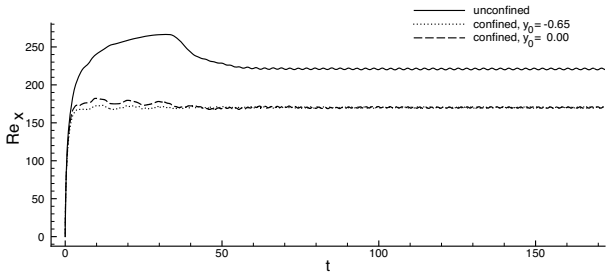

Figure 13: X-component of the velocity defined by $Re_x = U_x d/\nu$ versus dimensionless time for $Ga = 200$

The influence of the Galileo number on the mean terminal velocity and on its amplitude is represented in Figure (14). The amplitude of the oscillations of the velocity increases with the increase of the Galileo number in the unconfined case. To the contrary, for the confined falling cylinder, the amplitude of oscillations of the falling velocity does not increase with the increase of Galileo. The relation between the mean falling velocity and the Galileo number is practically linear. We found the relation $\overline{Re_x} = 1.092Ga + 2$ for the unconfined case and $\overline{Re_x} = 0.915Ga - 12$ for the confined cylinder. For the unconfined configuration, $Re > Ga$ and for the confined case $Re < Ga$.

The transverse velocity is represented by Re_y. The first observation is that its value is lower than 10% of the falling velocity. This velocity is just induced by the vortex shedding forces which are weaker than gravity

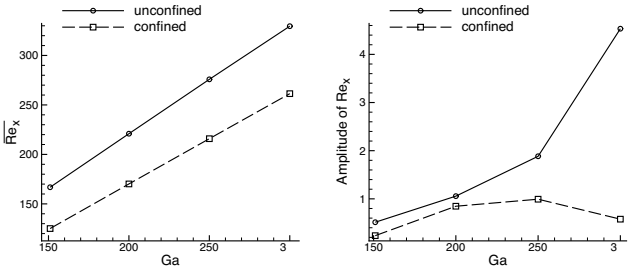

Figure 14: $\overline{Re_x}$ and amplitude of Re_x versus Galileo number for a confined and an unconfined falling cylinder and for $Ga = 200$

force. The Figure (15) show the time evolution of the transverse velocity for the confined and the unconfined cylinder with $Ga = 200$. The behaviour of the transverse velocity is similar for the unconfined cylinder and for the confined configuration with an initial position at tha middle axis. Oscillations increase progressively and these oscillations appear faster in the confined case. For the confined configuration with an initial position out the middle axis ($y_0/d = -0.65$), the oscillations appear immediately with an amplitude close to the final amplitude. The wall effect creates an asymmetric geometry, a powerful force appears, and the asymmetric geometry facilitates the onset of the vortex shedding.

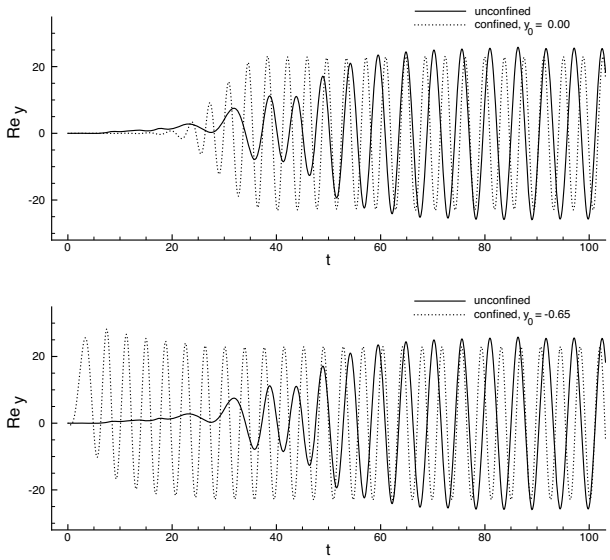

Figure 15: Y-component of the velocity defined by $Re_y = U_y d/\nu$ versus dimensionless time for $Ga = 200$

The evolution of Re_x and Re_y versus the transverse position y/d for the falling cylinder in the unconfined and confined cases for $Ga = 200$ during the periodic state is presented in (Figure (16)). The maximum of the transverse velocity appears when the cylinder is on the mean transverse position and the transverse velocity is equal to zero when the cylinder is at the extreme position of the motion.The behaviour of the falling velocity is opposite with a maximum velocity for the extreme position, and minimum velocity when the cylinder is at the mean position. The variation of the angular velocity is different and the maximum appears for 1/4 of the maximum displacement.

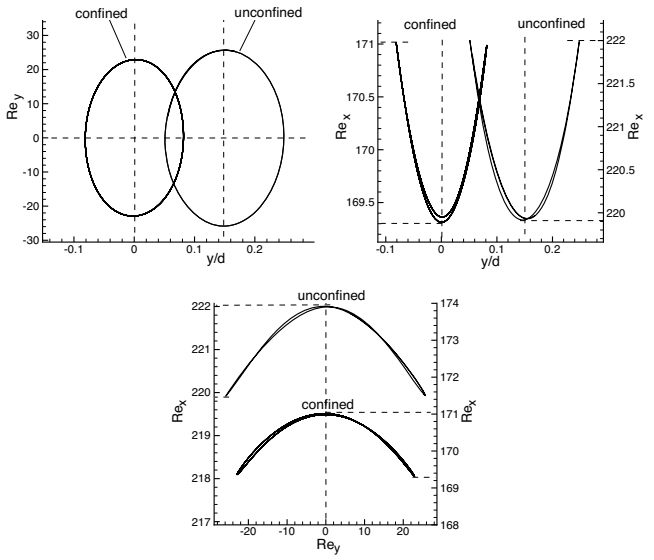

Figure 16: Relation between velocity (Re) and position (y/d) and between the translation velocities for $Ga = 200$

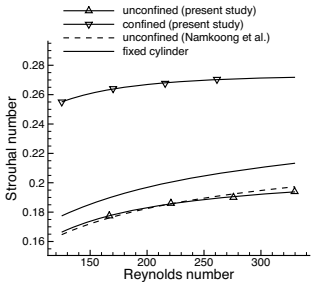

Figure 17: Data and fitted functions of the Strouhal number versus Galileo number

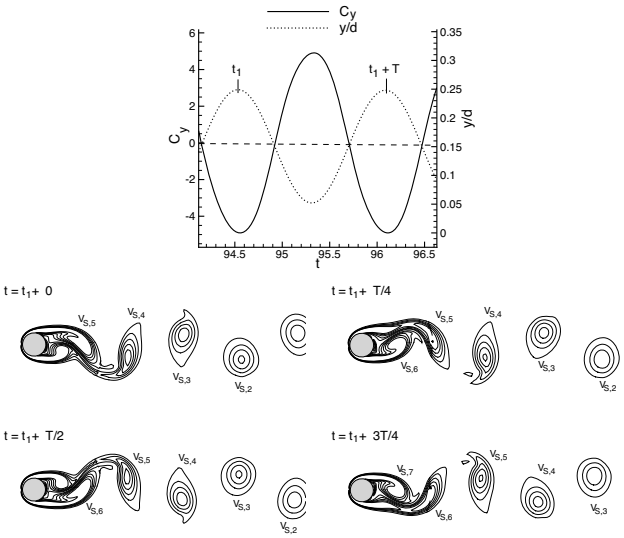

Figure 18: Isovorticities for unconfined falling cylinder and for $Ga = 200$

Frequencies of the falling cylinder

The frequency defined by the Strouhal number ($St = fd/U_x$) was first linked to the Reynolds number by Williamson et al. [34] for the fixed cylinder by the following function :

$$St = A + \frac{B}{\sqrt{Re}} + \frac{C}{Re} \tag{4}$$

This function can be simplified with $C = 0$ for the range of Reynolds number $Re < 188$. With the present results, the coefficients are determined and we have obtained the following coefficients :

$$\text{unconfined :} \qquad St = 0.2086 + \frac{0.0548}{\sqrt{Re}} - \frac{5.9004}{Re} \tag{5}$$

$$\text{confined :} \qquad St = 0.2527 + \frac{0.8581}{\sqrt{Re}} - \frac{9.3165}{Re} \tag{6}$$

$$\text{fixed cylinder :} \quad St = 0.27661 - \frac{1.1129}{\sqrt{Re}} - \frac{0.4821}{Re} \tag{7}$$

The fitted functions and the data are plotted in Figure (17). The behaviour of the the Strouhal number is well represented by the function [Eq. (4)]. The confinement accelerates the oscillation and the frequency is higher. The difference with the unconfined case is significant. The flow in the gap between the wall and the cylinder is more accelerated and drives the vortex out more rapidly.

Structure of the flow

The wake of the cylinder is due to the motion of the cylinder. The speed of the cylinder is such that the vortices at the rear of the cylinder are not steady but they are detached periodically resulting in the Von Kármán vortex shedding. This vortex shedding induces the oscillation of the position. In the unconfined case for $Ga = 200$, we choose the starting time t_1 when the cylinder is at the maximum transverse position and we examine the vortex structures over one period of oscillation (Figure (18)).

The transverse position is directly linked to the vortex shedding. At the time $t = t_1$, the vortex $V_{S,5}$ is ejected from the cylinder. This vortex is a clock-wise vortex with negative vorticity. At this time the lift is minimum. Then the vortex $V_{S,6}$ grows. It's a counter clock-wise vortex associated to positive vorticity and due to viscous effects it will attract the cylinder to it so that the cylinder will move to a negative y position. As a result of this positive vorticity the lift increases. At the time $t = t_1 + T/4$, the cylinder is at the axis. At the time $t = t_1 + T/2$ the vortex $V_{S,6}$ is ejected, the lift is maximum and the cylinder has reached its minimum position. The vortex $V_{S,7}$ grows. The negative associated vorticity will attract the cylinder to positive y positions. Again at $t = t_1 + 3T/4$ the cylinder crosses the y axis, the lift is zero.

4 Conclusion

We have implemented in our parallel Navier-Stokes solver a fast and efficient automatic chimera method for the simulation of static/moving complex geometries. We carried out a series of numerical test cases to validate the algorithm and to assess its feasibility in complex geometries. The computed results demonstrated that our method gives good results both for simple two-dimensional and three-dimensional complex confined configuration. The chimera method appears to be a

very simple and powerful tool to simulate flow around moving object. We are currently exploiting this solver on the simulation of free sphere falling in a tube.

The authors would like to thanks the national computing center CINES, the Direction Informatique of the University of Strasbourg and the Grid'5000 experimental testbed (being developed under the INRIA ALADDIN development action with support from CNRS, RENATER and several Universities as well as other funding bodies) for allowing us to use their computer.

References

[1] J. Vos, P. Leyland, P. Lindberg, V. Kemenade, C. Gacherieu, N. Duquesne, P. LÃűtstedt, C. Weber, and A. YtterstrÃűm. NSMB Handbook version 4.0. 1997.

[2] J. Vos, A. Rizzi, D. Darracq, and E. Hirschel. Navier-Stokes solvers in European aircraft design. *Progress in Aerospace Sciences*, 38:601–697, 2002.

[3] J. Vos, A. Rizzi, A. Orjon, E. Chaput, and E. Soinne. Recent Advances in aerodynamics inside the NSMB (Navier-Stokes Multiblock) Consortium. *AIAA paper*, 98-0225, 1998.

[4] A. Jameson. Analysis and design of numerical scheme for gas dynamics, 1 : artificial diffusion, upwind biased, limiters and their effect on accuracy and multigrid convergence. *Computational Fluid Dynamics*, 1995.

[5] P.L. Roe. Approximate riemann solvers, parameter vector and difference schemes. *J. of Comp. Phy.*, 43:357–372, 1981.

[6] M.-S Liou and C.J. Stephen. A new flux splitting scheme. *J. of Comp. Phys.*, 107:23–29, 1993.

[7] A.J. Chorin. Numerical solution of the navier-stokes equations. *J. Math. Computation*, 22:745, 1968.

[8] J. A. Benek, J. L. Steger, and F.C. Dougherty. A flexible grid embedding technique with application to the euler equations. *AIAA Paper*, 83-1944, 1983.

[9] W.D. Henshaw and D.W. Schwendeman. An adaptive numerical scheme for high-speed reactive flow on overlapping grids. *Journal of Computational Physics*, 191(2):420–447, 2003.

[10] W.D. Henshaw and D.W. Schwendeman. Moving overlapping grids with adaptive mesh refinement for high-speed reactive and non-reactive flow. *Journal of Computational Physics*, 216(2):744–779, 2006.

[11] AK Kapila, DW Schwendeman, JB Bdzil, and WD Henshaw. A study of detonation diffraction in the ignition-and-growth model. *Combustion Theory and Modelling*, 11(5):781–822, 2007.

[12] C. Kiris, D. Kwak, S. Rogers, and ID Chang. Computational approach for probing the flow through artificial heart devices. *Journal of biomechanical engineering*, 119:452, 1997.

[13] JY Tu and L. Fuchs. Calculation of flows using three-dimensional overlapping grids and multigrid methods. *International Journal for Numerical Methods in Engineering*, 38(2):259–282, 1995.

[14] PG Buning, IT Chiu, S. Obayashi, YM Rizk, and JL Steger. Numerical simulation of the integrated space shuttle vehicle in ascent. In *AIAA Atmospheric Flight Mechanics Conference, Minneapolis, MN*, pages 265–283, 1988.

[15] M. Hinatsu and JH Ferziger. Numerical computation of unsteady incompressible flow in complex geometry using a composite multigrid technique. *International Journal for Numerical Methods in Fluids*, 13, 1991.

[16] R.L. Meakin. Moving body overset grid methods for complete aircraft tiltrotor simulations. In *AIAA Computational Fluid Dynamics Conference, 11 th, Orlando, FL, Technical Papers. Pt. 2*, volume 6, 1993.

[17] D.G. Pearce, S.A. Stanley, F.W. Martin Jr, R.J. Gomez, G.J. Le Beau, P.G. Buning, W.M. Chan, I.T. Chiu, A. Wulf, and V. Akdag. Development of a large scale Chimera grid system for the space shuttle launch vehicle. In *AIAA, 31st Aerospace Sciences Meeting, Reno, NV*, volume 0533, 1993.

[18] R. Maple and D. Belk. A new approach to domain decomposition, the beggar code. *Numerical Grid Generation in Computational Fluid Dynamics and Related Fields, Pineridge Press Limited*, pages 305–314, 1994.

[19] D. Jespersen, TH Pulliam, and P. Buning. Recent enhancements to OVERFLOW. *AIAA paper*, 97–0644, 1997.

[20] R. L. Meakin. *Chapter 11 : Composite overset structured grids, in : Handbook of grid generation, J.F. Thompson, B.K. Soni and N.P. Weatherill.* CRC, 1999.

[21] Y. Tahara, R.V. Wilson, P.M. Carrica, and F. Stern. RANS simulation of a container ship using a single-phase level-set method with overset grids and the prognosis for extension to a self-propulsion simulator. *Journal of Marine Science and Technology*, 11(4):209–228, 2006.

[22] R.L. Meakin and N.E. Suhs. Unsteady aerodynamic simulation of multiple bodies in relative motion. In *AIAA Computational Fluid Dynamics Conference, 9 th, Buffalo, NY*, volume AIAA-89-1996, pages 643–657, 1989.

[23] G. Desquesnes, M. Terracol, E. Manoha, and P. Sagaut. On the use of a high order overlapping grid method for coupling in CFD/CAA. *Journal of Computational Physics*, 220:355–382, 2006.

[24] W.D. Henshaw and D.W. Schwendeman. Parallel computation of three-dimensional flows using overlapping grids with adaptive mesh refinement. *Journal of Computational Physics*, 227:7469–7502, 2008.

[25] B. Landmann and M. Montagnac. A highly automated parallel Chimera method for overset grids based on the implicit hole cutting technique. *International Journal for Numerical Methods in Fluids*, 2010.

[26] R.L. Meakin. A new method for establishing intergrid communication among systems of overset grids. *AIAA Paper*, 91-1586, 1991.

[27] H. Samet. *The design and analysis of spatial data structures*. Addison-Wesley, 1990.

[28] Timo L. Siikonen, Patrick P. Rautaheimo, and Esa J. Salminen. Numerical techniques for complex aeronautical flows. *European Congress on Computational Methods in Applied Sciences and Engineering ECCOMAS 2000*, 2000.

[29] Wei Liao, Jinsheng Cai, and Her Mann Tsai. A multigrid overset grid flow solver with implicit hole cutting method. *Computer Methods in Applied Mechanics and Engineering*, 196:1701 – 1715, 2007.

[30] C. Lei, L. Cheng, S.W. Armfield, and K. Kavanagh. Vortex shedding suppression for flow over a circular cylinder near a plane boundary. *Ocean Engineering*, 27:1109–1127, 2000.

[31] Lanying Zeng, S. Balachandar, and Paul Fischer. Wall-induced forces on a rigid sphere at finite Reynolds number. *J. Fluid Mech.*, 536:1–25, 2005.

[32] Fumio Takumura and Jacques Magnaudet. The transverse force on clean and contaminated bubbles rising near a vertical wall at moderate Reynolds number. *J. Fluid Mech.*, 495:235–253, 2003.

[33] Z. Yu, N. Phan-Thien, Y. Fan, and R.I. Tanner. Viscoelastic mobility problem of a system of particles. *Journal of Non-Newtonian Fluid Mechanics*, 104(2-3):87–124, 2002.

[34] CHK Williamson and GL Brown. A series in $1/\sqrt{}$ Re to represent the Strouhal–Reynolds number relationship of the cylinder wake. *Journal of Fluids and Structures*, 12:1073–1085, 1998.

A partitioned fluid-solid coupling scheme for numerical simulations of complex flow-structure interactions

Berland J.[1], Jus Y.[1], Longatte E.[1] and Baj F.[1]

[1] Laboratoire de Mécanique des Structures Industrielles Durables (LaMSID)

UMR CNRS/EDF/CEA 2832, Clamart, France

Abstract

The present paper presents a partitioned coupling procedure between a computational fluid mechanics solver and a computational solid mechanics solver in order to perform the calculation of fully-coupled fluid-solid systems. The fluid flow is governed by the incompressible Navier-Stokes equations and modeled using a fractional step scheme combined with a co-located finite volume method for space discretization. The motion of the fluid domain is accounted for by a moving mesh strategy through an Arbitrary Lagrangian-Eulerian (ALE) formulation. Solid dynamics is modeled by discrete or beam elements in the linear elasticity framework and systems are solved through a finite element method. The resulting strongly coupled fluid solid set of non linear equations is solved by means of a partitioned solution procedure. A fixed point method combined with an under-relaxation technique is designed to ensure the optimal convergence of the iterative procedure. The flutter phenomena of a flexible pipe conveying an internal fluid is numerically investigated to demonstrate the consistency of the present fluid-structure solver.

1 Introduction

Mechanical structures are, in many industrial applications, surrounded by complex turbulent highly energetic flows. Among others, tube bundles in heat exchangers [1], pipe systems [2] or buffeting airfoils [3] can undergo significant flow-induced loads causing possible vibrations and damages. Most of the predictive techniques available for these problems are semi-empirical models relying on experimental measurements. Alternatively, computational fluid dynamics now tends to encompass a large variety of flow phenomena and numerical simulations of turbulent motions along with a resolution of the structure dynamics are capable of providing comprehensive informations on fully coupled fluid-structure interaction phenomena. Such an approach is highly valuable and may shed a new light on the interplay between the turbulent flow development and the mechanical structure response [4, 5].

Solving a nonlinear fluid-structure problem is nonetheless a challenging task that inherits technicalities from both computational fluid dynamics and computational mechanics. Such calculations commonly relies on two main approaches: monolithic methods and partitioned coupling methods.

The monolithic methods treat the interaction between the fluid and the solid synchronously at the interface [6]. The approach is theoretically straightforward but the design of a specific solver is required for this purpose. Both sub-systems are formulated in the same framework and solved with the same numerical methods. Even though the method may have good convergence properties, taking into account both computational mechanics and computational fluid dynamics in a single numerical procedure dramatically increases the complexity of the practical implementation of the method.

To the contrary, for partitioned schemes, the fluid and the structure equations are alternately integrated in time and the interface conditions are solved asynchronously [7]. Different discretizations, either in space or in time, with possible non-matching interfaces, can be used. In spite of the extra computational cost required to ensure convergence of the fluid and structural solutions at the coupling interface, the approach is convenient since available softwares with minor changes may be used for this purpose.

The present paper presents a partitioned fluid-structure coupling between *Code_Saturne* and *Code_Aster*, two open-source solvers developed by Électricité de France (EDF) for computational fluid mechanics and computational solid mechanics, respectively. The basic features of the scheme are provided in section 2 and some results obtained with the coupled software are provided in sections 3 and 4. Conclusions are finally drawn in section 5.

2 Partitioned fluid-structure coupling scheme

2.1 Fluid and solid solvers

The partionned fluid-structure coupling scheme is based on two separate solvers, one for the fluid and one for the structure.

Flow motions are solved here using *Code_Saturne*, an EDF in-house open CFD tool [8] based on a collocated finite volume approach. The velocity-pressure coupling is treated using a SIMPLE[1] Consistent, or SIMPLEC, algorithm with a Rhie and Chow interpolation to avoid odd-even decoupling on structured meshes. The momentum equations are solved by considering an explicit mass flux so that the three components of the velocity are uncoupled. Further details about the solver *Code_Saturne* and its capabilities may be found in Archambeau *et al.* [8].

The structure dynamics is determined thanks to *Code_Aster*, a general mechanics solver also developed by EDF [9]. *Code_Aster* offers a large range of multiphysical analysis and modelling methods, including non-

1. Semi-Implicit Method for Pressure-Linked Equations

linear mechanics.

A key component within any solution procedure for coupled fluid-solid problems is the numerical implementation of the coupling mechanism between the turbulent flow and the structural displacement. Specific boundary conditions at the fluid and solid interfaces, respectively denoted $\Gamma_{s/f}$ and $\Gamma_{f/s}$, are required. In particular, one must ensure that the energy exchanges across the fluid-structure interface remains consistent. The energy transferred per unit of time and surface is given by the product of the mechanical stress acting on the interface and the interface displacement velocity. Therefore, the energy conservation is ensured if, at least, the velocity and the stress are continuous across the fluid-structure interface:

$$\begin{cases} u_i = \dfrac{Du_i^s}{Dt} & \text{on } \Gamma_{f/s} \\ \sigma_{ij} n_j = T_{ij} n_j & \text{on } \Gamma_{s/f} \end{cases} \tag{1}$$

where u^s designates the displacement of the interface, u the fluid velocity field, D/Dt the material derivative and T_{ij} the solid stress tensor. After space and time discretization, these conditions must still be fulfilled.

2.2 Solving fluid motions around moving bodies

Fully coupled fluid-structure interaction problems may involve multiple moving bodies. The computational fluid dynamic numerical procedure must therefore have the capability to handle moving boundaries. Several techniques may be implemented such as the penalization methods [10], the so-called *Chimera* techniques [11]. The present solver makes use of the the Arbitrary Lagrangian-Eulerian (ALE) approach which is based on a moving reference frame [12]. An arbitrary referential coordinate is then introduced in addition to the Lagrangian and Eulerian coordinates. The cells themselves are deformable so that the mesh topology may be adjusted in order to always enforce body-fitted boundary conditions.

Within the ALE theoretical framework, the continuity equation and the momentum equations are given by,

$$\begin{aligned} &\rho \frac{\partial u_i}{\partial x_i} = 0 \\ &\frac{\partial u_i}{\partial t} + (u_i - v_i)\frac{\partial u_i}{\partial x_j} = -\frac{1}{\rho}\frac{\partial p}{\partial x_i} + \nu \frac{\partial^2 u_i}{\partial x_j \partial x_j} \end{aligned} \tag{2}$$

where v designates the cell velocity evaluated at the center of the gravity of the cell in a framework of collocated finite volume approach, and ρ and p the density and the pressure.

Solving the Navier-Stokes equations on an arbitrary referential frame requires to introduces in the momentum equations a new convective terms based on the mesh velocity v. For incompressible flow, the Geometry Conservation Law (GCL)[13] is ensured for uniform flows with a first order approximation. It ensures numerical conservation of physical fields: the variation of an elementary volume during a time step Δt is balanced by the flux through the volume faces during the same period. The integral form of the GCL is provided by,

$$\frac{\partial}{\partial t}\int_V dV = \int_{\delta V} vc \cdot n dS \tag{3}$$

Several formulations are possible to impose the grid velocity. In the present work, a Poisson elliptic equation is used to control the cell deformation [12]:

$$\begin{cases} \nabla \bullet (\overline{\overline{\lambda}} \nabla(v)) = 0 \\ v = \frac{Du_s}{Dt} \quad \text{on } \Gamma_{f/s} \\ v = 0 \quad \text{on } \partial\Omega f \setminus \Gamma_{f/s} \end{cases} \tag{4}$$

where the boundary conditions are defined according the displacement of the moving or non-moving domain boundaries. The parameter $\overline{\overline{\lambda}}$ is a specific so-called "mesh viscosity" allowing a fine control of the cell deformations. In the mesh regions with large viscosity $\overline{\overline{\lambda}}$ the cell shapes will undergo few changes. Such a procedure enables for instance to keep a constant mesh size close to solid surfaces.

2.3 Solution convergence at the solid/fluid interface

The present strategy relies on a partitioned coupling scheme between the fluid and solid solvers. The fluid and the structure equations are alternately integrated in time and the interface conditions are solved asynchronously. In order to provide a solution continuous at the interface at each time step, an iterative procedure is implemented. The major features of the iterative process are based on the following steps:

- the displacement of the structure is transfered to the fluid solver;
- the position of the fluid mesh is updated;
- the fluid system is advanced in time and the new pressure field is computed;
- the new structural load is deduced from the new pressure field;
- the structural system is advanced in time under the fluid-induced load;
- one checks that a convergence criterion is fulfilled. If not, another iteration is performed.

A schematic view of the iteration process is proposed in Figure (1). After the initialization stage, the flow field is determined for the current mesh geometry and friction and pressure forces acting on the fluid/solid interface are determined. These loading data are sent to the structural solver as boundary conditions. The structural solver then computes the deformations, which are used to update the geometry of the fluid mesh. Afterwards the flow solver is started again.

A fixed point method is used here along with a consistent predictor and corrector terms for kinematics and stress field transfer in order to improve the convergence of the coupling scheme. In addition, data transfers between the fluid mesh and the solid mesh are carried out using a projection algorithm. A condensation scheme is also available when simplified structural modelling (*e.g.* one-degree-of-freedom or lineic modelization) are used while the fluid domain is three-dimensional.

As pointed out, the partitioned coupling iteration loop is repeated until an arbitrary convergence criterion ε^{FSI} is reached. This work makes use of a single scalar which is

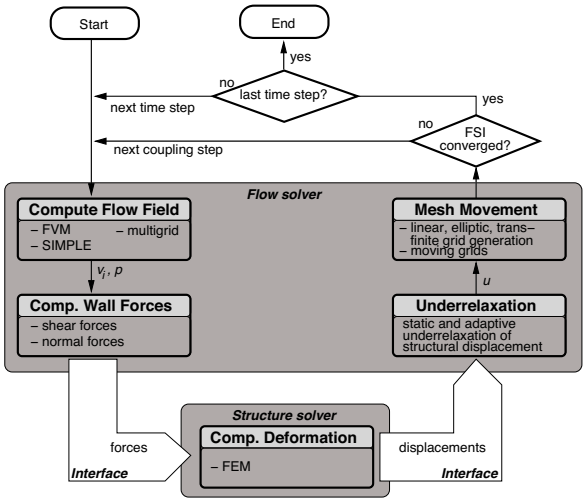

Figure 1: Flow chart of partionned coupling procedure for fluid-structure simulations.

defined using the displacement averaged over the structure:

$$\varepsilon^{\mathrm{FSI}} = \frac{1}{N}\sum_{k=1}^{N}\frac{\|\boldsymbol{u}^{k,m-1} - \boldsymbol{u}^{k,m}\|_\infty}{\|\boldsymbol{u}^{k,m}\|_\infty} < \varepsilon\,, \qquad (5)$$

where m is the FSI iteration counter, N is the number of interface nodes, and $\|\cdot\|_\infty$ denotes the infinite norm. A one-step implicit scheme is equivalent to an explicit coupling method.

It should be pointed out that various test computations have shown that the coupling scheme is rather sensitive with respect to the deformations, especially in the first FSI iterations. Situations that are far away from the physical equilibrium can consequently arise and may lead to instabilities or even the divergence of the FSI iterations. In order to counteract this effect an adaptive under-relaxation can be employed. By using a relaxation factor α^m_{FSI} the computed displacements $\tilde{\boldsymbol{u}}^m$ are linearly weighted with the values $\boldsymbol{u}^{m-1}$ from the preceding iteration to give the new displacements $\boldsymbol{u}^{m+1}$:

$$\boldsymbol{u}^{m+1} = \alpha^m_{\mathrm{FSI}}\ \tilde{\boldsymbol{u}}^m + (1-\alpha^m_{\mathrm{FSI}})\boldsymbol{u}^{m-1}\,, \qquad (6)$$

where $0 < \alpha^m_{\mathrm{FSI}} \leq 1$. Note that the under-relaxation does not change the final converged solution.

3 Oscillation of a flexible duct conveying an internal axial fluid flow

The dynamical system involving a fluid-conveying pipe has been mainly studied because of its applications. This is a system of great relevance in the field of fluid structure interaction as this is a model problem for a large variety of fluid structure interaction systems [14]. The identification of the dynamical instability threshold in such a configuration has been extensively studied from an experimental point of view under many mechanical and hydraulical conditions. Analytical models have been derived and good agreement has been obtained between analytical predictions and experimental observations. Numerical simulations have although been performed by using boundary condition linearized formulations for example [15].

One considers a flexible cylinder of circular cross section of diameter D and length L conveying a fluid. The flow is incompressible and the velocity v_f^0 is uniform along the initial axis of the cylinder (see Figure (2)). The cylinder is fixed upstream in the flow direction and it is free downstream. This means that the motion of the downstream extremity of the duct depends on the interaction with the fluid flow and conversely. The cross section diameter is uniform and only small flexion motion is allowed along the cross direction. Gravity and external perturbations are neglected. Only fluid forces acting on the cylinder wall are taken into account. Reference analytical solutions are available [16].

A two-dimensional modeling is used. Until a laminar Poiseuille flow profile has been reached, solid walls are fixed. The coupling process is then ignited. An initial impulsion is introduced in order to create an asymmetry by using the mode shape of the second mode of the structure. The second mode is chosen because it is expected to be unstable in the configuration that is considered according to the analytical theory [16]. The solid modeling is formulated along the mean axis of the cylinder. Using a two-dimensional modeling implies connecting solid walls at each time step of the computation so that they move in accordance. For fluid mesh deformation and node displacement computation an algebraic method combined with an adjacent cell tracking process is involved.

Examples of meshes used for fluid and solid modeling are shown in Figure (3). The configuration parameters are described in Table (1) and correspond to those of a previous work [15]. Results are compared to those obtained by a non-moving mesh method in a small displacement framework with a boundary condition linearization approach. Two instantaneous mode shapes are plotted in Figure (4) for reduced velocities 4.0 and 4.5 where the reduced velocity is defined by the ratio between the flow velocity and the product between the duct diameter and the frequency of the second mode of the solid. According to the Argand diagram, the critical velocity corresponds to the dynamic instability threshold where the damping of the system falls to zero. The critical threshold is in between 4.0 and 4.5 as shown in Figure (5). The numerical results are therefore consistent with previous solutions established numerically [15] in terms of critical reduced velocity threshold estimate.

Figure 2: Snapshot of the pressure field in the pipe at the initial stage of the coupled fluid-structure simulation.

Moreover the solution obtained in the present work may be more consistent in the post-instability range since the solution resulting from the boundary linearization method is not reliable for large motion magnitudes. From these first results one can conclude that the partitioned procedure is convenient for simulation of flutter and identification of instability threshold. The full system damping estimate seems to be acceptable which tends to show that the numerical diffusion generated by the partitioned procedure does not affect the results significantly.

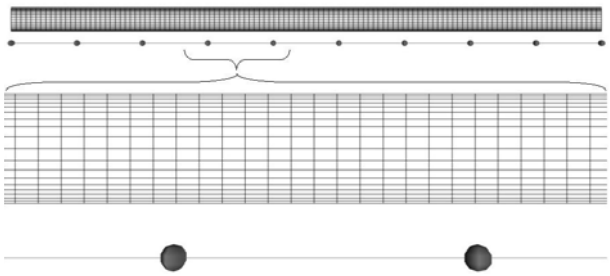

Figure 3: View of the fluid and solid meshes. The solid mesh is one-dimensional whereas the fluid mesh is fully three-dimensional.

Table 1: Parameters of the simulation of a flexible duct conveying fluid.

Tube length	L	=	1.0	m
Tube diameter	D	=	$4.0\ 10^{-2}$	m
Young modulus	E_s	=	$1.5.10^{9}$	Pa
Poisson coefficient	ν_s	=	0.3	
Solid density	ρ_s	=	160	$kg.m^{-2}$
Fluid density	ρ_f	=	$1.0\ 10^{3}$	$kg.m^{-3}$
Dynamic viscosity	η	=	$5.0\ 10^{-2}$	$kg.m^{-1}.s^{-1}$
Reduced velocity	$\bar{v}_{red}$	$\in$	$[0, 7]$	
Initial magnitude motion	$Ampl$	=	$1.84\ 10^{-6}$	$m.s^{-1}$

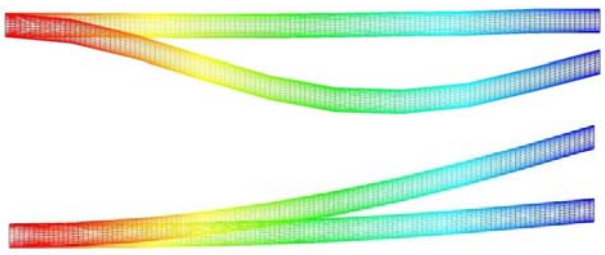

Figure 4: Instantaneous snapshots of the cylinder mode shape obtained for a reduced velocity equal to 4.0 (top), and 4.5 (bottom).

4 Instability threshold in tube array under cross flow

The stability of a flexible tube in a rigid tube array under cross flow has also been investigated. The details of the study are not reproduced here but they may be found in Huvelin *et al.* [17]. The results turn out to be encouraging. In particular, it is shown that the critical reduced velocity deduced from the simulation is in good agreement with the one predicted by Connors theory [18].

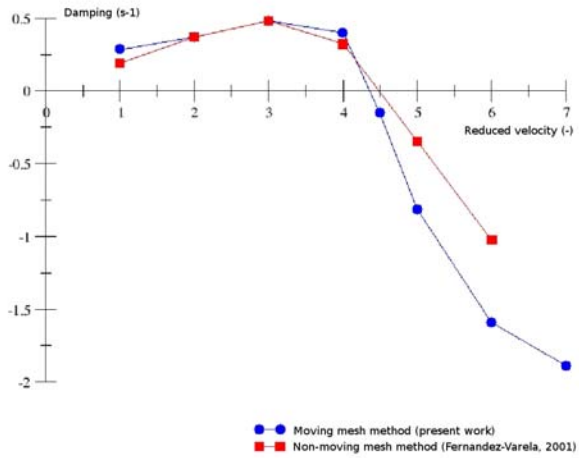

Figure 5: Evolution of the total damping (fluid and structural) as a function of the reduced velocity.

5 Conclusion

A partitioned coupling scheme between a computational fluid mechanics and a computational solid mechanics solver has been presented. The CFD simulation relies on the ALE procedure to allow the calculation of unsteady flow motions around moving bodies and an interpolation procedure has been designed to permit information exchanges between the flow and solid solutions. The fluid and the structure equations are alternately integrated in time and the interface conditions are solved asynchronously. An iterative algorithm along with a relaxation procedure is implemented to improve convergence at the solid-fluid interface. To illustrate the ability of the present solver to tackle complex fully coupled fluid-structure problems, the oscillations of a fluid-conveying pipe have been computed. A good agreement has been found with the previous numerical investigation of Fernández Valera [15], hence demonstrating the consistency of the proposed partitioned fluid-structure solver.

References

[1] Weaver, D. & Fitzpatrick, J. A review of cross-flow induced vibrations in heat exchanger tube arrays J. Fluid Struct., 1988, 2(1), 73-93

[2] Païdoussis, M. Dynamics of tubular cantilevers conveying fluid J. Mech. Eng., 1970, 12, 85-103

[3] Theodorsen, T. & Garrick, T. Mechanism of flutter NACA Technical Report TR-685, 1940

[4] Kevlahan, N.-R. & Wadsley, J. Suppression of three-dimensional flow instabilities in tube bundles J. Fluid Struct., 2005, 20(4), 611-620

[5] Longatte, E., Bendjeddou, Z. & Souli, M. Methods for numerical study of tube bundle vibrations in cross-flows J. Fluid Struct., 2003, 18(5), 513-528

[6] Blom, F. A monolithical fluid-structure interaction algorithm applied to the piston problem Comput. Meth. Appl. Mech. Eng., 1998, 167(3-4), 369-391

[7] Felippa, C., Park, K. & Farhat, C. Partitioned analysis of coupled mechanical systems Comput. Meth. Appl. Mech. Eng., 2001, 190(24-25), 3247-3270

[8] Archambeau, F., Sakiz, M. & Namane, M. Code Saturne: a finite volume code for turbulent flows Int. J. Finite Vol., 2004, 1(1), 1-62

[9] Code_Aster, *Analysis of structures and thermomechanics for studies & research*, http:www.code-aster.org.

[10] Schneider, K. & Farge, M. Numerical simulation of the transient flow behaviour in tube bundles using a volume penalization method J. Fluid Struct., 2005, 20(4), 555-566

[11] Sherer, S.E. & Scott, J.N. High-order compact finite-difference methods on general overset grids J. Comput. Phys., 2005, 210(2), 459-496

[12] Souli, M., Ouahsine, A. & Lewin, L. ALE formulation for fluid-structure interaction problems Comput. Meth. Appl. Mech. Eng., 2000, 190(5-7), 659-675

[13] Farhat, C., Geuzaine, P. & Grandmont, C. The discrete geometric conservation law and the nonlinear stability of ALE schemes for the solution of flow problems on moving grids J. Comp. Phys., 2001, 174(2), 669-694

[14] Blevins, R.D., Flow-induced vibrations, *Van Nostrand Reinhold*, 1977

[15] Fernández Varela, M., Modèles simplifiés d'interaction fluide-structure, Ph.D. Thesis, Université Paris IX Dauphine, 2001

[16] Païdoussis, M. Fluid structure interaction: slender structures and axial flow, Volume 1, *Academic Press Inc.*, 2003

[17] Huvelin, F., Morais, M., Baj, F., Magnaud, J.P., Longatte, E., Souli, M. Numerical simulation of tube bundle vibrations under cross flow, PVP 2007-26595, *ASME Pressure Vessels and Piping Conference*, July 22-26, San Antonio, Texas, U.S.A., 2007

[18] Connors, H. Fluidelastic vibration of heat exchanger tube arrays J. Mech. Design, 1978, 100, 347-353

INTRODUCTION ON LARGE EDDY SIMULATION OF A SINGLE CYLINDER VORTEX-INDUCED VIBRATION UNDER SUBCRITICAL CROSS FLOW

Yoann Jus[1], Elisabeth Longatte[1], Jean-Camille Chassaing[2] and Pierre Sagaut[2]

[1] LaMSID UMR CNRS/EDF/CEA 2832, Clamart, France

[2] UPMC Paris 6 University

Abstract

The present work focuses on Vortex-Induced Vibrations (VIV) of an elastically mounted cylinder in a cross flow at moderate Reynolds number. The dynamic response of the cylinder freely moving in the lift direction is investigated by means of a three-dimensional Large Eddy Simulation (LES) in an Arbitrary Lagrangian Eulerian (ALE) framework using an iterative method for computation of flow interaction with solid moving boundary. Numerical simulations are performed at Reynolds number 3900 in several configurations, at low mass-damping ratio, for several reduced velocity values. A brief physical analysis is provided. This work has been performed in the framework of a PhD Thesis. It will be published in further articles.

1 Introduction

Fluid structure interactions occur in a wide range of industrial domains including vibrations of mechanical structures submitted to external thermohydraulics flows in nuclear devices such as those encountered in steam exchanger cylinder arrangements. Vortex-Induced Vibrations (VIV) have been extensively studied over the last past decades [1, 2, 3, 4]. In the case of an elastically mounted cylinder at low mass-damping, three types of responses can be observed as described in [5, 6, 7]. For low reduced velocities, an *initial* branch is associated with a vortex shedding mode involving two-single vortices shed per cycle (2S mode). For intermediate and larger reduced velocities, an *upper* and a *lower* branches associated with a vortex shedding mode emission involving two pairs of vortices shed per cycle (2P mode) are observed [5, 6].

The article is organized as follows : firstly, recall on numerical background, secondly, discussion on numerical results and comparisons to reference solutions.

2 Numerical Background

Navier-Stokes equations governing an incompressible fluid flow in interaction with freely moving solid boundaries are considered. Space discretization relies on a collocated finite volume approach on unstructured mesh and a fractional time step procedure is involved for fluid pressure velocity coupled computation through a projection method [8]. An Arbitrary Lagrangian Eulerian (ALE) approach is involved to describe solid boundary motion by introducing an arbitrary referential domain for Navier-Stokes system computation. The associated time-depending reference space mapping is used to derive the full system in the computational coordinate system. Governing equations for incompressible flow are written as follows :

$$\frac{\partial \overline{u}_i}{\partial x_i} = 0$$

$$\frac{\partial \overline{u_i}}{\partial t} + (\overline{u_i} - v_{gi})\frac{\partial \overline{u_i}}{\partial x_j} = -\frac{1}{\rho}\frac{\partial \overline{p}}{\partial x_i} + \nu\frac{\partial^2 \overline{u_i}}{\partial x_j \partial x_j} - \frac{\partial \tau_{\mathrm{ij}}}{\partial x_j}$$

where v_g represents the grid cell velocity, $\overline{u}$ and $\overline{p}$ designate the spatially filtered velocity and pressure respectively, with local coordinates (x, t) in the space time domain. ρ and ν designate respectively fluid density and viscosity. The subgrid scale tensor $\underline{\overline{\tau}}$ is modeled by the Smagorinsky model which is based on Germano identity[9] and Lilly minimization[10]. The deviatoric part of the subgrid-scale tensor is given by :

$$\tau_{\mathrm{ij}} - \frac{1}{3}\tau_{\mathrm{kk}}\delta_{\mathrm{ij}} = -2\nu_t S_{ij} = -2(C_s\overline{\Delta})^2\|S\|S_{ij}$$

where S_{ij} represents the filtered strain rate tensor, $\|S\| = \sqrt{2S_{ij}S_{ij}}$, ν_t denotes the subgrid-scale viscosity, $\overline{\Delta}$ is the filter width and C_s is the Smagorinsky constant ($C_s = 0.065$). Only hexahedral computational cells with volume Ω are considered in the present work and one uses $\overline{\Delta} = 2\Omega^{\frac{1}{3}}$. The term $\frac{1}{3}\tau_{\mathrm{kk}}\delta_{\mathrm{ij}}$ is taken into account in the pressure gradient.

From a mathematical point of view, the introduction of an arbitrary computational reference system means the introduction of a grid mesh impacting convective terms in the momentum equation. For incompressible flow, the Geometry Conservation Law (GCL) [11] is ensured for uniform flows with a first order approximation.

Several formulations are possible for the choice of grid velocity dynamics like transfinite mapping strategy, spring analogy or linear elasticity approach.

The assumption that LES filtering commutes with partial derivatives is generally considered valid on fixed grids with uniform cell width. On deforming unstructured grid, Temporal Commutation Errors (TCE) must be taken into account[12]. In the framework of the present work it is assumed that these errors can be neglected.

At fluid solid interface, conditions describe continuity of velocity and stress. The former corresponds to the kinematic no-slip condition and the latter is the equilibrium condition as follows :

$$\begin{cases} u_i = \dfrac{Du_i^s}{Dt} & \text{on } \Gamma_{f/s} \\ \sigma_{ij} n_j = T_{ij} n_j & \text{on } \Gamma_{s/f} \end{cases}$$

where u^s designates the displacement of the interface, $\frac{D}{Dt}$ the material derivative and T_{ij} the solid stress tensor. The interfaces of solid and fluid domains are $\Gamma_{s/f}$ and $\Gamma_{f/s}$ respectively.

The motion of an elastically rigid circular cylinder oscillating freely in a cross-flow is considered. The one-degree-of-freedom dynamic equation of the structure reads :

$$m\ \ddot{y} + c\ \dot{y} + k\ y \quad = \quad F_y$$

where y is the solid displacement in the cross direction, $\dot{y}$ the velocity, $\ddot{y}$ the acceleration, m, c and k are the structural mass, damping and stiffness respectively and F_y represents the action exerted by fluid in the lift direction. In the framework of rigid motion theory (similarly for linear elasticity), a lagrangian formulation is used to describe the time evolution of the solid kinematics. System remains linear and time integration relies on a Newmark algorithm.

To deal with computation of the fully-coupled fluid solid system, an iterative method is involved in order to look for a solution ensuring continuity conditions through the interface [13, 14, 15, 16, 17]. A fixed point method is used with consistent predictor and corrector terms for kinematics and stress field transfer. A projection and a condensation methods are used in order to enable one-degree-of-freedom systems for modeling solid dynamics [18]. Under-relaxation may be introduced to improve the convergence properties of the iterative process.

3 Results and Discussion

Low mass-damping LES computations are performed at $Re = 3900$ for various reduced velocities. A particular attention is paid to high amplitude response corresponding to the upper branch. The size of the computational domain is $20D \times 20D$ in axial and cross directions and the length upstream the cylinder is equal to $10D$ where D designates the cylinder diameter. The spanwise length of the domain is set to $4D$. Computations are performed using 32 grid points along the spanwise direction. The total number of cells is equal to 2.10^6. The time step is $\Delta t = 0.001D/U_0$ and U_0 is the inlet velocity. The corresponding maximum CFL number is equal to 0.8. As far as boundary conditions are concerned, a constant velocity in both space and time is specified at inlet boundary. Laminar flow conditions are considered upstream of the cylinder and periodic boundary conditions are used in the spanwise direction. Dirichlet conditions for pressure and homogeneous Neumann conditions for velocity are applied at the outer boundary. At the fluid solid moving boundary Dirichlet conditions are imposed on the velocity field with respect to the kinematic consistency condition. Finally, symmetry boundary conditions are employed at upper and lower transverse boundary faces. One considers the numerical parameters of experimental work providing reference solutions[19]. Low mass-damping conditions are studied for $m^*\xi = 0.04$ where ξ the reduced damping is defined by $c = 2\ m\ \omega_0\ \xi$ with ω_0 the system pulsation. The mass ratio is set to $m^* = 1$. Several reduced velocity values are investigated.

Figure (1) displays an example of flow field in the wake of a static single cylinder submitted to a cross flow at Reynolds number 3900. Figure (2) shows results provided by computation of dynamic single cylinder response. It is pointed out that LES succeeds in computing the typical branch responses for low mass-damping configurations. Simulation at $U^* = 3$ corresponds to the *initial* small amplitude response branch. The high amplitude *upper* branch can be clearly identified for the range $U^* = [4 - 5]$. In particular, the highest amplitude response is close to those observed experimentally [19]. Finally, the reduced velocity range corresponding to the small amplitude *lower* branch is approximatively defined by $U^* = 5.5 - 10$. A qualitatively good agreement is retrieved with reference experimental data[19].

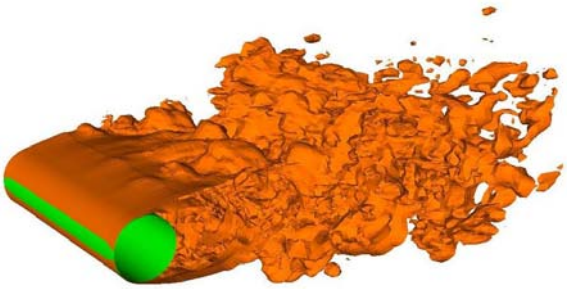

Figure 1: Flow field ($Re = 3900$, static cylinder)

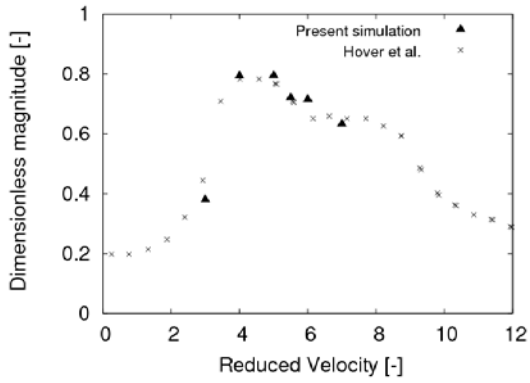

Figure 2: Comparison of the response amplitude with the experimental data[19] ($Re = 3900$, $m^* = 1$ and $m^*\xi = 0.04$)

Table (1) summarizes the value of the mean amplitude A_{mean} based on the average of the peak amplitude of the tenth last periods of oscillations provived by computation. The coefficient of variation COV = STD/A_{mean} ranges from 6.5% to 23.45%. The linear growth of the response is expected up to $U^* = 7$. As far as the *lock-in* region is concerned, LES simulations predict a reduced frequency close to one which indicates that the synchronization regime has been reached.

4 Conclusion

VIV of a rigid cylinder freely vibrating in a cross-flow is investigated by means of LES at Re=3900. A wide range of reduced velocities is examined in order to characterize the three-branches response model for low mass-damping. The displacements amplitude on the *upper* branch as well as the reduced frequency in the lock-in

U^*	A_{mean}/D	A_{max}/D	A_{min}/D	STD
3	0.380	0.416	0.352	0.02
4	0.794	0.892	0.663	0.052
5	0.795	1.01	0.639	0.056
5.5	0.721	0.898	0.562	0.107
6	0.715	1.08	0.547	0.149
7	0.661	0.821	0.550	0.072

Table 1: Statistical properties of the amplitude response as a function of the reduced velocity at $m^* = 1$ and $m^*\xi = 0.04$

region are compared to experimental results. The transition from the upper branch to the lower one is retrieved.

References

[1] E. Guilmineau and P. Queutey. Numerical simulation of vortex-induced vibration of a circular cylinder with low mass-damping in a turbulent flow. *Journal of Fluids and Structures*, 19:449–466, 2004.

[2] Z. Pan, W. Cui, and Q. Miao. Numerical simulation of vortex-induced vibration of a circular cylinder at low mass-damping using rans code. *Journal of Fluids and Structures*, 23:23–37, 2007.

[3] J. Sigrist, C. Allery, and C. Beghein. A numerical simulation of vortex induced vibrations on a elastically mounted circular rigid cylinder at moderate reynolds numbers. *ASME Conference Proceedings: Pressure Vessel and Piping*, 2008:83–92, 2008.

[4] D. Lucor, J. Foo, and G. Karniadakis. Vortex mode selection of a rigid cylinder subject to viv at low mass damping. *Journal of Fluids and Structures*, 20:483–503, 2005.

[5] A. Khalak and C. Williamson. Motions, forces and mode transitions in vortex-induced vibrations at low mass damping. *Journal of Fluids and Structures*, 13:813–851, 1999.

[6] R. Govardhan and C. Williamson. Modes of vortex formation and frequency response of a freely vibrating cylinder. *Journal of Fluid Mechanics*, 420:85–130, 2000.

[7] C. Williamson and R. Govardhan. Vortex-induced vibrations. *Annual Review of Fluid Mechanics*, 36:413–455, 2004.

[8] F. Archambeau, N. Méchitoua, and M. Sakiz. A finite volume code for the computation of turbulent incompressible flows–industrial applications. *International Journal of Finite Volumes*, 1:1–59, 2004.

[9] M. Germano, U. Piomelli, P. Moin, and W. Cabot. A dynamic subgrid-scale eddy viscosity model. *Physics of Fluids*, 3:1760–1765, 1991.

[10] D. Lilly. A proposed modification of the germano subgrid-scale closure method. *Physics of Fluids*, 4:633–635, 1992.

[11] M. Lesoinne and C. Farhat. A geometric conservation for flow problems with moving boundaries and deformable meshes, and their impact on aeroelastic computations. *Computer Methods in Applied Mechanics and Engineering*, 134:71–90, 1996.

[12] V. Moureau, O. Vasilyev, C. Angelberger, and T.J. Poinsot. Commutation errors in les on moving grids: Application to piston engine flows. In *Center for Turbulence Research Stanfort, Proceedings of the Summer Program*, 2004.

[13] F. Huvelin. *Couplage de codes en interaction fluide-structure et applications aux instabilités fluide- élastiques*. PhD thesis, Lille University, 2008.

[14] E. Longatte, V. Verreman, and M. Souli. Time marching for simulation of fluid structure interaction problems. *Journal of Fluids and Structures*, 25:95–111, 2009.

[15] S. Piperno. Explicit/implicit fluid/structure staggered procedure with a structural predictor and fluid subcycling for 2d inviscid aeroelastic simulations. *International Journal of Numerical Methods In Fluids*, 25:1207–1226, 1997.

[16] S. Piperno and C. Farhat. Partitionned procedures for the transient solution of coupled aeroelastic problems. *Computer Methods in Applied Mechanical and Engineering*, 190:3147–3170, 2001.

[17] M. Schaefer, M. Heck, and S. Yigit. An implicit partitioned method for the numerical method of fluid-structure interaction. In *Fluid-Structure Interaction, LNCSE 53*. Springer, 2007.

[18] N. Maman and C. Farhat. Matching fluid and structure meshes for aero-elastic computations : a parallel approach. *Computers & Structures*, 54:779–785, 1995.

[19] F. Hover, A. Techet, and M. Triantafyllou. Forces on oscillating uniform and tapered cylinders in cross-flow. *Journal of Fluid Mechanics*, 363:97–114, 1998.

Simulation of fluid structure interaction in a tube array under cross flow at high Reynolds number

T. Marcel[1], M. Braza[1], Y. Hoarau[2], G. Harran[1], F. Baj[3], JP. Magnaud[3] and E. Longatte[4]

[1] Institut de Mécanique des Fluides de Toulouse (IMFT-UMR CNRS 5502)

[2] Institut de Mécanique des Fluides et des Solides de Strasbourg (IMFS)

[3] Commissariat à l'Énergie Atomique (CEA)

[4] Lab. de Méc. des Structures Industrielles Durables (LaMSID-UMR EDF CNRS 2832)

marcel@imft.fr

Abstract

The fluid-structure interaction in a tube bundle is studied at high Reynolds number by means of URANS and Hybrid turbulence modelling, to analyse the origins of appearance of fluid-elastic instabilities at high Reynolds number. Especially the Organised Eddy Simulation (OES) approach [1] is used to allow development of fluid-structure interaction modes. The simulations are carried out by means of the code NSMB (Navier-Stokes Multi Block).

A comparative study between the $k-\varepsilon-$OES, $k-\omega-$OES and URANS $k-\omega-$SST [2] turbulence models is provided with a discussion of their predictive capabilities. The study is carried out for two geometries of (3×3) and (4×5) cylinders, first on a static configuration and second in case of one cylinder oscillation. The contributions of the structural motion and of the turbulence on the unsteady loads due to the fluid-structure interaction are quantified.

Finally a $3D$ simulation using a Delayed Detached Eddy Simulation approah with the Spalart-Allmaras (SA) [3] turbulence modeling in the URANS part is used in order to quantify the $3D$ aspects of the flow.

1 Introduction

The prediction of fluid-elastic instabilities developped in a tube bundle is of major importance for the current design of heat exchangers for cooling the nuclear plants and for the prevention of accidents associated with material fatigue, shock between beams and severance of solid walls. The fluid-elastic instabilities in tube arrays appear in the laminar regime and persists up to the turbulent regime.

In the industrial context, the high Reynolds number gives a complex interaction between non-linear instability due to the movement of the solid structure and the near-wall unsteady turbulence around the cylinders. To correctly take into account this interaction and efficiently predict the unsteady loads, it is necessary to develop reliable turbulence modeling approaches, able to separate the effects due to the structure motion (low freqyebcues, well distinct peaks) and the random effects due to the turbulence background.

The development of near-wall turbulence around moving cylinders produces an interaction with non-linear modes from the structure and requires specific turbulence modelling approaches. Indeed, approaches such as URANS, derived from assumptions of statistical equilibrium, tend to underestimate the global coefficients (drag, lift) and their amplitudes (see the European program DESIDER, Detached Eddy Simulation for Industrial Aerodynamics [4]).

The LES approach is less suitable for *high Reynolds* number wall flows as the present industrial problem. Hybrid-type approaches (URANS near the obstacle and LES into the regions of flow detachment) are more promising, and especially the Detached Eddy Simulation, (DES). Furthermore the Organised Eddy Simulation, (OES) approach ([1], [5] and [6]), being in between the URANS and the DES, is quite promising, based on a number of previous studies [7], for capturing predominant instability modes around bodies at high Reynolds number. OES uses a separation of the ernergy spectrum into an organised part (resolved turbulence), that includes all the predominant wavenumber and a chaotic part (continuous spectrum) that extends from the low to the high wavenumber range and constitutes the part to be modeled. OES uses the phase-averaged Navier-Stokes equations system and modified URANS turbulence modelling closures to take into account non-equilibrium turbulence effects by using DRSM (Differential Reynolds Stress transport Modelling) towards adapted two-equation modelling. In recent works, the turbulence stresses by means are modeled by means of a tensorial eddy viscosity concept [8] and [1]. This is derived by means of experimental studies in the research team "Interaction Fluide-Structure Sous Turbulence" carried out in the wind tunnels of IMFT [9] by using phase-averaged three-component PIV for flows around a circular cylinder at high Reynolds number (The IMFT's circular cylinder "DESIDER test-case").

In this paper URANS, OES and DES approaches are compared for predicting the fluid-elastic instabilities in the tube array at Reynolds number 20 000, corresponding to an inter-tube Reynolds number of 60 000, based on the inter-tube distance. This study is a collaboration between EDF, CEA and IMFT. Comparisons with experimental results from industrial partners will be presented. In the present study, an adaptation of OES to scalar eddy-viscosity is used [5].

2 Configuration

The fluid structure interaction is studied on two different meshes : the $2D-20$ cylinders, and the $3D-20$ cylinders.

configuration	cells	blocks	near-wall grid spacing
$2D-20$	392 600	80	$1,5.10^{-4}\ D$
$3D-20$	21 930 648	560	$1,5.10^{-4}\ D$

Table 1: Meshes configuration (D = cylinder's diameter, array of 20 cylinders)

At the the entrance of the computationnal domain, the boundary conditions are freestream. At the outlet boundary, non-confining boundary conditions are used, corresponding to non-reflective equations [10].

In the spanwise direction, (spanwise length $3D$), periodic boundary conditions are used to simulate an infinite bundle.

3 Numerical Method

The computations are carried out with the code NSMB, *Navier-Stokes Multi Block*, (NSMB) [11]. This is a structured finite volume solver used by a number of european Institutes and aeronautics industries in the context of the NSMB consortium. IMFT participates in the consortium for the development of turbulence modelling. The multi-bloc approach allows mesh production of realistic industrial configurations, like the tube bundle. Moreover, thanks to the multi-block approach, NSMB is a massively parallelised software in MPI architectures and offers increased efficiency in current super computers platforms.

The numerical scheme used for the convection terms, is an upwind 3$^{\text{rd}}$ order Roe scheme [12], with the MUSCL[1] limiter. The diffusion terms are discretised by central differencies. The temporal integration is performed by an implicit Runje-Kutta 3$^{\text{rd}}$ order scheme, using dual time-stepping.

For the mesh deformation, the *Arbitrary Langrangian Eulerian* (ALE) method is used [14] with a Newmark algorithm for the structural modal analysis.

4 Results

All the computations detailled in the following section, are time-dependent simulations that need an order of 30 000 hours of CPU time for a whole $3D$ computation, using 64 parallel processors on the supercomputer "JADE" (*SGI Altix ICE 8200 EX*) at the CINES (Centre Informatique National de l'Enseignement Supérieur) in Montpellier.

4.1 Static configuration

First, the fixed cylinders configuration is computed. The values of drag coefficients obtained with the $k-\omega-$SST model are higher than those derived from the $k-\varepsilon-$OES

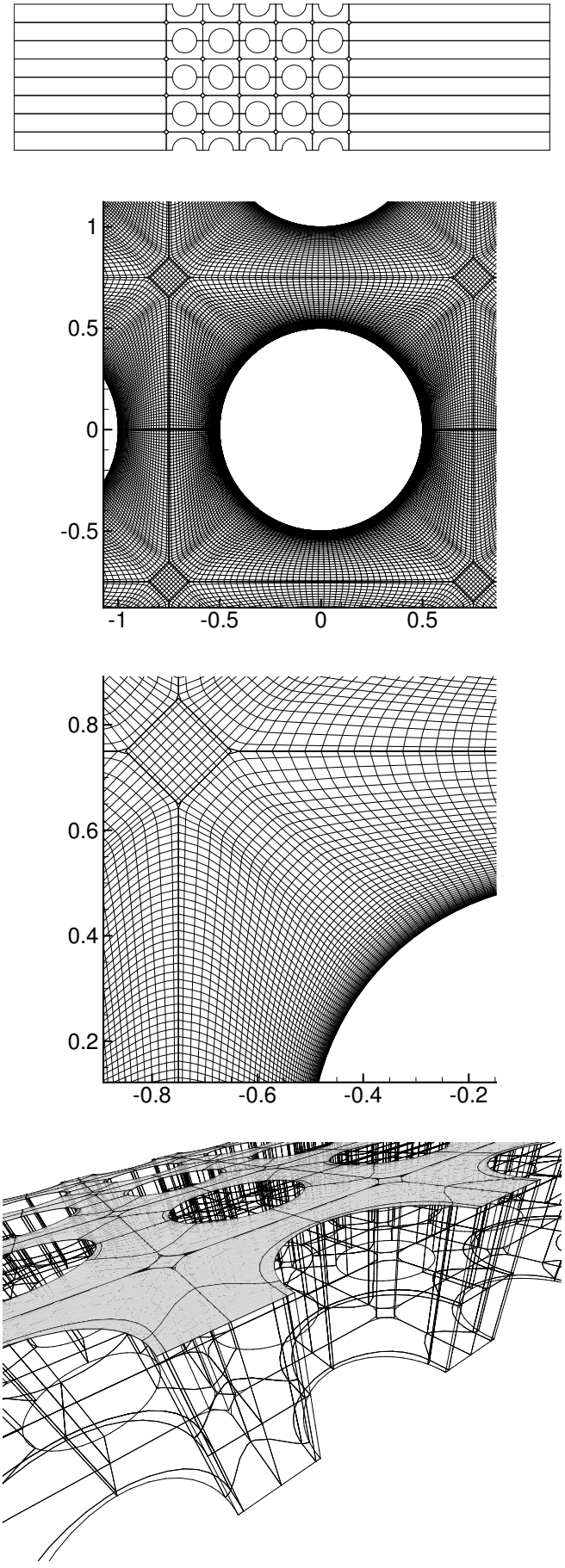

Figure 1: Meshes and cells details

1. Monotone Upwind Scheme for Conservation Laws [13]

and from the $k-\omega-$OES models. This behaviour confirms that conventional URANS models tend to overestimate the drag.

The velocity-pressure fields obtained by OES modeling show the wake effect. The statistically averaged velocity fields show a "triangle-like" shape of the iso-contours downstream of the last column of cylinders array (Figure (4)).

Model	$\overline{C_L}$	St_{C_L}	$\overline{C_D}$	St_{C_D}	$\mathrm{St}_{C_D}/\mathrm{St}_{C_L}$
$k-\omega-$SST	0,07	0,36	0,37	0,67	1,87
$k-\omega-$OES	0,09	0,39	0,22	0,74	1,88
$k-\varepsilon-$OES	0,01	0,43	0,20	0,61	1,43

Table 2: Frequences ratio on drag and lift instationnary loads. St_{C_L} and St_{C_D} are the most energetic dimensionless predominant frequency peaks in the spectra of the drag and lift coefficients respectively.

The spectra of the hydrodynamic global coefficients allow evaluation of the predominant frequencies of the fluid instability of Von Kàrmàn type. The drag coefficient oscillations of the fundamental frequency are approximately doubly faster than the fundamental oscillations of the lift coeffcient. The predominant frequencies are of the same order as in the experiments by CEA and EDF. A more detailed comparison is under way.

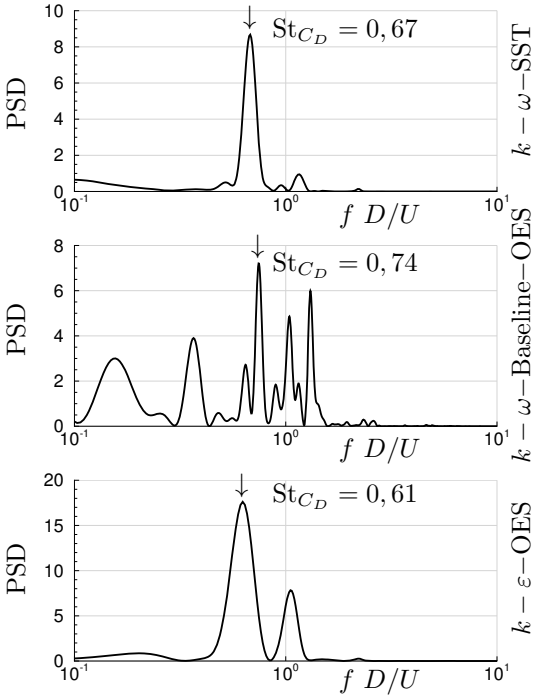

Figure 2: Power spectral density of the drag coefficient, $k-\omega-$SST, $k-\omega-$OES and $k-\varepsilon-$OES models.

Figure (5) shows that the turbulent kinetic energy is symetric and increases due to the cylinders bundle : there is no turbulent energy in the entry of the computation domain.

On Figure (6) and Figure (7), it can be seen that the $3D$ turbulence structure is developed. We can also observe on the slice (Figure (6)) that $3D$ vertical vorticity seems to aglomerate with the flow : there are around 8 layers of vortices on the first vertical row and around 5 in the last one. The size of the structure becomes higher downstream, corresponding to the turbulence development.

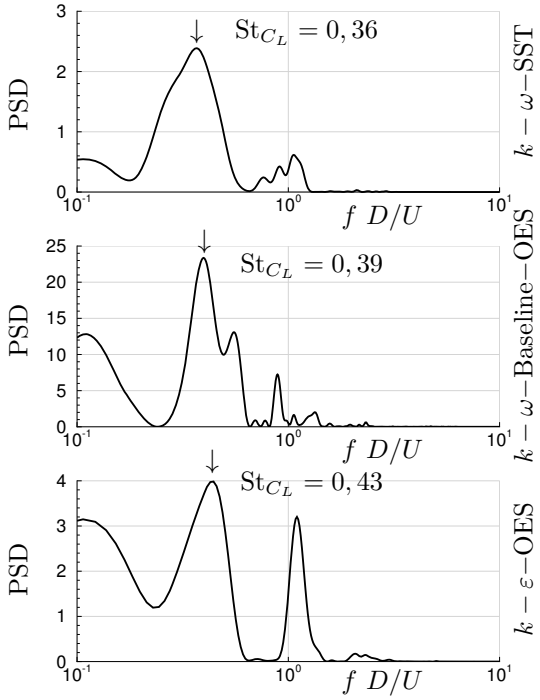

Figure 3: Power spectral density of the lift coefficient, $k-\omega-$SST, $k-\omega-$OES and $k-\varepsilon-$OES models.

Drag coefficient values on Table (2), obtained with URANS$-k-\omega-$SST model are higher than these are obtained with OES in both $k-\omega-$OES and $k-\varepsilon-$OES.

Moreover, it can be seen in the vorticity pattern of Figure (5) that OES, which is a sort of modification of URANS modeling, reveals more structures in the flow than URANS standard approaches. The evaluation of the unsteady loads on the solid structure including *the turbulence effects* is very important in fluid-structure interaction, and for this reason, this modeling aspect can be of importance for the design.

The results obtained by means of the OES approach in $2D$ configuration are quite promising, given the rich statistical content of the simulations and the tendency of not overestimating the dragh coefficient. Consequently, a $3D$ DDES [15] using OES approach in the URANS part near the bodies is carried out in comparison with DDES-SA. The hybridation of DES and of OES is presented in detail in [1].

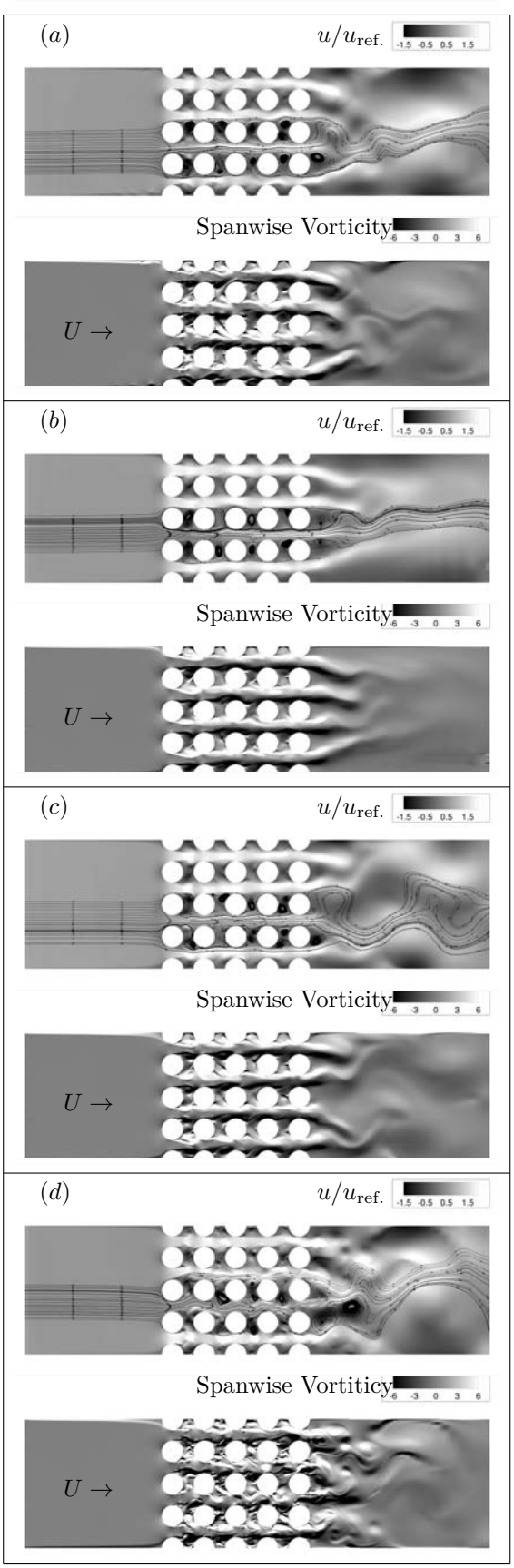

Figure 4: Instantaneous longitudinal velocity and spanwise vorticity with $k-\omega-$OES (a), $k-\varepsilon$ OES (b), $k-\omega-$SST (c), SA(d).

4.2 Dynamic configuration, free motion

To reproduce the fluid elastic instabilty, the central cylinder is allowed mooving vertically, according to one degree of freedom (Figure (8)), with modal parameters in the Table (3)

A comparative study between 1 and 2 degrees of freedom can be done in the future.

The dynamics equations are resolved with Newmark algorithm [16], (Eq. (2)), with parameters :

$$(\alpha_s \ ; \ \delta_s) = (1/4 \ ; \ 1/2) \tag{1}$$

(constant averaged acceleration hypothesis). The mesh is modified by means a the ALE method [14].

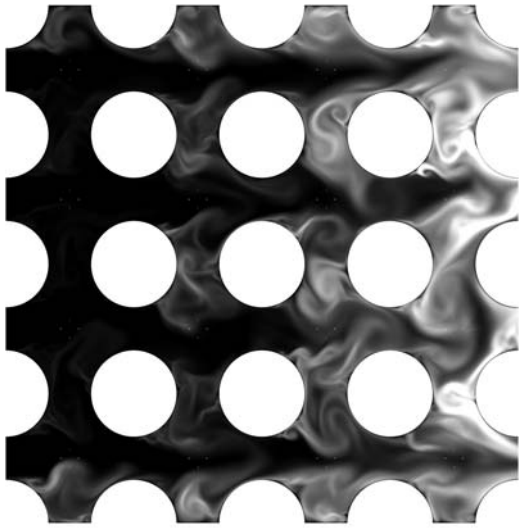

Figure 5: Instantaneous turbulent kinetic energy k, $k-\omega-$OES.

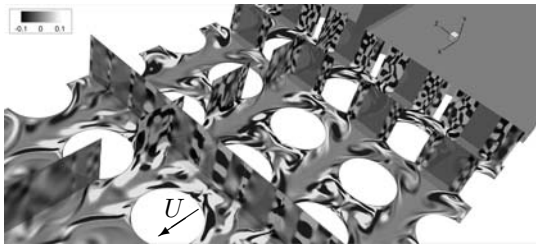

Figure 6: Instantaneous vorticity slices, DDES$-k-\omega-$SST.

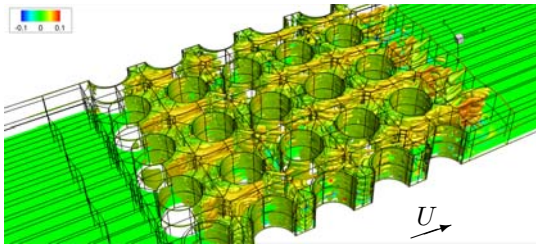

Figure 7: Instantaneous vorticity isosurfaces, DDES$-k-\omega-$SST.

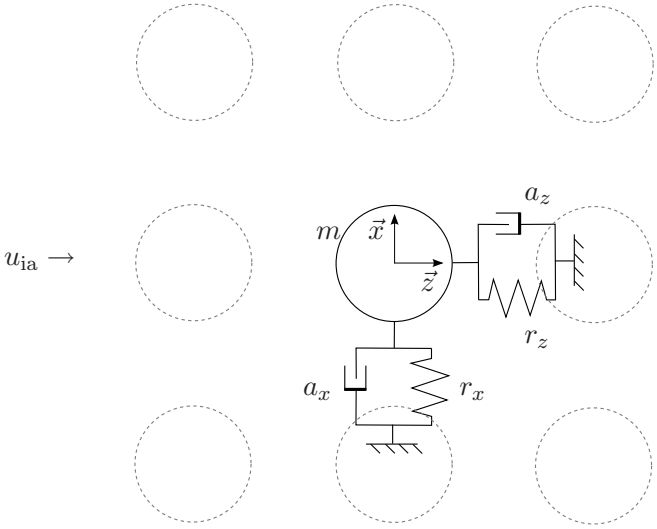

Figure 8: Schematic representation with middle cylinder motion, in the general case of two-degrees of freedom.

$$
\begin{aligned}
(x_s)_i^{n+1} = & \left[a_0\ M + a_1\ A + R\right]^{-1} \\
& \times \left\{F^{n+1} + M\ \left[a_0\ (x_s)_i^n + a_2\ (\dot{x}_s)_i^n + a_3\ (\ddot{x}_s)_i^n\right]\right. \\
& \left. + A\ \left[a_1\ (x_s)_i^n + a_4\ (\dot{x}_s)_i^n + a_5\ (\ddot{x}_s)_i^n\right]\right\}
\end{aligned}
\tag{2}
$$

$(M,\ A,\ R)$ are the mass, damping and stiffness matrices, $[(x_s)_i,\ (\dot{x}_s)_i,\ (\ddot{x}_s)_i]$ is the position, the speed and the acceleration of the structure on the i axis. $(a_0,\ \cdots,\ a_5)$ are function of $(\alpha_s,\ \delta_s)$.

The dimentionless equation for 1 degree of freedom ($\vec{z}$, crossflow direction), (Eq. (3)), used allowes evaluation of the drag and lift coefficients.

$$
m^*\ \frac{\partial^2 z_s^*(t)}{\partial t^{*2}} + a^*\ \frac{\partial z_s^*(t)}{\partial t^*} + r^*\ z_s(t)^* = C_z(t) \tag{3}
$$

with :

$$
z_s^* = \frac{z_s}{d} \qquad C_z = \frac{2\ f_z}{\rho_{\text{ref.}}\ d\ u_{\text{ref.}}^2\ l}
$$

$$
t^* = \frac{t\ u_{\text{ref.}}}{d} \qquad a^* = \frac{2\ a}{\rho_{\text{ref.}}\ d\ u_{\text{ref.}}\ l}
$$

$$
m^* = \frac{2\ m}{\rho_{\text{ref.}}\ d^2\ l} \qquad r^* = \frac{2\ r}{\rho_{\text{ref.}}\ u_{\text{ref.}}^2\ l}
$$

d and l the diameter and the length of the structure, $u_{\text{ref.}}$ and $\rho_{\text{ref.}}$ the flow reference speed and density.

Mass m [kg]	3.384
Damping c [kg/s]	0.00286
Stiffness k [N/m]	1.44
Natural frequency f_0 [Hz]	0.1
Reduced velocity	1.18
Mass-damping	0.013

Table 3: Caracteristic parameters of the structure (tube)

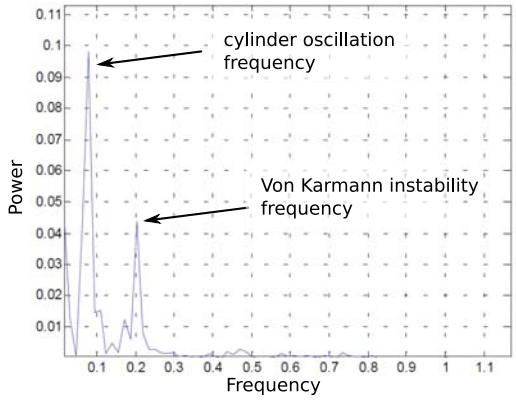

Figure 9: Lift coefficient spectrum of the central cylinder motion and Von Kàrmàn frequency after order shedding

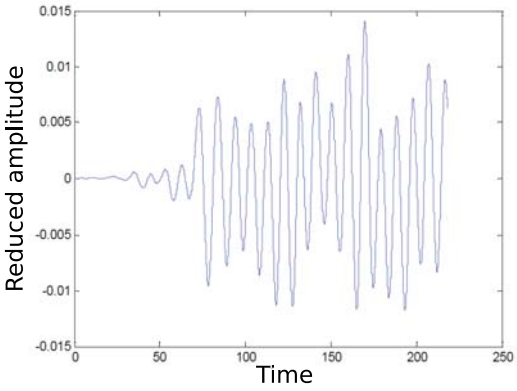

Figure 10: Reduced amplitude (A/D) of the cylinder displacement as a function of time

On Figure (10), the displacement of the free motion cylinder is shown. This motion leads to the appearance of a second high-energy frequency peak on the spectrum of the lift coefficient on Figure (9). This means that the motion is not only due to the Von Kàrmàn instabilty, but also ruled by a fluid-structure interaction process that induces a new frequency.

5 Conclusions

This present study discusses the prediction of fluid elastic instability, and of the unsteady loads in a tube bundle at high Reynolds number. The NSMB, *Navier-Stokes Multi Block*, code has been used.

Comparison of turbulence modeling approaches has been carried out to capture the unsteady dynamic loads due to the fluid-structure interactions. The oscillatory caracteristics is well predicted, particulary concerning the drag coefficients. The OES modelling improves the coherent structure prediction in the cylinders bundle that is attenuated in classic URANS approach.

The dynamic case allowed evaluation loads evolution in case of fluid structure interaction, and quantification of the loads due to turbulence as well as of those due to the structure's motion, by comparison of the static case to the dynamic one.

The DDES approach is promising for the generation of three-dimensionnality and for creation os spanwise pre-

dominant wavenumbers. These $3D$ computations are continued to provide converged statistics and a detailed comparison with the experiments.

In future developments, a comparison will be carried out between experimental results provided by CEA, EDF and simulation results provided by IMFT, for this typical configuration.

Acknowledgments

This study has been carried out by using High Performance computing services of the nationals centres as CINES, IDRIS, CALMIP and GRID5000. The authors thank Dr. J. Vos, (CFS Engineering and EPFL), G. Barbut and V. Bodoc for their contribution in the adaptation of the NSMB code for this new configuration.

References

[1] R. Bourguet, M. Braza, G. Harran, and R. El Akoury. Anisotropic organised eddy simulation for the prediction of non-equilibrium turbulent flows around bodies. *J. Fluids Struct.*, 24(8):1240–1251, 2008.

[2] F.R. Menter. Two-equation eddy-viscosity turbulence models for engineering applications. *AIAA J.*, 32(8):1598–1605, 1994.

[3] P.R. Spalart and S.R. Allmaras. A one-equation turbulence model for aerodynamic flows. *AIAA Paper*, 439, 1992.

[4] W. Haase, M. Braza, and A. Revell. *DESider – a European effort on hybrid RANS LES modelling: results of the European Union funded project, 2004-2007*, volume 103 of *Notes on Numerical Fluid Mechanics and Multidisciplinary Design*. Springer, 2009.

[5] M. Braza, R. Perrin, and Y. Hoarau. Turbulence properties in the cylinder wake at high reynolds number. *J. Fluids Struct.*, 22:7551–771, 2006.

[6] Y. Hoarau. *Analyse physique par simulation numérique et modélisation des écoulements décollés instationnaires autour de surfaces portantes*. Thèse de doctorat, INP de Toulouse, 2002.

[7] S. Bourdet, M. Braza, Y. Hoarau, R. El Akoury, A. Ashraf, G. Harran, P. Chassaing, and H. Djeridi. Prediction and physical analysis of unsteady flows around a pitching airfoil with the dynamic mesh approah. *Eur. J. Comp. Mech.*, 16(3/4):451–476, 2007.

[8] R. Bourguet, M. Braza, R. Perrin, and G. Harran. Anisotropic eddy-viscosity concept for strongly detached unsteady flows. *AIAA J.*, 45(5):1145–1149, 2007.

[9] R. Perrin, E. Cid, S. Cazin, A. Sévrain, M. Braza, F. Moradei, and G. Harran. Phase-averaged measurements of the turbulence properties in the near wake of a circular cylinder at high reynolds number by 2c-piv and 3c-piv. *Exp. Fluids*, 42:93–109, 2007.

[10] G. Jin and M. Braza. A nonreflecting outlet boundary condition for incompressible unsteady navier-stokes calculations. *J. Computat. Phys.*, 107(2):239–253, 1993.

[11] J.B. Vos, E. Chaput, B. Arlinger, A. Rizzi, and A. Corjon. Recent advances in aerodynamics inside the NSMB (Navier-Stokes Multi-Block) consortium. *AIAA Paper*, 0802, 1998.

[12] P.L. Roe. Approximate riemann solvers, parameter vectors, and difference schemes. *J. Comp. Phys.*, 43:357–372, 1981.

[13] B. Van Leer. Towards the ultimate conservative difference scheme. v. a second-order sequel to godunov's method. *J. Comp. Phys.*, 32:101–136, 1979.

[14] J. Donea, P. Fasolli-Stella, and J.P. Halleux. An arbitrary lagrangian eulerian finite element method for transient dynamic fluid-structure interaction. *Comp. Meth. Appl. Mech. Eng.*, 33:689–723, 1982.

[15] P.R. Spalart, S. Deck, M.L. Shur, K.D. Squires, M.Kh. Strelets, and A. Travin. A new version of detached-eddy simulation, resistant to ambiguous grid densities. *Theor. Comput. Fluid Dyn.*, 20:181–195, 2006.

[16] N.M. Newmark. A method of computation for structural dynamics. In ASCE, editor, *J. of the Engineering mechanics division*, volume 3, pages 67–94, 1959.

ERCOFTAC Special Interest Groups

1. Large Eddy Simulation

Geurts, B.J.
University of Twente, Holland.
Tel: +31 53 489 4125
Fax: +
b.j.geurts@math.utwente.nl

4. Turbulence in Compressible Flows

Comte, P.
University of Poitiers, France.
Tel: +33 5 49 36 60 11
Fax: +33 5 49 36 60 01
Pierre.comte@tea.univ-poitiers.fr

5. Environmental CFD

Morvan, H.
University of Nottingham, England.
Tel: +44 115 846 6374
Fax: +44 115 951 3898
herve.morvan@nottingham.ac.uk

10. Transition Modelling

Dick, E.,
University of Gent, Belgium.
Tel: +32 9 264 3301
Fax: +32 9 264 3586
erik.dick@ugent.be

12. Dispersed Turbulent Two Phase Flows

Sommerfeld, M.
Martin-Luther University, Germany.
Tel: +49 3461 462 879
Fax: +49 3461 462 878
martin.sommerfeld@iw.uni-halle.de

14. Stably Stratified and Rotating Flows

Redondo, J.M.
UPC, Spain.
Tel: +34 93 401 7984
Fax: +34 93 401 6090
Redondo@fa.upc.es

15. Turbulence Modelling

Jakirlic, S.
Darmstadt University of Technology, Germany.
Tel: +49 6151 16 3554
Fax: +49 6151 16 4754
s.jakirlic@sla.tu-darmstadt.de

20. Drag Reduction and Flow Control

Choi, K-S.
University of Nottingham, England.
Tel: +44 115 9513 792
Fax: +44 115 9513 800
kwing-so-choi@nottingham.ac.uk

24. Variable Density Turbulent Flows

Anselmet, F.
IMST, France.
Tel: +33 4 91 505 439
Fax: +33 4 91 081 637
fabian.anselmet@irphe.univ-mrs.fr

28. Reactive Flows

Tomboulides, A.
Aristotle University of Thessaloniki, Greece.
Tel: +30 2310 991 306
Fax: +30 2310 991 304
ananiast@enman.auth.gr

32. Particle Image Velocimetry

Stanislas, M.
Ecole Centrale de Lille, France.
Tel: +33 3 20 337 170
Fax: +33 3 20 337 169
stanislas@ec-lille.fr

33. Transition Mechanisms, Prediction and Control

Hanifi, A.
FOI, Sweden.
Tel: +46 8 5550 4334
Fax: +46 8 5550 3481
ardeshir.hanifi@foi.se

34. Design Optimisation

Giannakoglou, K.
NTUA, Greece.
Tel: +30 210 772 1636
Fax: +30 210 772 3789
kgianna@central.ntua.gr

35. Multipoint Turbulence Structure and Modelling

Cambon, C.
ECL Ecully, France.
Tel: +33 4 72 186 161
Fax: +33 4 78 647 145
claude.cambon@ec-lyon.fr

36. Swirling Flows

Braza, M.
IMFT, France.
Tel: +33 5 61 285 839
Fax: +33 5 61 285 899
braza@imft.fr

37. Bio-Fluid Mechanics

Van Steenhoven, A.A.
Eindhoven University of Technology, Holland.
Tel: +31 40 2472 722
Fax: +31 40 2433 445
a.a.v.steenhoven@wtb.tue.nl

38. Microfluids and Micro Heat Transfer

Tardu, S.
Laboratoire des Ecoulements Géophysiques et Industriels, France.
sedat.tardu@hmg.inpg.fr

39. Aeroacoustics

Bailly, C.
Ecole Centrale de Lyon, France.
Tel: +33 4 72 186 014
Fax: +33 4 72 189 143
christophe.bailly@ec-lyon.fr

40. Smoothed Particle Hydrodynamics

Le Touzé, D.
Ecole Centrale de Nantes, France.
Tel: +33 2 40 37 15 12
Fax:
david.letouze@ec-nantes.fr

41. Fluid Structure Interaction

Longatte, E.
EDF, France.
Tel: +33 1 30 87 80 87
Fax: +33 1 30 87 77 27
elisabeth.longatte@edf.fr

42. Synthetic Models in Turbulence

Nicolleau, F.
University of Sheffield, England.
Tel: +44 114 22 27867
Fax: +44 114 22 27890
f.nicolleau@sheffield.ac.uk

43. Fibre Suspension Flows

Hämäläinen, J.
University of Kuopio, Finland.
Tel: +358 17 162279
Fax: +358 17 162585
jari.hamalainen@uku.fi

101. Quality and Trust in Industrial CFD

Hutton, A.G.
Airbus UK, England.
Tel: +44 117 936 7519
Fax:
anthony.hutton@airbus.com

102. ERCOFTAC Database Interests Group

Laurence, D.
UMIST, England.
Tel: +44 161 200 3704
Fax: +44 161 200 3723
dominique.laurence@manchester.ac.uk

ERCOFTAC Pilot Centres

Alpe – Danube – Adria

Reichl, C.
Austrian Institute of Technology,
Giefinggasse 2,
A-1210 Wien,
Austria.

Tel: +43 1 50550 6605
Fax: +43 1 50550 6439
christoph.reichl@arsenal.ac.at

Belgium

Geuzaine, P.
Cenaero,
CFD Multi-physics Group,
Rue des Frères Wright 29,
B-6041 Gosselies,
Belgium.

Tel: +32 71 919 334
philippe.geuzaine@cenaero.be

Czech Republic

Bodnar, T.
Institute of Thermomechanics AS CR,
5 Dolejskova,
CZ-18200 Praha 8,
Czech Republic.

Tel: +420 224 357 548
Fax: +420 224 920 677
bodnar@marian.fsik.cvut.cz

France – Henri Bénard

Cambon, C.
Ecole Centrale de Lyon.
LMFA,
B.P. 163,
F-69131 Ecully Cedex,
France.
Tel: +33 4 72 18 6161
Fax: +33 4 78 64 7145
claude.cambon@ec-lyon.fr

France South

Braza, M.
IMF Toulouse,
CNRS UMR – 5502,
Allée du Prof. Camille Soula 1,
F-31400 Toulouse Cedex,
France.
Tel: +33 5 61 28 5839
Fax: +33 5 61 28 5899
marianna.braza@imft.fr

France West

Bonnet, J-P.
Université de Poitiers,
Centre d'Etudes Aérodyn. et Thermiques,
43 Route de l'Aérodrome,
F-86036 Poitiers Cedex,
France.
Tel: +33 5 49 36 60 31
Fax: +33 5 49 45 60 01
jean-paul.bonnet@univ-poitiers.fr

Germany North

Gauger, N.
German Aerospace Center – DLR,
Institute of Aerodynamics,
Lilienthalplatz 7,
D-38108 Braunschweig,
Germany.
Tel: +49 531 295 3339
Fax: +49 531 295 2914
nicolas.gauger@dlr.de

Germany South

von Terzi, D.
Inst. Thermische Strömungsmaschinen,
Universität Karlsruhe (TH),
Kaiserstr. 12 (Geb. 10.91, Zi. 201)
D-76131 Karlsruhe,
Germany.

Tel: +49 721 608 6829
vonterzi@its.uni-karlsruhe.de

Germany West

Schröder, W.
RWTH – Aachen,
Institute of Aerodynamics,
D-52062 Aachen,
Germany.

Tel: +49 241 809 5410
Fax: +49 241 809 2257
ek@aia.rwth-aachen.de

Greece

Papailiou, K.D.
National Tech. University of Athens,
Laboratory of Thermal Turbomachines,
9 Iroon Polytechniou,
P.O. Box 64069,
Gr-15710 Athens, Greece.
Tel: +30 210 772 1634
Fax: +30 210 772 1658
kpapail@ltt.ntua.gr

Iberian East

Onate, E.
Universitat Politecnica de Catalunya,
Edificio C-1, Campus Norte,
Gran Capitan s/n,
E-08034 Barcelona,
Spain.
Tel: +34 93 401 6035
Fax: +34 93 401 6517
onate@cimne.upc.es

Iberian West

Theofilis, V.
Universidad Politécnica de Madrid,
Plaza Cardenal Cisneros 3,
E-28040 Madrid,
Spain.

Tel: +34 91 336 3291
Fax: +34 91 336 6371
vassilis@torroja.dmt.upm.es

Italy

Martelli, F.
University of Florence,
Department of Energy,
Via Santa Marta 3,
I-50139 Firenze,
Italy.
Tel: +39 055 479 6237
Fax: +39 055 479 6342
francesco.martelli@unifi.it

Nordic

Wallin, S.
Swedish Defence Research Agency FOI,
Computational Physics,
S-16490 Stockholm,
Sweden.

Tel: +46 8 5550 3184
Fax: +46 8 5550 3062
stefan.wallin@foi.se

Poland

Drobniak, S.
Technical University of Czestochowa,
Thermal Machinery Institute,
Al. A. Krajowej 21,
PL-42200 Czestochowa,
Poland.
Tel: +48 34 325 0507
Fax: +48 34 325 0555
drobniak@imc.pcz.czest.pl

Switzerland

Jenny, P.
ETH Zürich,
Institute of Fluid Dynamics,
Sonneggstrasse 3, ML H 38,
CH-8092 Zürich,
Switzerland.
Tel: +41 44 632 6987
Fax: +41 44 632 1147
jenny@ifd.mavt.ethz.ch

Netherlands

Ooms, G.
J.M. Burgerscentrum,
Research School for Fluid Mechanics,
Mekelweg 2,
NL-2628 CD Delft,
Netherlands.
Tel: +31 15 278 1176
Fax: +31 15 278 2979
g.ooms@wbmt.tudelft.nl

United Kingdom

Barton, I.
BAE Systems,
ATC – Sowerby, FPC 267,
P.O. Box 5,
Bristol BS34 7QW,
England.
Tel: +44 117 302 8251
Fax: +44 117 302 8007
iain.barton@baesystems.com

Best Practice Guidelines for Computational Fluid Dynamics of Dispersed Multi-Phase Flows

Editors

Martin Sommerfeld, Berend van Wachem
&
René Oliemans

The simultaneous presence of several different phases in external or internal flows such as gas, liquid and solid is found in daily life, environment and numerous industrial processes. These types of flows are termed multiphase flows, which may exist in different forms depending on the phase distribution. Examples are gas-liquid transportation, crude oil recovery, circulating fluidized beds, sediment transport in rivers, pollutant transport in the atmosphere, cloud formation, fuel injection in engines, bubble column reactors and spray driers for food processing, to name only a few. As a result of the interaction between the different phases such flows are rather complicated and very difficult to describe theoretically. For the design and optimisation of such multiphase systems a detailed understanding of the interfacial transport phenomena is essential. For single-phase flows Computational Fluid Dynamics (CFD) has already a long history and it is nowadays standard in the development of air-planes and cars using different commercially available CFD-tools.

Due to the complex physics involved in multiphase flow the application of CFD in this area is rather young. These guidelines give a survey of the different methods being used for the numerical calculation of turbulent dispersed multiphase flows. The Best Practice Guideline (BPG) on Computational Dispersed Multiphase Flows is a follow-up of the previous ERCOFTAC BPG for Industrial CFD and should be used in combination with it. The potential users are researchers and engineers involved in projects requiring CFD of (wall-bounded) turbulent dispersed multiphase flows with bubbles, drops or particles.

Table of Contents

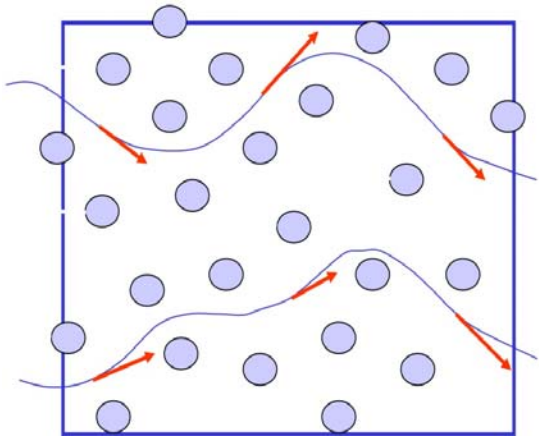

Copies of the Best Practice Guidelines can be acquired electronically from the ERCOFTAC website:

www.ercoftac.org

Or from:

ERCOFTAC ADO
Chaussée de la Hulpe 189 Terhulpsesteenweg
B-1170 Brussels
Belgium

Tel: +32 2 643 3572
Fax: +32 2 647 9398
Email: anne.laurent@ercoftac.be

The price per copy (not including postage) is:

ERCOFTAC members	
First copy	*Free*
Subsequent copies	45 Euros
Students	30 Euros
Non-ERCOFTAC academics	90 Euros
Non-ERCOFTAC industrial	180 Euros